Experimental and theoretical characterization of the low frequency acoustic transmission through centrifugal pumps

Guidong Li

Universidad de Oviedo

Doctoral Thesis presented in the Doctoral Program
of Energy and Process Control

Gijón, September 2020

Experimental and theoretical characterization of the low frequency acoustic transmission through centrifugal pumps

Guidong Li

Universidad de Oviedo

Supervisor: Prof. Dr. Jorge Luis Parrondo Gayo

Doctoral Thesis presented in the Doctoral Program
of Energy and Process Control

Gijón, September 2020

SUMMARY OF THE PhD THESIS CONTENTS

1.- Title of the Thesis	
Spanish/other languages: Caracterización experimental y teórica de la transmisión acústica de baja frecuencia a través de bombas centrífugas	English: Experimental and theoretical characterization of the low frequency acoustic transmission through centrifugal pumps

2.- Author	
Name: Guidong Li	ID/Passport/NIE number:
PhD Programme: Energía y Control de Procesos	
Body responsible: Comisión Académica del Programa de Doctorado	

SUMMARY (in Spanish)

El ruido fluidodinámico en sistemas hidráulicos ha cobrado gran atención en las últimas décadas debido a que en muchas áreas de aplicación cada vez hay requisitos más exigentes de reducción de niveles de ruido y vibraciones. Las principales fuentes de ruido en estos sistemas suelen ser las propias máquinas de fluidos, tales como las bombas centrífugas, en las que se generan pulsaciones de flujo con amplitud que depende de las condiciones de operación (velocidad y caudal). Las fluctuaciones de presión inducidas en una cierta posición de los conductos y a una cierta frecuencia también dependen de la respuesta acústica del sistema, es decir, de cómo los pulsos acústicos son transmitidos o reflejados en cada componente del sistema, incluidas las propias bombas. Por tanto, la medida directa de fluctuaciones de presión en una tubería no es reflejo directo de las propiedades acústicas de las bombas, pues el acoplamiento con el sistema hidráulico puede llevar a situaciones de gran amplitud por resonancia.

La mayor parte de la energía sonora en sistemas de tuberías hidráulicas es de baja frecuencia, es decir, su transmisión solo sucede en modo de onda plana. Por ello, las bombas pueden asimilarse a elementos acústicos de dos puertos con ciertas propiedades de generación (activas) y de reflexión-transmisión (pasivas). Estas últimas se suelen caracterizar mediante una matriz de dispersión o una matriz de transmisión, que establecen relaciones lineales entre las variables acústicas (como las ondas de presión o las fluctuaciones de velocidad) de cada puerto de la bomba (aspiración y descarga). El objeto de esta tesis ha sido el estudio de esas matrices de dispersión y de transmisión para bombas centrífugas convencionales (sin difusor y con voluta) mediante ensayos sobre una bomba de laboratorio y mediante el desarrollo de un modelo acústico de las bombas capaz de estimar ambas matrices.

Para los ensayos de laboratorio se sometió una bomba a diferentes cargas acústicas, inducidas mediante otra bomba auxiliar, mientras se grababan las señales de presión en distintas posiciones a lo largo de los conductos de aspiración e impulsión. Después las señales se post-procesaron en el dominio de frecuencia para obtener los respectivos frentes de onda hacia aguas arriba y abajo. Por último, entre los frentes de onda de cada frecuencia se impusieron las relaciones asociadas a los elementos de la matriz de dispersión, formándose un sistema de ecuaciones sobre-determinado que se puede resolver mediante un procedimiento de mínimos cuadrados para obtener los elementos de la matriz de dispersión.

Por otro lado, se elaboró un modelo acústico de parámetros agrupados para simular el campo sonoro interno en bombas centrífugas ante la acción de fuentes ideales de baja frecuencia. El modelo se basa en una red de nodos distribuidos en la bomba, con matrices de transferencia local entre parejas de nodos de regiones vecinas. Este modelo se incorporó en un procedimiento numérico para determinar las matrices de dispersión o de transmisión de bombas centrífugas en función de la frecuencia y de los principales parámetros geométricos de las bombas. Tras analizar la sensibilidad de los resultados respecto a varios parámetros de cálculo, las predicciones se contrastaron frente a los datos experimentales obtenidos para la bomba de

ensayo así como frente a los datos publicados en la literatura técnica para otras nueve bombas distintas. En conjunto, las diez bombas cubren un rango de velocidad específica adimensional de 0.25 a 1.01. Este contraste se extendió a las predicciones del modelo clásico de Stirnemann, basado en una analogía eléctrica.

Los resultados muestran que las predicciones del nuevo modelo propuesto siempre están en buen acuerdo cuantitativo con las medidas, y que, al subir la frecuencia, su capacidad de predicción supera claramente a la del modelo de analogía eléctrica, con independencia de la velocidad específica o de las características geométricas.

SUMMARY (in English)

Fluid-dynamic noise in hydraulic systems has gained high attention in the last decades due to the increasing requirements of vibration and noise reduction in many fields. Usually the most significant sound sources in the system are fluid machines such as centrifugal pumps, in which flow pulsations are generated with amplitude that depends on the operating conditions (velocity and flow-rate). The resulting pressure fluctuations induced at a given frequency and position along the pipes also depend on the acoustic response of the system, i.e., on how the acoustic pulsations are transmitted or reflected at each system component, including the pump itself. Therefore, the direct measurement of pressure pulsations in a pipeline of a test pump does not directly reflect the acoustic properties of the pump itself, because the coupling effects of the hydraulic system, which can even cause standing waves, may be seriously misleading.

Most of the sound energy in piping systems lays in a range of frequencies low enough for sound to be transmitted only in plane wave mode. In consequence, centrifugal pumps can be considered as two-port acoustic elements with sound generation and sound reflection-transmission properties. The latter are characterized by means of the scattering matrix or the transmission matrix, which establish linear relationships between the acoustic variables (like pressure waves or velocity fluctuations) at the upstream inlet and downstream outlet ports of the pump. This thesis has aimed to investigate the characteristics of the scattering and the transmission matrices of conventional centrifugal pumps with vaneless volute casing, by means of an experimental study on a laboratory pump combined with the development of a special acoustic model.

First, experiments were conducted on a test pump when subject to different acoustic loads that could be induced from an auxiliary pump of the same hydraulic system. In particular, the pressure signals at several positions along the suction and discharge pipes of the test pump were acquired and recorded for a variety of acoustic load configurations. Then, signals were post-processed in the frequency domain to determine the pressure waves travelling up and downstream. And finally, the relationships between the pressure waves at a given frequency imposed by the scattering matrix formed an overdetermined equation system, from which the elements of the scattering matrix could be obtained based on a least square error procedure.

On the other hand, an acoustic lumped-parameter model has been developed to simulate the internal sound field in centrifugal pumps when subject to ideal low-frequency sound sources. The model is based on a network of nodes distributed through the pump, with local transfer matrices connecting pairs of nodes at neighboring regions. This model has been implemented in a numerical procedure to determine the pump passive acoustic properties, either in terms of a transmission matrix or a scattering matrix, as a function of frequency and depending on the main geometrical parameters of the pump. After analyzing the sensitivity of the results with respect to several calculation parameters, predictions have been contrasted against the experimental data obtained for the test pump as well as against the data published in the open

technical literature for other nine different pumps. All together, the ten pumps cover a range of non-dimensional specific speeds from 0.25 to 1.01. That contrast was extended to the predictions of the classical Stirnemann's pump model based on an electrical system analogy.

The results show that the predictions of the new transfer matrix model are always in reasonable quantitative agreement with measurements, and that, as frequency is increased, its prediction capability clearly outperforms that of the electrical analogy model regardless the pump specific speed or geometrical features.

DIRECTOR OF THE DEPARTMENT OF *ENERGÍA*
PRESIDENT OF THE ACADEMIC COMMISSION OF THE PhD PROGRAMME IN *ENERGÍA Y CONTROL DE PROCESOS*

Abstract

Fluid-dynamic noise in hydraulic systems has gained high attention in the last decades due to the increasing requirements of vibration and noise reduction in many fields. Usually the most significant sound sources in the system are fluid machines such as centrifugal pumps, in which flow pulsations are generated with amplitude that depends on the operating conditions (velocity and flow-rate). The resulting pressure fluctuations induced at a given frequency and position along the pipes also depend on the acoustic response of the system, i.e., on how the acoustic pulsations are transmitted or reflected at each system component, including the pump itself. Therefore, the direct measurement of pressure pulsations in a pipeline of a test pump does not directly reflect the acoustic properties of the pump itself, because the coupling effects of the hydraulic system, which can even cause standing waves, may be seriously misleading.

Most of the sound energy in piping systems lays in a range of frequencies low enough for sound to be transmitted only in plane wave mode. In consequence, centrifugal pumps can be considered as two-port acoustic elements with sound generation and sound reflection-transmission properties. The latter are characterized by means of the scattering matrix or the transmission matrix, which establish linear relationships between the acoustic variables (like pressure waves or velocity fluctuations) at the upstream inlet and downstream outlet ports of the pump. This thesis has aimed to investigate the characteristics of the scattering and the transmission matrices of conventional centrifugal pumps with vaneless volute casing, by means of an experimental study on a laboratory pump combined with the development of a special acoustic model.

First, experiments were conducted on a test pump when subject to different acoustic loads that could be induced from an auxiliary pump of the same hydraulic system. In particular, the pressure signals at several positions along the suction and discharge pipes of the test pump were acquired and recorded for a variety of acoustic load configurations. Then, signals were post-processed in the frequency domain to determine the pressure waves travelling up and downstream. And finally, the relationships between the pressure waves at a given frequency imposed by the scattering matrix formed an overdetermined equation system, from which the elements of the scattering matrix could be obtained based on a least square error procedure.

On the other hand, an acoustic lumped-parameter model has been developed to simulate the internal sound field in centrifugal pumps when subject to ideal low-frequency sound sources. The model is based on a network of nodes distributed through the pump, with local transfer matrices connecting pairs of nodes at neighboring regions. This model has been implemented in a numerical procedure to determine the pump passive acoustic properties, either in terms of a transmission matrix or a scattering matrix, as a function of frequency and depending on the main

geometrical parameters of the pump. After analyzing the sensitivity of the results with respect to several calculation parameters, predictions have been contrasted against the experimental data obtained for the test pump as well as against the data published in the open technical literature for other nine different pumps. All together, the ten pumps cover a range of non-dimensional specific speeds from 0.25 to 1.01. That contrast was extended to the predictions of the classical Stirnemann's pump model based on an electrical system analogy.

The results show that the predictions of the new transfer matrix model are always in reasonable quantitative agreement with measurements, and that, as frequency is increased, its prediction capability clearly outperforms that of the electrical analogy model regardless the pump specific speed or geometrical features.

Resumen

El ruido fluidodinámico en sistemas hidráulicos ha cobrado gran atención en las últimas décadas debido a que en muchas áreas de aplicación cada vez hay requisitos más exigentes de reducción de niveles de ruido y vibraciones. Las principales fuentes de ruido en estos sistemas suelen ser las propias máquinas de fluidos, tales como las bombas centrífugas, en las que se generan pulsaciones de flujo con amplitud que depende de las condiciones de operación (velocidad y caudal). Las fluctuaciones de presión inducidas en una cierta posición de los conductos y a una cierta frecuencia también dependen de la respuesta acústica del sistema, es decir, de cómo los pulsos acústicos son transmitidos o reflejados en cada componente del sistema, incluidas las propias bombas. Por tanto, la medida directa de fluctuaciones de presión en una tubería no es reflejo directo de las propiedades acústicas de las bombas, pues el acoplamiento con el sistema hidráulico puede llevar a situaciones de gran amplitud por resonancia.

La mayor parte de la energía sonora en sistemas de tuberías hidráulicas es de baja frecuencia, es decir, su transmisión solo sucede en modo de onda plana. Por ello, las bombas pueden asimilarse a elementos acústicos de dos puertos con ciertas propiedades de generación (activas) y de reflexión-transmisión (pasivas). Estas últimas se suelen caracterizar mediante una matriz de dispersión o una matriz de transmisión, que establecen relaciones lineales entre las variables acústicas (como las ondas de presión o las fluctuaciones de velocidad) de cada puerto de la bomba (aspiración y descarga). El objeto de esta tesis ha sido el estudio de esas matrices de dispersión y de transmisión para bombas centrífugas convencionales (sin difusor y con voluta) mediante ensayos sobre una bomba de laboratorio y mediante el desarrollo de un modelo acústico de las bombas capaz de estimar ambas matrices.

Para los ensayos de laboratorio se sometió una bomba a diferentes cargas acústicas, inducidas mediante otra bomba auxiliar, mientras se grababan las señales de presión en distintas posiciones a lo largo de los conductos de aspiración e impulsión. Después las señales se post-procesaron en el dominio de frecuencia para obtener los respectivos frentes de onda hacia aguas arriba y abajo. Por último, entre los frentes de onda de cada frecuencia se impusieron las relaciones asociadas a los elementos de la matriz de dispersión, formándose un sistema de ecuaciones sobre-determinado que se puede resolver mediante un procedimiento de mínimos cuadrados para obtener los elementos de la matriz de dispersión.

Por otro lado, se elaboró un modelo acústico de parámetros agrupados para simular el campo sonoro interno en bombas centrífugas ante la acción de fuentes ideales de baja frecuencia. El modelo se basa en una red de nodos distribuidos en la bomba, con matrices de transferencia local entre parejas de nodos de regiones vecinas. Este modelo se incorporó en un procedimiento numérico para determinar las matrices de dispersión o de transmisión de bombas centrífugas en función de la frecuencia y de los principales parámetros geométricos de las bombas. Tras analizar la sensibilidad de

los resultados respecto a varios parámetros de cálculo, las predicciones se contrastaron frente a los datos experimentales obtenidos para la bomba de ensayo así como frente a los datos publicados en la literatura técnica para otras nueve bombas distintas. En conjunto, las diez bombas cubren un rango de velocidad específica adimensional de 0.25 a 1.01. Este contraste se extendió a las predicciones del modelo clásico de Stirnemann, basado en una analogía eléctrica.

Los resultados muestran que las predicciones del nuevo modelo propuesto siempre están en buen acuerdo cuantitativo con las medidas, y que, al subir la frecuencia, su capacidad de predicción supera claramente a la del modelo de analogía eléctrica, con independencia de la velocidad específica o de las características geométricas.

Acknowledgements

I would like to express my gratitude to all people who helped me during the writing of this thesis.

First and foremost, my deepest gratitude are Prof. Jorge Parrondo and Prof. Yang Wang. It was Prof. Jorge Parrondo that offered me this valuable opportunity to conduct further study on fluid machineries in University of Oviedo and has given me great help in both study and life during my four years stays in Gijon, like a teacher and a father. He has taught me a lot of advanced and professional knowledge and technologies in aspects of noise of fluid machineries, supplied me with a good condition of experiments and worked with me to solve problems in the research, all of these have made me progress greatly. Meanwhile, Prof. Yang Wang has provided me with great support and significantly instructive advices in my master and doctoral study. It is impossible for me to finish this thesis without their valuable and detailed guidance.

Second, I would like to sincerely thank my colleagues and friends in University of Oviedo, Prof. Adrián, Dr. Andrés, Dr. Manu, Dr. Celia, who have helped me a lot in my study and life and always been full of passion when I asked them for help. Besides, I want to give my special thanks to my Spanish friends, Joseta, Pablo and Celia, for their kind company and cares. At the same time, I also would like to express the depth of my gratitude to all the colleagues in National Research Center of Pumps, Prof. Jinfeng Zhang, for their valuable advices and help. Especially, I give many thanks to Dr. Puyu Cao, who has given me consistent cares and selfless help for these years.

Moreover, I really appreciate that China Scholarship Council, University of Oviedo and Jiangsu University can offer me this precious chance to study, supporting my study and life in Spain, so that I can concentrate on my research.

Finally, I would like to give the greatest gratitude to my family who has always given me the greatest support. My beloved wife Jieyun Mao and our wonderful son Maoyi Li are the origins of my motivation and they have supplied me with endless encouragements, company and love.

Guidong Li

Contents

List of Figures

List of Tables

Nomenclature

Latin symbols

A_P	average of the pump eye section and the throat section [m^2]
A_S	cross-section area of the pipeline [m^2]
A_T	volute throttle cross-section [cm^2]
$A(x)$	cross-sections at the longitudinal coordinate *x*
A_0	cross-sectional area at narrow side of the tongue [cm^2]
$A_{2\pi}$	cross-sectional area at wide side of the tongue [cm^2]
b_2	width at impeller outlet [mm]
b_3	volute width [mm]
c_0	sound speed [m/s]
C_{res}	sum of squares of residuals
C_{tot}	total sum of squares
d_D	diameter of discharge port [mm]
d_S	diameter of suction port [mm]
$E_1,\ E_2$	experimental measurement errors
f	frequency [Hz]
f_B	blade passing frequency [Hz]
f_S	shaft frequency [Hz]
H	head [m]
i	imaginary part of the physical variables
j	imaginary unit, equal to $\sqrt{-1}$
k	wave number [1/m]
k_0	wave number at position x
k_P	peripheral expansion factor at impeller outlet
k_R	reflection coefficient
$k_\mathrm{TS},\ k_\mathrm{TD}$	transmission coefficient
$\Delta l,\ \Delta l_1,\ \Delta l_2$	distance between the sensors [mm]
L_{SE}	length suction port to impeller eye [mm]
L_{TD}	length throttle to discharge port [mm]
t	time [s]
N	number of segments for passages with variable cross-section
n	pump rotational speed [rpm]
n_im	node located in region R_i
n_jn	node located in region R_j
n_s	non-dimensional specific speed
n_S	node at suction port
n_D	node at discharge port
n_{00}	one single node facing the impeller eye
n_{10}	one central node facing the pump inlet

n_{100}	one single node facing the throttle
$p_{a,u}$, $p_{b,u}$	acoustic pressure at upstream position a, b [Pa]
$p_{a,d}$, $p_{b,d}$	acoustic pressure at downstream position a, b [Pa]
p_{im}	acoustic pressure in the impeller region [Pa]
p	acoustic pressure [Pa]
p_i	transient pressure fluctuation at position i=1, 2 ... n [Pa]
p_{suc}^{+}	entering pressure wave at the suction pipe [Pa]
p_{suc}^{-}	exiting pressure wave at the suction pipe [Pa]
p_{dis}^{+}	entering pressure wave at the discharge pipe [Pa]
p_{dis}^{-}	exiting pressure wave at the discharge pipe [Pa]
p^{+}	radiated pressure wave along *x*-direction [Pa]
p^{-}	returning pressure wave along *x*-direction [Pa]
Q	flow rate [m^3/h]
Q_{BEP}	flow rate at the best efficiency point [m^3/h]
R^2	determination coefficient
R_i	region, i=0, 1 … 10
R_j	neighboring region to R_i
r	real part of the physical variables
r_1	radius at impeller inlet [mm]
r_2	radius at impeller outlet [mm]
r_3	radius at tongue tip [mm]
S	scattering matrix
T	transmission matrix
t	time variable [s]
u	acoustic volume velocity [m^3/s]
V_{IMP}	volume of the impeller [m^3]
V_{PUMP}	volume of the pump [m^3]
VR	variance ratio
v_{im}	acoustic mass velocity In the impeller region [m/s]
v_i	transient acoustic mass velocity at position i=1, 2 ... n [m/s]
$v_{a,u}$, $v_{b,u}$	acoustic mass velocity at upstream position a, b [m/s]
$v_{a,d}$, $v_{b,d}$	acoustic mass velocity at downstream position a, b [m/s]
x, *y*, *z*	coordinate: *x*-direction, *y*-direction, *z*-direction
Δx	a slice of thickness [mm]
Y_1, Y_3	Admittance [S]
y_0	acoustic characteristic impedance [m^{-1} s^{-1}]
Z, Z_2	acoustic impedance [Pa s / m^3]
Z_v	acoustic impedance based on acoustic mass velocity [m^{-1} s^{-1}]
Z_R	acoustic impedance at the boundary [Pa s / m^3]
Z_R'	resonator impedance
Z_0	specific acoustic impedance [Pa s / m]
z_B	number of blades

Greek symbols

β_2	outlet angle relative to tangent [deg]
δ	blade thickness at trailing edge [mm]
ρ	density of liquid [kg/m^3]
φ_1	angular position of first blade (trailing edge) relative to tongue [deg]
φ^+	phase corresponding to the pressure wave p^+ [deg]
φ^-	phase corresponding to the pressure wave p^- [deg]
ω	angular frequency [rad/s]

Superscripts

$+$	radiated component
$-$	returning component

1 Introduction

1.1 Research background

As a simple type of rotating machine, centrifugal pumps increase the pressure of the liquid through the interaction of the impeller blades and the liquid, thereby transporting the fluid from one place to another. In other words, these machines transfer the mechanical energy of the prime mover to the working media through their own rotating impellers, thereby generating kinetic energy and pressure energy in the liquid. Centrifugal pumps are widely used in modern society to transport different working media in a large variety of fields. For example, they are an indispensable facility in agricultural irrigation, drought-resistant irrigation and drainage. In the water supply and sewerage system, the pump and the pump station play the role of water intake, transportation and wastewater collection, and it is one of the most important facilities in modern cities. In hydroelectric power plants, pumps are responsible for pumping and storing energy. In nuclear power plants, pumps act as a high-pressure water supply for the safety injection system of the pressurized water reactor (PWR). In aerospace engineering, centrifugal pumps provide lubricating oil for the normal operation of aircraft engines, and liquid nitrogen, liquid oxygen and other propellants for liquid rocket engines. Furthermore, centrifugal pumps are also suitable for petroleum, metallurgy, pharmaceutical and synthetic fibre industries to transport corrosive aggressive media (e.g. acidity and alkaline) at various temperatures or media with high physical and chemical properties. Therefore, it can be said that there are pumps wherever there is fluid transport.

Due to the development of technology and the automation of modern industrial equipment, the connection between the different devices in the hydraulic circulation system is getting closer. Centrifugal pumps, as the core components of the hydraulic circulation system, and the piping system jointly determine the operating flow rate of the pump. The requirement is to match the maximum efficiency point on the pump curve to the desired operating point of the system during the design process. In actual operation, centrifugal pumps not only operate in the vicinity of the optimum efficiency point but also may operate at off-design conditions depending on work requirements. That is, it is unrealistic to offer appropriate and satisfactory performance under all operating conditions. Based on the design mechanism of centrifugal pumps, deviation from the maximum efficiency point usually results in hydraulic losses (efficiency decrease) and unstable operation (e.g. vibration and noise) within the pump (Wang et al. 2003, Pedersen et al. 2003, Yang et al. 2014, Zhang et al. 2020). The long-term periodic unstable operation may cause system instability, and failure will occur when the allowable value is exceeded (Guan 2011). In addition, the structure of the pump hydraulic circulation system is complicated and may also cause the pump to produce unstable vibration and noise because of different mechanisms

(includes mechanical vibration, fluid-dynamic interaction and cavitation phenomenon and so on), especially under high-speed operating conditions. Occasionally, severe vibration and noise can even cause equipment damage up to the shutdown of a full hydraulic system, thereby causing huge economic losses and serious harm to enterprises and society.

Conventional centrifugal pumps usually have a simple structure consisting of a bladed rotor (impeller) inside a static volute casing, with one inlet and one outlet port. However, the Coriolis and centrifugal forces generated by the impeller rotation and surface curvature effects cause the flow in the impeller to be very complicated, with fully 3D and unsteady features (Brun et al. 2005, Li et al. 2016). Flow in pumps is often accompanied by phenomena such as pre-rotation, recirculation, flow separation and high levels of turbulence. Besides, other phenomena can take place such as cavitation, rotating stall or surge pulsations, which affect the stable operation of centrifugal pumps. The parameters related to the hydraulic design of the volute, such as the throat area of the volute, the radius of the tongue, the placement angle of the tongue, the base circle diameter of the volute and the flow angle of the tongue, also have a significant effect on the internal flow states of the centrifugal pump (Guan 2011, Yang et al. 2011). The asymmetric structure of the volute in the circumferential direction results in the uneven flow state of the impeller exit area, at the same time, the interaction generated by the intermittent relative motion between the rotating impeller and the stationary volute tongue creates an unstable flow field. The instability of the fluid flow in the above main components not only affects the efficiency and working range of the centrifugal pump but also is the main reason for inducing the vibration and noise of the centrifugal pump and affecting the stable operation (Cai et al. 2014, Zhang et al. 2016, Si et al. 2020, Cheng et al. 2020). The pulsating pressure caused by the instability of the fluid flow also directly leads to the mechanical vibration of the pipe. In particular, the resonance will occur when the pulsation frequency is close to the natural frequency of the piping system. The pressure pulsation generated in the resonance state is well larger than the pressure pulsation in the non-resonant state. It not only affects the working quality of system components and the accuracy of system parameter testing but also causes structural noise and nozzle radiation noise, etc., which are very harmful.

With the development of centrifugal pumps in the direction of high-speed, multi-purpose, centralized and automated, the requirements of stability and low noise are becoming more and more demanding in the design stage of centrifugal pumps. The noise of centrifugal pumps is a combination of sounds under different frequencies and intensities. According to the previous studies, the excitation of fluid-dynamic noise inside the centrifugal pump is a primary noise source for the hydraulic system formed by the external piping, particularly at off-design operating conditions (Barrio et al. 2008, Keller et al. 2014, Zhang et al. 2015). Effectively suppressing or improving the occurrence of noise level is very significant to the performance of the overall hydraulic circulatory system. In the actual design and selection process of the

centrifugal pumps, the noise level as a critical indicator must be suitable for the expected service (Morgenroth et al. 1998, Larralde et al. 2010, Guo et al. 2020). It has become an important factor in limiting product quality. Therefore, the identification and control of noise are vital in the hydraulic circulatory system. However, the prediction of noise at the design stage of the centrifugal pump is more difficult and less precise than for other performance characteristics, e.g. pump head and efficiency.

1.2 Noise in pump hydraulic systems

In a centrifugal pump hydraulic system, the excitation noise sources come from many aspects even without considering the influence of the external environment. The noise generated in the flow passage components can be simply divided into noise sources in the piping system and noise sources in the centrifugal pump. Classifying the primary source is the basis for analysing and diagnosing the noise of centrifugal pumps.

1.2.1 Noise sources in piping systems

Piping systems with centrifugal pumps, consisting mainly of valves, branch pipes, elbow pipes and measuring instruments and so on, is a network to transfer fluid medium from one place to another. It builds the connection between the medium transmission device and the upstream/downstream devices, and can only be operation in a complete loop. The piping system acts as a transmission channel for different sources of noise (Hambric et al. 2002), and also radiate undesirable noise as a sound source at some positions (e.g. valve, regulator, bend, joint pipe, expansions and contractions, etc.).

Valve is a control component in the fluid transfer system with functions such as regulation, diversion and shunt, etc. Meanwhile, it can also be an important noise source in the pump piping system. Faulkner (1976) and Barron (2003) thought that mechanical noise and fluid-dynamic noise are the two main noise sources generated by the valve. The mechanical noise is mainly derived from the valve plug, the valve stem and some moving parts. The reason is that these components are subjected to impact from fluid and effect from fluid-induced pressure fluctuations within the valve, results in mechanical vibration further generating noise. Fluid-dynamic noise originates from several sources of noise, including turbulent velocity fluctuations induced by changes in liquid velocity and cavitation noise caused by collapse of vapor bubbles.

1.2.2 Noise sources in centrifugal pumps

Centrifugal pumps can not only radiate sound directly to the external environment through the pump casing but also can transmit through the flowing fluid

along the upstream and downstream pipelines. In general the excitation mechanisms can be divided into mechanical noise and hydraulic noise (Durrer et al. 2006, Si et al. 2019). Both types of noise propagate simultaneously but their relative contributions on the hydraulic system are different.

Mechanical noise:

The most common mechanical noise sources are mainly caused by poor machining accuracy of the components, dynamic friction and mounting error of the installation (Birajdar et al. 2009). For example:

(1) rotor vibration caused by shaft misalignment between the motor and the centrifugal pump;
(2) friction generated by load unbalance on the impeller;
(3) friction induced by defects or wear of bearings and seals;
(4) high vibration and unbalance emerged by the rotational speed of centrifugal pump being near or pass through a lateral critical speed, etc.

The generation of mechanical noise is often accompanied by the vibration of the pump, which threatens the safe operation of the hydraulic system. In the modern industry, with the continuous improvement of manufacturing and processing technology, the mechanical noise has been gradually improved.

Instability flow generated noise:

The internal flow of the centrifugal pump is fully three-dimensional unsteady and turbulent flow, with regions of swirling flow (Elholm et al. 1990), flow separation (Sinha et al. 2000) and secondary flow (Westra et al. 2010), etc. The mechanism of noise generated by the internal flow is more complicated than the noise generated by the mechanical structure, and the frequency range involved is wider. The sources of hydraulic noise in the centrifugal pump are mainly caused by flow separation, rotating stall, rotor and stator interaction and cavitation, etc. (Majidi 2005, Birajdar et al. 2009, Ni et al. 2020). In the case of single-stage centrifugal pump with a vaneless volute casing, the hydraulic noise caused by instability flow perturbation is associated with the shaft frequency, blade passing frequency (including their harmonics) and broadband phenomena. It is a common and unavoidable phenomenon due to the finite blade number and finite blade thickness.

For a centrifugal pump with a well-structured design, the fluid-dynamic noise sources are the main noise sources. In general, the excitation at the blade passing frequency as the noise dominant excitation is a consequence of the intermittent impeller-tongue interaction and periodic non-uniform outflow from the impeller. When two consecutive blades pass through the tongue region, the fluid flowing out from the impeller channels between them is subject to obstructed and creates pulse flows. These pulse flows as sound waves propagate along the piping system and may lead to annoying noise (Langthjem et al. 2004). The magnitude of this fluid-dynamic excitation is dependent on the geometries of the machine at the impeller and volute tongue regions (including the radial gap between the impeller and the tongue edge, the

blades number and the volute tongue shape, etc.) (Dong et al. 1997, Solis et al. 2009, Gao et al. 2016, Guo et al. 2019) and on the pump operating conditions (Parrondo et al. 2010, Yuan et al. 2012, Guo et al. 2017 and 2018). In addition, the periodic interaction between the spatially distorted inlet flow field and the rotating impeller may also produce a noise excitation similar to the interaction of impeller outflow and volute tongue. The fluid-dynamic noise propagates along the piping system and acoustic energy is not easily attenuated. Meanwhile, new noise sources may be generated due to strong coupling with other pipe components. Standing waves and fluid resonant feedback may also form due to the arrangement of the pipes.

During the operation of the centrifugal pump, especially under off-design conditions, the sources of broadband noise as important components of hydraulic noise are mainly caused by large-scale flowfield instabilities in the impeller channels. The instability of the flow is related to the unsteady turbulence flow (induced by separating flow and recirculating flow from the impeller channel) and the nonuniform discharge flow (caused by wake flow from the velocity difference on both pressure and suction sides). According to the researches (Guelich et al. 1992, Choi et al. 2003, Durrer et al. 2006), these instability flow produce dynamic fluctuating pressure forces on the blade surface and thereby generate noise by a trailing edge generation mechanism.

Another important cause of instability in the centrifugal pump is cavitation. Cavitation, generated by the formation and collapse of vapour bubbles due to change in pressure, is a common phenomenon in the centrifugal pump. Cavitation emerges in the low static pressure region of the impeller blades inlet and the bubbles produced extinguishes in the high-pressure region of the impeller blade trailing edge. This phenomenon usually generates high-frequency pulses, thereby accompanying excessive vibration and noise, and destructs the surface layer of the impeller blades (Chudina. 2003, Al Thobiani. 2011). Cavitation noise with wideband frequency presents different acoustic spectrum characteristics in different cavitation stages. Some scholars (Neill et al. 1997, Alfayez et al. 2005, Čudina. 2009, Mousmoulis et al. 2019) used the noise spectra structure to investigate the cavitation inception and its development process. Experimental results show that the maximum high-frequency noise occurred before the drop of the pump head.

At present, the noise caused by structural vibration in the pump hydraulic system can be reduced and isolated by relatively mature measures, so it does not contribute much to the pipe nozzle radiation noise. The fluid-dynamic noise generated in the centrifugal pump can radiate directly to the outside of the pipe port through the fluid itself, and this part of the noise reduction is difficult.

1.3 Acoustic characteristics and analysis approaches of pumps

1.3.1 Experimental measurement of noise sources

During the experiment, the excitation noise of the centrifugal pump is usually measured by a monitoring instrument such as microphone, accelerometer, pressure sensor or hydrophone, etc. The acoustic signals or vibrational signals measured by the microphone or accelerometer are often used to indirectly reflect the noise characteristics of centrifugal pumps. However, the correspondence between airborne noise (or vibrational signals from the walls) and fluid-dynamic noise is very complicated. Airborne noise is very susceptible to background noise. Due to the stiffness of the pump surrounding wall, the noise energy radiated from the pump will also be greatly attenuated, especially high-frequency noise. Therefore, these test methods outside the pump are difficult to accurately describe the fluid-dynamic noise.

The hydrophone or pressure sensor, which is mounted directly on the pump wall or its pipeline and is in direct contact with the transmission medium, can be used to capture the acoustic signals of hydraulic noise in centrifugal pumps. For example, Simpson H. C. et al. (1966) used the experimental method to examine the hydraulic noise of two types of centrifugal pumps with different structures (volute pump and diffuser pump). The dominant frequencies of the hydraulic noise in the noise spectrum are the same as the rotational frequency of the impeller and its harmonics. Choi et al. (2003) used hot wire probes and pressure sensors to investigate the noise generation mechanism caused by the unsteady flow field in a centrifugal impeller with air as working medium. Kergourlay et al. (2007) analysed the effect of splitter blades on performance and pressure pulsation of the centrifugal pump through the piezoelectric pressure sensors. The results reveal that adding splitter blades have a positive effect on the pressure fluctuation and decrease the radiated noise. Yuan et al. (2009) employed pressure sensors and hydrophones to collect and analyse the pressure pulsation signal and flow noise signal at the outlet of the centrifugal pump. The results show that the blade passing frequency is the main frequency of the pressure pulsation and the flow noise signal. In addition, the noise also has obvious peaks in the second-order harmonic frequency and shaft frequency. Liu et al. (2012 and 2013) pointed out through experiments that the width of the blade outlet has different degrees of influence on the flow induced vibration intensity and noise signal of the centrifugal pump. Wang et al. (2013) adopted hydrophone to measure and analysis the noise power spectral density of the centrifugal pump at different impeller outlet angles. Christopher et al. (2013) investigated the cavitation in a centrifugal pump for three different leading edge shapes of the impeller blade based on cavitation noise and vibration signal detected by hydrophone and accelerometer. The experimental results exhibited that the noise and vibration signals were better predictor of cavitation inception and its development.

The emergence of particle image velocimetry (PIV) technology allows

researchers to directly extract the abundant flow field information from a large number of spatial points, and use this as a basis to obtain the required data. Therefore, visualization technology is also combined with pressure transducer or hydrophones to study the mechanism of noise generation. For example, Chu et al. (1995) utilized PIV measurement to determine the velocity distribution of the internal flow field of the centrifugal pump and obtained the pressure field through correlation calculation. The results show that the uneven flow of the impeller outlet and the mutual interference between the blade and the volute tongue are the main causes of the pressure pulsation and far-field noise inside the pump. Dong et al. (1997) carried out a series of experiments to show the interrelationship among the internal flow structure, pressure value and noise level (measured by PIV technique, pressure transducer and hydrophone respectively) in a centrifugal pump. They revealed the primary sources of noise originated by the interaction of the impeller non-uniform outflow with the tongue. The magnitude of the clearance between the impeller and the tongue has an important impact on the noise of the pump. Wu et al. (2017) obtained that the broadband frequency of the pressure pulsation frequency of the centrifugal pump is mainly induced by the unstable separating vortex in the impeller channels, and it is closely related to the relative position of the volute tongue. This is because the effect of the volute tongue enhances the strength of the vortex.

Experimental measurement has the advantage of providing accurate and reliable test results for many engineering research using modern advanced testing techniques. These results have an irreplaceable role in the study of complex flow mechanisms and the design of fluid-related engineering structures and machinery.

1.3.2 Theoretical analysis of noise sources

The premise of low noise pump retrofit design is to establish the relationship between pump structural and operating condition parameters and its vibration and noise characteristics through theoretical or experimental methods. However, in practical engineering applications, the experiment method requires a large number of model tests to summarize the rules, which is costly and has a long research period, and some flow conditions (such as corrosive flow, high-temperature flow, etc.) are difficult to achieve by experimental means and are also affected by model size limitations and boundary conditions. Therefore, in order to optimize the design of centrifugal pumps with low noise, the related theoretical model would be helpful.

The noise generated by the unstable flow inside the centrifugal pump produces sound waves that propagate through the main components (such as impeller, volute, inlet and outlet pipeline, etc.) and radiate to the external environment. During the operation of the centrifugal pump, not only the generation of sound pressure needs attention, but also the transmission characteristics of the sound pressure need to be taken into account. For example, Stirnemann et al. (1987) developed an electrical network model related to the pump geometry, which describes the passive acoustic properties of the pump by means of a dynamic transmission matrix. They determined this transmission matrix for a pump under noncavitating and slightly cavitating conditions. Bardeleben et al. (2002) presented a new model to investigate the acoustic

scattering matrix for a centrifugal pump, which can be used to evaluate how the centrifugal pump interacts with acoustic pressure waves from the pump inlet and outlet ports. Carta et al. (2002) used the transmission matrix model to obtain experimental results of the matrix elements in the static and operational state of the impeller, and get the difference between the active source parameters of the two centrifugal pumps. The results show that the passive source characteristic matrix is basically unaffected by the operating conditions. Parrondo et al. (2011) built an acoustic model, which is made up of a succession of cells with independent sound reflection and transmission coefficients, to determine the ideal noise sources. Moreover, the acoustic model developed was verified in a real centrifugal pump by comparing the experimental and theoretical values of the sound reflection coefficient of the pump outlet. The results showed that the proposed acoustic model can be used to characterize the internal sound field of the pump related to low frequency fluid-dynamic mechanisms.

Through theoretical analysis, noise generation mechanism and acoustic propagation characteristics can be obtained to a certain extent, thereby guiding experimental design and product development. Simplified acoustic model research can extract more concise calculation and analysis model, thereby improving computational efficiency and saving manpower and resources. The study of theoretical method and the analysis of simplified acoustic models are necessary. In addition to making researchers understand the mechanism of fluid-dynamic noise generation, the more significant purpose is to analyse the acoustic characteristics of the actual product, reduce product noise and ultimately design different series of low-noise centrifugal pumps, which is also in line with the actual needs of enterprises and users. Therefore, the analysis of the acoustic propagation characteristics of the centrifugal pump combined with the actual product has great practical value based on the theoretical analysis of the acoustic model. Even these analytical results can be applied to other related industrial products for acoustic improvement, providing some practical ideas for the low noise design of other related types of industrial machinery.

1.3.3 Computational fluid dynamics analysis of noise sources

Computational fluid dynamics (CFD) technique have been verified by many theories and experiments that can be used to predict the performance parameters of centrifugal pumps, such as the head, efficiency and power, etc. Many pump manufacturers adopt this technique to analyse the interrelationship between internal flow properties and geometric parameters and then optimize their pump products. However, the flow-dynamic behaviour to estimate the flow-dynamic noise generated in centrifugal pumps, which can then be used for noise reduction, needs further verification in numerical simulation.

So far, it has not been practical to use CFD to evaluate the pressure amplitude in an industrial piping system if taking into account the resonance conditions (Hayashi et al. 2014). The reason is that numerical solution of the fluid-dynamic noise of the

centrifugal pump needs to solve the unsteady velocity and pressure distributions of the internal flow field of the pump through the CFD code and establish the monopole, dipole and quadrupole sound sources based on the Lighthill acoustic analogy (Lighthill, 1952). Then, the boundary conditions and constraints are set up in the inlet and outlet ports of the pump and inner surface of the volute, respectively. Finally, the sound pressure values on the inlet and outlet ports of the centrifugal pump are calculated and use these parameters to characterize the fluid-dynamic noise properties of the pump (Sun et al. 2016). This numerical simulation process is very complicated. Considering the impact of the entire hydraulic piping system, the practical application methodology of the pump-piping system has not been established due to the high cost of numerical calculation.

In addition, the working medium usually is treated as an ideal fluid (incompressible and homogeneous) in these simulations, resulting in sound pressure transmission and acoustic coupling effect are not taken into consideration (Keller et al. 2014). The selections of the appropriate boundary conditions, turbulence model and pipe material properties, etc. all need to receive an accurate definition. For example, boundary conditions for infinitely long pipe or non-reflective terminations are difficult to achieve in the actual test. As a result, while this precludes the analytical determination of fluid-dynamic variables of centrifugal pumps, the prediction of the internal fluid-dynamic noise is even more difficult and the estimations are little reliable. Therefore, investigation of the acoustic properties of centrifugal pumps requires the support and validation of more detailed and accurate experimental data in hydraulic piping systems.

1.4 Objectives and methodologies intended for the present study

The noise of centrifugal pumps is unavoidable and detrimental: it not only worsens the working environment but also affects the normal operation of the equipment. In the environment outside the test system of centrifugal pumps, the noise measured by any instrument cannot directly reflect the fluid-dynamic noise inside the pump. It may come from multiple sources such as radiating noise from pipe wall vibration, valve vibration, motor vibration, external environmental noise, etc. Each of these sources of noise can interact through the fluid-structure interaction and propagate through the structural vibration to the acoustic environment, thereby becoming difficult to achieve a separation of noise sources. That is, the relationship between fluid-dynamic noise and the noise obtained by this measurement method is complex (Tao 2004). Therefore, accurately estimating and measuring the acoustic characteristics of fluid-dynamic noise in centrifugal pumps is the basic guarantee to complete the study of its noise mechanisms, verify noise reduction measures and design lower noise products.

With the changes in centrifugal pump models and changes in operating conditions, such as impeller diameter, inlet/outlet area of the impeller, blade number, volute structure, pump flow, rotational speed, etc., the main spectral components of

fluid-dynamic noise as the main noise source are bound to change accordingly. In engineering practice, it is impossible to test for each operating condition or each type of model, which is not allowed by time and manpower. This highlights the importance of mathematical models. The accurate establishment of the acoustic model in centrifugal pumps is bound to greatly improve the analysis efficiency and provide a reliable basis for the acoustic improvement. However the effective sound pressure levels induced by the pumps at a given location and frequency is not only dependent on the pump internal generation sources but on how the pipeline systems behaves to the pump acoustic excitation, i.e. on how noise is transmitted or reflected back when approaching every element of the system. This accounts for the pumps themselves. In consequence, on one hand there is a need to characterize pumps as fluid-dynamic sound sources but, on the other hand, it is also necessary to characterize them as acoustic passive elements with specific properties of sound transmission and reflection.

In practice, most of the sound energy propagating along pipelines corresponds to a frequency range low enough as to preclude transmission in acoustic modes higher than the fundamental mode of plane waves across the ducts. Under this assumption of plane wave mode transmission, pumps can be considered as linear acoustic two-port elements. This means that the sound emitted to and received from the suction and discharge pipes can be described in terms of two acoustic state variables at each pump port that are related by linear relationships involving both the source and transmission features of the pump. The source features are usually represented in a vector with two components and the transmission features are represented by a 2x2 matrix, where all the elements depend on frequency. Many scholars (To and Doige 1979, Stirnemann et al. 1987, Lavrentjev et al. 1995, Bardeleben. 2005, Yamamoto et al. 2014, Lehr et al. 2019) have verified the feasibility and correctness of determining acoustic parameters of two-port elements through experimental methods. According to the selected state parameters of the inlet and outlet ports, there are mainly two methods to describe the noise transmission characteristics of those two-port elements: the transmission matrix method and the scattering matrix method. However, though there has been a considerably high number of recent studies devoted to estimate and analyze the sound excitation sources in centrifugal pumps, there have been very few recent studies devoted to analyze their passive properties of sound reflection and transmission.

In consequence, the research of this thesis was designed to cover that gap, i.e. the main objective of the thesis was to characterize the acoustic properties of reflection and transmission of centrifugal pumps by studying and analyzing their scattering matrices or their transmission matrices. To achieve that general purpose, the following specific objectives and methodologies were considered:

1. Conduct an experimental characterization in laboratory of the scattering matrix corresponding to a conventional centrifugal pump. This requires the design and mounting of a special set-up in which the test pump can be subjected to external acoustic loads on the suction and discharge ports, as well as the capture and post-processing of pressure signals along the pipes connected to the pump. Besides,

this experimental determination of the scattering matrix should cover a range of frequencies as wide as possible.

2. Elaborate a theoretical model capable to describe the acoustic field inside centrifugal pumps when subject to low frequency ideal sound sources under the following constraints：

- consider the main geometrical parameters of the pumps as input data,

- consider the main acoustic phenomena that govern the internal sound propagation in pumps under the assumption of plane wave mode,

- produce predictions with little computational effort so that computations can easily cover a wide frequency range.

- allow estimating the scattering or transmission matrices by incorporating sound sources at the suction and discharge ports.

Based on this model, a resolution algorithm was to be elaborated and implemented in a calculation program, so that the elements of either the scattering or the transmission matrix can be computed for each pump geometry as a function of frequency.

3. Validate the theoretical model and the calculation program by contrasting predictions against the experimental data obtained for the laboratory pump.

4. Once validated, apply the calculation program on pumps with different specific speeds and geometrical parameters, especially if there are experimental data available in the technical literature for those geometries, so that general trends of geometrical dependence can be inferred.

1.5 Document structure

The chapters of this thesis document are organized as follows：

(1) An introduction to the area of noise in pump machinery, including a classification of noise sources in the pump hydraulic circulation system and the identification method of the internal noise of the centrifugal pump. The objectives and methodologies of this thesis are proposed.

(2) This chapter discusses the transmission characteristics of acoustic noise along pipelines, and the elements of the transmission and the scattering matrices between the upstream and downstream ports of the centrifugal pump are identified based on the acoustic two-port model.

(3) This chapter describes the equipment and instrumentation used in laboratory for the acquisition of hydrodynamic noise signals from a centrifugal pump. The experimental set-up includes a test pump, an auxiliary pump, a hydraulic circulation system, an operation control system and a signal acquisition system. The effects of

different piping schemes on the hydrodynamic noise induced by centrifugal pumps with constant operating conditions are tested.

(4) After introducing the classic simple model for centrifugal pumps proposed by Stirnemann et al. (1987), based on an electric analogy, this chapter presents the new acoustic model developed to estimate the elements of the transmission matrix and the scattering matrix between the upstream and downstream ports of the centrifugal pump. This includes the model hypothesis, a network of calculation nodes, the estimation of internal transfer matrices and the implementation in a calculation algorithm. Besides, the effect of several calculation parameters on the predictions is analyzed for the case of a reference pump.

(5) This chapter starts presenting the experimental results on the scattering matrix corresponding to the test pump of the current research, which are compared to the predictions of the theoretical model described in the previous chapter. Thereafter that contrast is extended to other sets of data obtained by different researchers and collected from the technical literature, which correspond to measurements on pumps with a variety of specific speeds and geometrical features. Predictions obtained from Stirnemann's classical model are also considered in the comparisons.

(6) The main conclusions of the study are summarized and some future research directions are suggested.

2 Acoustic transmission characteristics in pump hydraulic system

This chapter briefly discusses the transmission characteristics of the noise produced by acoustic source in the pipeline and introduces the identification method of signal parameters based on two-sensor measurement. A direct connection between the measurable pressure fluctuation parameters in the piping system and the parameters of the acoustic two-port model in a centrifugal pump is derived. Here these two different acoustic two-port models, which one is the pulsating pressure and mass velocity as port variables and another is the plane pressure waves in opposite directions as port variables, are adopted as the extraction method of transmission matrix parameters and scattering matrix parameters of the centrifugal pump, respectively. These models consider the coupling characteristics of the acoustic field parameters between the suction and discharge pipe under a specific hydraulic circulation system.

2.1 Acoustic sources in pipelines

Pipelines as the most basic components in the medium transmission systems are widely used in various fields. The hydraulic noise in the hydraulic piping system containing the centrifugal pump is usually associated with pressure pulsations of flow excitation.

The main ways in which acoustic source in the pipeline radiates noise towards outside are flowing medium and pipe wall. The expression of radiated noise of acoustic sources in pipeline is mainly divided into direct description and indirect description. For example, the noise intensity of the sound source in the pipeline can be indirectly reflected by measuring the vibrations of the pipe wall or measuring the noise signals of the external air environment. However, this indirect expression is not very rigorous and accurate. This is because the decomposition of the pipe wall vibration signals is a very difficult task and the measured noise signals will be affected by the external environmental noise. The direct method is to use the hydrophone or the dynamic pressure sensor, which is flush-mounted on the wall of the pipeline and contact with the transmission medium, to reflect the characteristics of the noise source in the pipeline. This method is relatively good at avoiding the influence of background noise in the external environment.

The main factors affecting the measurement accuracy of the noise intensity in the pipeline are: the separation of sound sources, the influence of the impedance at the tube end, the coupling effect of fluid-structure and the correct installation of sensors (Chen et al. 2005). Due to the presence of different types of piping components, valves, and measuring components in the pump hydraulic circulation system, therefore, fluid passing through these pipe elements produces a secondary sound

source that radiates noise along the upstream and downstream of the pipeline. At the same time, the noise generated by these secondary sources is superimposed on the flow noise generated by the centrifugal pump. When evaluating the sound source characteristics and propagation characteristics of the noise, the interference of these secondary sources must be considered. The amplitude of the sound pressure at different locations in the test pipe section is usually affected by standing waves. The installation conditions at both ends of the test pipe are different, and the acoustic impedance is also different, so that the results of measurement at different positions vary greatly. Due to the different boundary conditions of the upstream and downstream pipelines of the centrifugal pump, the impedance treatment method should be considered during the test. The pipe and its components are deformed by the action of the fluid and these deformations in turn act on the fluid. This coupling between the fluid and the mechanical structure exists along the entire pipe. If the length-to-diameter ratio of the test pipe section is large and the thickness is relatively small, this effect cannot be ignored in a centrifugal pump whose medium is water.

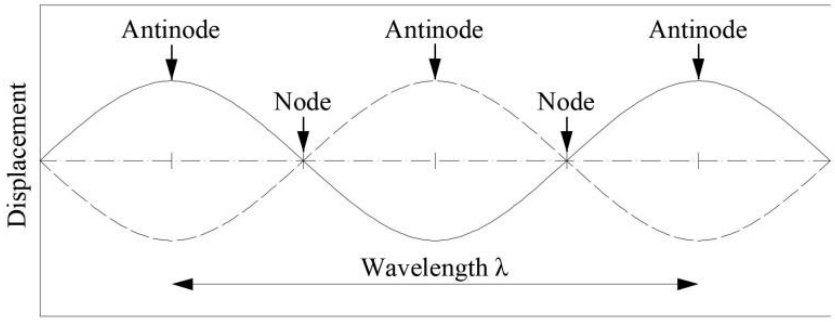

Fig. 2.1. Schematic view of standing wave in a rigid straight pipe

Therefore, if the influence of external factors on the acoustic characteristics of the acoustic source can be eliminated as much as possible during the measurement process, and then obtain the properties of the acoustic source itself, so it has great significance for the study of the acoustic wave transmission characteristics of the acoustic source along the pipeline.

2.2 Plane wave assumption and acoustic impedance

Centrifugal pump is the main noise source of the whole hydraulic system, and its fluid-dynamic excitation noise is dominated by the low frequency noise. Transmission of the sound in a fluid-filled pipeline is a very complicated problem. If the transmission medium of low frequency noise is confined to a relatively long cylindrical pipe with rigid walls, then a simple plane wave model can be employed to describe the transmission of sound waves. The sound propagates along the axial direction of the pipeline, and the axial dimension is much larger than the other two directions. Therefore, the one-dimensional acoustic theory is usually used to analyse the transmission characteristics of sound in the pipeline.

Under the assumption of plane waves, the transmission of wave energy is non-attenuating and non-dispersive. In other words, the plane wave is easily formed in the pipeline, which is not easily attenuated and can usually travel far without acoustic treatment. In the case of the plane wave, the wave front or phase surface is a plane perpendicular to the wave transmission direction, and they have the same amplitude and phase at all points.

In this study, the wavelength generated by pulsating pressure waves in the low frequency range is considerably well larger than the diameter of the suction/discharge pipes and the cross-sectional area of main components (including the impeller channel and volute casing) for all test cases. In addition, the radial inertia and viscosity of the medium are insignificant and negligible compared to their motion variables due to the slight compressibility between the fluid and the wall of the pipeline. Therefore, the proposal of one-dimensional plane wave assumption in such acoustic pressure field is necessary and reasonable to fully describe the physical features and to simplify mathematical expressions for the study of acoustic pressure waves propagating in hydraulic piping systems. Many studies have also demonstrated the justifiability and reliability of the plane wave assumption in hydraulic system applications (Lavrentjev et al. 1995, Parrondo et al. 2002, Hayashi et al. 2014, Kabral et al. 2018).

In an acoustic system transmitted along the simple pipeline, the acoustic pressure wave, are considered to be uniform plane waves propagating along a certain direction (e.g. *x*-direction), satisfies the one-dimensional wave equation as follows (Munjal 1987):

$$\frac{\partial^2 p(x,t)}{\partial x^2} - \frac{1}{c_0^2} \cdot \frac{\partial^2 p(x,t)}{\partial t^2} = 0 \tag{2.1}$$

where c_0 is the velocity of wave propagation or is known as the speed of sound, p indicates acoustic pressure. The one-dimensional acoustic theory means that the acoustic pressure field does not depend on the coordinates *y*, *z* and is only a function of the coordinate *x* and time variable *t*.

According to one-dimensional plane wave assumption, the solution of the above Eq. (2.1) can be written as:

$$p(x,t) = C_1 \cdot e^{j(\omega t - kx)} + C_2 \cdot e^{j(\omega t + kx)} \tag{2.2}$$

where $j = \sqrt{-1}$ is the imaginary unit, $\omega = 2\pi f$ denotes an angular frequency and $k = \omega / c_0$ indicates the wave number (neglect wave attenuation). For the right part of the Eq. (2.2), the first term represents the wave travelling in the positive direction, and the second term is the wave travelling in the negative direction. That is, the one-dimensional acoustic pressure $p(x,t)$ at a certain position in an acoustic piping system indicates the superposition of two plane waves travelling in opposite directions.

Meanwhile, the acoustic volume velocity u in the pipeline also applies to the above wave equation. The general solution is as follows:

$$u(x,t) = C_3 \cdot e^{j(\omega t - kx)} + C_4 \cdot e^{j(\omega t + kx)} \tag{2.3}$$

According to the dynamic equilibrium equation:

$$\rho \cdot \frac{\partial u}{\partial t} + \frac{\partial u}{\partial x} = 0 \tag{2.4}$$

Substituting Eq. (2.2) and Eq. (2.3) into the Eq. (2.4) shows that

$$C_3 = \frac{C_1}{\rho c_0}, \quad C_4 = -\frac{C_2}{\rho c_0}$$

therefore the following expression for the acoustic velocity fluctuations in the *x*-direction is obtained:

$$u(x,t) = \frac{1}{\rho c_0} \cdot [C_1 \cdot e^{j(\omega t - kx)} - C_2 \cdot e^{j(\omega t + kx)}] \tag{2.5}$$

where ρ is the fluid density. For plane wave transmission and small enough acoustic pressure variation in a certain medium, the product of $Z_0 = \rho c_0$ is defined as the specific acoustic impedance of a plane wave. C_1, C_2, C_3 and C_4 are frequency-dependent complex numbers that represent the acoustic properties of the pipeline.

For a plane wave travelling along the pipeline, the acoustic impedance Z is defined as the ratio of acoustic pressure and acoustic volume velocity,

$$Z = \frac{p}{u} = \rho c_0 \tag{2.6}$$

which describes the reflection, transmission and absorption characteristics of acoustic waves as they encounter boundaries, e.g. different media or terminals during transmission.

Based on the relationship between mass velocity v and volume velocity u,

$$v = \rho u A_S \tag{2.7}$$

Therefore, the acoustic impedance based on acoustic mass velocity Z_v in a stationary medium is

$$Z_v = \frac{p}{v} = \frac{c_0}{A_S} \tag{2.8}$$

where the variable A_S is the cross-section area of the pipeline, which varies with the diameter of the pipeline.

2.3 Identification of acoustic two-port components

Centrifugal pumps are the primary sources of pressure pulsation and flow fluctuation in a hydraulic piping system, resulting in undesired vibration and noise. Perturbations caused by these fluctuations transmit towards the piping system of the centrifugal pump at the sound speed and reflect at some components such as branch pipes or regulating valves (Keller et al. 2013).

Due to the size limitations of the centrifugal pump piping operating system, it is not possible to separately place the centrifugal pump in an acoustic laboratory for measurement using standard monitoring methods. Therefore, the acoustic characteristics of the centrifugal pump can only be accurately measured from the pipe in which it is connected to the system. However, the acoustic characteristics of the centrifugal pump sound source are directly described by the noise at a certain point in the piping system, and the results often cause significant differences in measurement results depending on the system and measurement position. This undoubtedly brings great difficulties to theoretical research and experimental measurements. Therefore, it is necessary to propose a method that can describe the characteristics of the sound source while being independent of the test system.

In the investigation of acoustic transmission for a pipeline system, the acoustic two-port model established by the experimental measurement has become a significant analytical means for plane wave regions (Åbom et al. 1991, 2011 and 2018, Carta et al. 2000, Rzentkowski et al. 2000, De Roeck et al. 2008). Acoustic two-port model is generally utilized to identify the transmission characteristics of acoustic waves in a continuous container or pipe, such as water supply and drainage pipes, filters, fans, centrifugal pumps, etc. It has the advantage of describing only the selected pipe element while independent of the acoustic impedance of the upstream and downstream sections. This makes the acoustic two-port model a practical and intuitive modelling tool for studying the acoustic properties of hydraulic systems.

Centrifugal pumps which have a piping system connected with an upstream inlet port and a downstream outlet port, which is acoustically coupled, can be depicted in the plane wave region. In this study, the geometric size of the centrifugal pump (as a noise source) is significantly smaller than the acoustic wavelength of the main noise bands and the length of the pipe that the acoustic wave propagates along the axial direction of the pipeline. Therefore, the fluid-dynamic noise source inside the centrifugal pump can be viewed virtually as a point source between the two ports of the pump inlet and outlet, and an acoustic two-port model is established based on the relationship between the acoustic state variables at the two ports. According to the selected different state parameters of the inlet and outlet, there are mainly two methods for describing the transmission characteristics of the sound source: the transmission matrix method and the scattering matrix method.

2.3.1 Pulsating pressure and mass velocity as port variables

Fig. 2.2 presents the pressure and flow fluctuations radiated by the sound source transmit towards downstream along a rigid straight pipe. The dynamic pressure sensors at different locations, separated by a distance Δl, measure the transient pressure fluctuations p_1 and p_2, respectively.

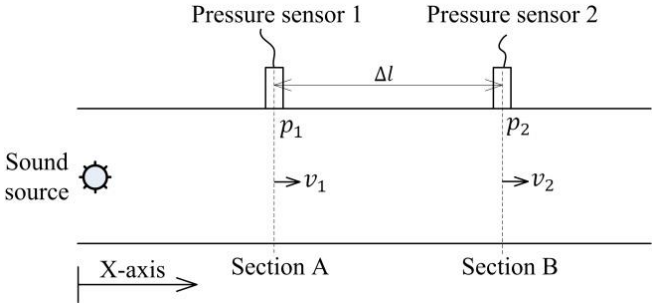

Fig. 2.2. Schematic view of plane wave transmission in a rigid straight pipe

The transmission of the plane wave in a rigid straight pipe with a constant cross section, according to the boundary conditions of Section A and Section B and combining with the above Eq. (2.2) and Eq. (2.5), the state variables of Section B can be represented by the state variables of Section A.

Assume that the position coordinate of Section A is $x = 0$, therefore, C_1 and C_2 can be obtained,

$$C_1 = \frac{p_1 + \rho c_0 v_1}{2} \tag{2.9}$$

$$C_2 = \frac{p_1 - \rho c_0 v_1}{2} \tag{2.10}$$

Then substituting the above two formulas and distance Δl into Eq. (2.2) and Eq. (2.5) based on the position coordinate $x = \Delta l$ of Section B,

$$\begin{aligned} p_2 &= \frac{p_1 + \rho c_0 v_1}{2} \cdot e^{-j \cdot k \cdot \Delta l} + \frac{p_1 - \rho c_0 v_1}{2} \cdot e^{j \cdot k \cdot \Delta l} \\ &= p_1 \cos(k \cdot \Delta l) - j \cdot \rho c_0 v_1 \cdot \sin(k \cdot \Delta l) \end{aligned} \tag{2.11}$$

$$\begin{aligned} v_2 &= \frac{1}{\rho c_0} \cdot [\frac{p_1 + \rho c_0 v_1}{2} \cdot e^{-j \cdot k \cdot \Delta l} - \frac{p_1 - \rho c_0 v_1}{2} \cdot e^{j \cdot k \cdot \Delta l}] \\ &= v_1 \cos(k \cdot \Delta l) - j \cdot \frac{p_1}{\rho c_0} \sin(k \cdot \Delta l) \end{aligned} \tag{2.12}$$

In this case, if written in matrix form, Eq. (2.11) and Eq. (2.12) can be transformed as follows,

$$\begin{bmatrix} p_2 \\ v_2 \end{bmatrix} = \begin{bmatrix} \cos(k \cdot \Delta l) & -j \cdot \rho c_0 \cdot \sin(k \cdot \Delta l) \\ -\frac{j}{\rho c_0} \cdot \sin(k \cdot \Delta l) & \cos(k \cdot \Delta l) \end{bmatrix} \cdot \begin{bmatrix} p_1 \\ v_1 \end{bmatrix} \quad (2.13)$$

The passive two-port transmission matrix **T** can be obtained by correlating the state variables pulsating pressure p and mass velocity v at the upstream section A and downstream section B.

$$[\mathbf{T}] = \begin{bmatrix} T_{11} & T_{12} \\ T_{21} & T_{22} \end{bmatrix} = \begin{bmatrix} \cos(k \cdot \Delta l) & -j \cdot \rho c_0 \cdot \sin(k \cdot \Delta l) \\ -\frac{j}{\rho c_0} \cdot \sin(k \cdot \Delta l) & \cos(k \cdot \Delta l) \end{bmatrix} \quad (2.14)$$

This transmission matrix **T** is called passive, meaning that there is no sound source between the two-port studied. It is independent of the type of pipe before or after the pipe segment. If there is an active condition between the two ports, the transmission matrix **T** will depend on the entire piping system, not just the pipe segment between section A and section B. In addition, the transmission matrix **T** is a frequency-dependent characteristic.

In practice, different components are connected together in the hydraulic piping system, for example, as shown in Fig. 2.3. If the piping system can be decomposed in different pipe segments with different cross-sectional areas (such as sudden expansion or contraction pipe connected in series), the parts with the same diameter in each pipe segment can be respectively represented by a transmission matrix which depends on its geometric parameters and port flow states. Therefore, it is essential to identify each segment and then contact them to gain the overall acoustic characteristics of the hydraulic piping system.

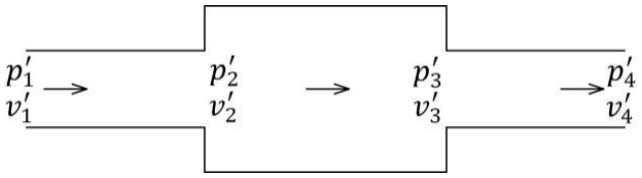

Fig. 2.3. Schematic view of plane wave transmission in a variable diameter rigid pipe

The transmission matrix of the whole system with no internal sources can be easily given by the product of the transmission matrix of each pipe segment. Expression can be represented as,

$$\begin{bmatrix} p_n \\ v_n \end{bmatrix} = \mathbf{T_1} \cdot \mathbf{T_2} \cdot \ldots \cdot \mathbf{T_{n-1}} \cdot \mathbf{T_n} \cdot \begin{bmatrix} p_1 \\ v_1 \end{bmatrix} = \prod_{i=1}^{n} \mathbf{T_i} \cdot \begin{bmatrix} p_1 \\ v_1 \end{bmatrix} \quad (2.15)$$

which describes the state variables for the upstream and downstream ports in the pipeline.

The transmission matrix method is one of the effective methods for

fluid-dynamic noise analysis in pump pipeline systems. It divides the complex fluid piping system into a finite number of interconnected units in accordance with different acoustic structures such as connecting pipes, elbow sections, valves, flow meter and the centrifugal pump. The acoustic transfer characteristics of the individual elements are represented by a matrix of features. Then multiply these matrices to obtain the acoustic transmission matrix of the whole system. Finally, the fluid-dynamic noise characteristics of the hydraulic piping system are obtained by using the acoustic boundary conditions of the two ports of the pipeline. The flow velocity of the liquid in the hydraulic pipeline system is small relative to the speed of sound and can be ignored, so the Mach number is not considered in the transmission matrix of the hydraulic pipeline system (Bardeleben 2005).

In the pipeline system, the acoustic state variables of the upstream and downstream ports of the centrifugal pump under passive conditions can be expressed by the acoustic two-port model based on acoustic pulsating pressure and acoustic mass velocity as port variables. Fig. 2.4 presents the acoustic transmission matrix representation based on port variables in an acoustic system consisting of a centrifugal pump and pipelines. The pulsating pressure values of the monitoring positions 1 to 4 can be directly measured by the pressure sensors and the corresponding acoustic mass velocity can be obtained according to Eqs. (2.11) and (2.12). Therefore, the transmission matrix elements of the centrifugal pump can be identified based on these measurement results.

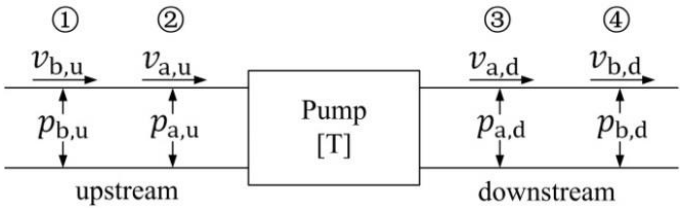

Fig. 2.4. Acoustic transmission matrix representation based on pulsating pressure and mass velocity as port variables

The upstream inputs are variables acoustic pressure $p_{a,u}$, $p_{b,u}$ and acoustic mass velocity $v_{a,u}$, $v_{b,u}$ at the different positions, downstream outputs are the corresponding variables $p_{a,d}$, $p_{b,d}$ and $v_{a,d}$, $v_{b,d}$. Define the transmission matrix of the centrifugal pump as $\mathbf{T_m}$, the correspondence relationship between the variables at positions 2 and 3 and between the acoustic variables at positions 1 and 4 can be written as a single matrix equation, respectively:

$$\begin{bmatrix} p_{a,u} \\ v_{a,u} \end{bmatrix} = [\mathbf{T_m}] \cdot \begin{bmatrix} p_{a,d} \\ v_{a,d} \end{bmatrix} \tag{2.16}$$

$$\begin{bmatrix} p_{b,u} \\ v_{b,u} \end{bmatrix} = [\mathbf{T_m}] \cdot \begin{bmatrix} p_{b,d} \\ v_{b,d} \end{bmatrix} \tag{2.17}$$

Written into the equation sets are:

$$p_{\mathrm{a,u}} = \mathrm{T}_{m11} \cdot p_{\mathrm{a,d}} + \mathrm{T}_{m12} \cdot v_{\mathrm{a,d}} \tag{2.18}$$

$$v_{\mathrm{a,u}} = \mathrm{T}_{m21} \cdot p_{\mathrm{a,d}} + \mathrm{T}_{m22} \cdot v_{\mathrm{a,d}} \tag{2.19}$$

$$p_{\mathrm{b,u}} = \mathrm{T}_{m11} \cdot p_{\mathrm{b,d}} + \mathrm{T}_{m12} \cdot v_{\mathrm{b,d}} \tag{2.20}$$

$$v_{\mathrm{b,u}} = \mathrm{T}_{m21} \cdot p_{\mathrm{b,d}} + \mathrm{T}_{m22} \cdot v_{\mathrm{b,d}} \tag{2.21}$$

According to Eq. (2.18) and Eq. (2.20), elements T_{m11} and T_{m12} in the transmission matrix of the centrifugal pump can be solved as follows:

$$\mathrm{T}_{m11} = \frac{p_{\mathrm{a,u}} \cdot v_{\mathrm{b,d}} - p_{\mathrm{b,u}} \cdot v_{\mathrm{a,d}}}{p_{\mathrm{a,d}} \cdot v_{\mathrm{b,d}} - v_{\mathrm{a,d}} \cdot p_{\mathrm{b,d}}} \tag{2.22}$$

$$\mathrm{T}_{m12} = \frac{p_{\mathrm{a,u}} \cdot p_{\mathrm{b,d}} - p_{\mathrm{a,d}} \cdot p_{\mathrm{b,u}}}{v_{\mathrm{a,d}} \cdot p_{\mathrm{b,d}} - p_{\mathrm{a,d}} \cdot v_{\mathrm{b,d}}} \tag{2.23}$$

Similarly, elements T_{m21} and T_{m22} can be calculated according to Eq. (2.19) and Eq. (2.21):

$$\mathrm{T}_{m21} = \frac{v_{\mathrm{a,u}} \cdot v_{\mathrm{b,d}} - v_{\mathrm{a,d}} \cdot v_{\mathrm{b,u}}}{p_{\mathrm{a,d}} \cdot v_{\mathrm{b,d}} - v_{\mathrm{a,d}} \cdot p_{\mathrm{b,d}}} \tag{2.24}$$

$$\mathrm{T}_{m22} = \frac{v_{\mathrm{a,u}} \cdot p_{\mathrm{b,d}} - p_{\mathrm{a,d}} \cdot v_{\mathrm{b,u}}}{v_{\mathrm{a,d}} \cdot p_{\mathrm{b,d}} - p_{\mathrm{a,d}} \cdot v_{\mathrm{b,d}}} \tag{2.25}$$

2.3.2 Plane wave decomposition method

Because of the reflective characteristics of hydraulic components and ports, the plane wave decomposition method based on multi-sensor identification technique has adopted and verified experimentally in many fluid machine fields (e.g. fan and centrifugal pump, Lavrentjev et al. 1995 and 1996, Rzentkowski et al. 2000, Garnell et al. 2019) to establish an acoustic two-port model and analyse source-load interaction effects within the frequency range of plane wave transmission.

Fig. 2.5 presents a schematic view of a pipe section with two pressure sensors and plane pressure waves travelling in opposite directions. At the left side of the pipe an ideal sound source is radiating plane pressure waves while the right side of the pipe has an equivalent acoustic impedance Z_{R}. The flush-mounted dynamic pressure sensors at positions x_1 and x_2, separated by a distance Δl, measure the transient pressure fluctuations $p_1(x,t)$ and $p_2(x,t)$, respectively. The superscript "+" and "−" denote pressure wave transmission along the positive and negative *x*-direction, that is, the radiated component and the returning component of the sound source.

The amplitudes p^+, p^- and phases φ^+, φ^- of each plane pressure wave must satisfy the following relationships for each frequency:

$$p_1(x,t) = p^+ \cdot e^{j(\omega t - k x_1 + \varphi^+)} + p^- \cdot e^{j(\omega t + k x_1 + \varphi^-)} \tag{2.26}$$

$$p_2(x,t) = p^+ \cdot e^{j(\omega t - kx_2 + \varphi^+)} + p^- \cdot e^{j(\omega t + kx_2 + \varphi^-)} \tag{2.27}$$

$$\Delta l = x_2 - x_1 \tag{2.28}$$

The incident and reflected pressure wave amplitudes p^+ and p^- can be calculated using Eq. (2.26) and Eq. (2.27). The results are as follows

$$p^+ = \frac{p_1(x,t) \cdot e^{j(\omega t + kx_2 + \varphi^-)} - p_2(x,t) \cdot e^{j(\omega t + kx_1 + \varphi^-)}}{e^{j(2\omega t + k\cdot\Delta l + \varphi^+ + \varphi^-)} - e^{j(2\omega t - k\cdot\Delta l + \varphi^+ + \varphi^-)}} \tag{2.29}$$

$$p^- = \frac{p_1(x,t) \cdot e^{j(\omega t - kx_2 + \varphi^+)} - p_2(x,t) \cdot e^{j(\omega t - kx_1 + \varphi^+)}}{e^{j(2\omega t - k\cdot\Delta l + \varphi^+ + \varphi^-)} - e^{j(2\omega t + k\cdot\Delta l + \varphi^+ + \varphi^-)}} \tag{2.30}$$

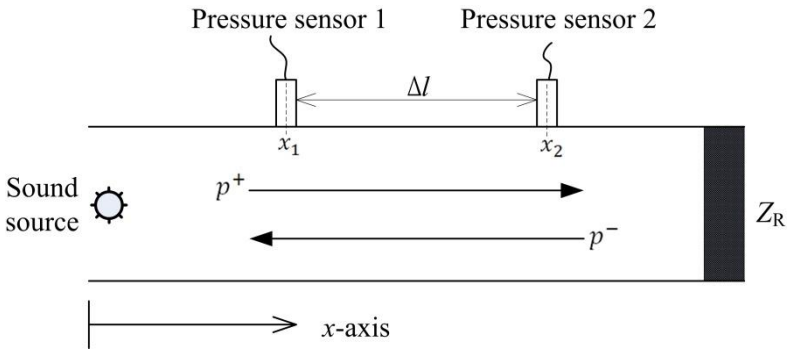

Fig. 2.5. Schematic view of the plane wave decomposition method based on multi-sensor identification technique

The pressure waves travelling in opposite directions so obtained result from the acoustic interaction between the external sound source and the piping system and so they are different when modifying the acoustic impedance Z_R (boundary condition) at the right side of the pipe in case the sound source remains unchanged. In addition, different plane wave pressure amplitudes can also be obtained by using the different acoustic loads for the external sound source (external excitation source). It is worth noting that the incident sound wave and the reflected sound wave in the pipeline can be decomposed by the plane wave decomposition technique through the experimental measurement of the multi-sensor, but the characteristics of the sound source (including sound source intensity and transmission characteristics) cannot be described by means of the travelling wave from the direction of the sound source.

The ratio between the reflected wave and the incident wave is defined as the reflection coefficient. The range of its value varies between zero and one. The magnitude of the reflection coefficient indicates the amount of reflection of the acoustic energy at the pipe termination. When the boundary condition of the pipe termination is a rigid wall (total reflection port), all of the incident sound waves are reflected back, that is, the termination does not have any sound absorption capability, and the reflection coefficient reaches a maximum value of one. In contrary, when the

pipe termination is an infinitely long pipe or sound-absorbing wall, the reflection coefficient is a minimum value of zero. This boundary condition is named non-reflective boundary condition. All sound pressure waves propagate perfectly through such boundary.

2.3.3 Plane pressure waves in opposite directions as port variables

The scattering matrix is a common method to characterize the acoustic two-port characteristics of centrifugal pumps, which describes the linear relationship between the pressure variables at the upstream inlet and downstream outlet ports in the frequency range of plane wave transmission. The major advantage of using the scattering matrix is that the acoustic properties of the component to be detected in the two-port model are independent of the other components of the system.

Fig. 2.6 presents a scheme of a centrifugal pump considered as a linear acoustic two-port model with two state variables at each port: the entering (radiated) and exiting (returning) pressure waves (p^+ and p^-) at the suction and discharge pipes. To determine the elements of the scattering matrix of the centrifugal pump through the experimental measurement, two pairs of highly sensitive pressure sensors separated by distances Δl_1 and Δl_2 were installed at the suction and discharge pipes of pump, respectively. Based on the above approaches, plane pressure waves travelling in opposite directions as port variables are adopted to identify the scattering matrix **S** of the centrifugal pump. The relation between those state variables is given by the so-called scattering matrix **S** in the frequency domain when the sound source is external and the centrifugal pump is at a standstill, defined as:

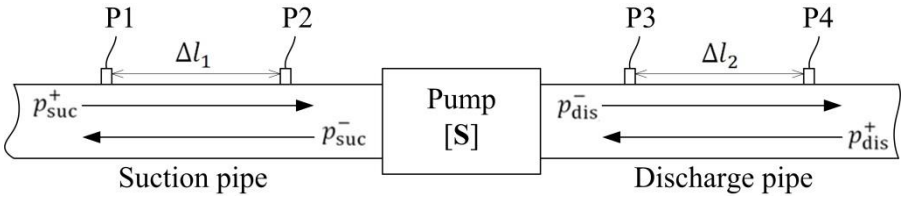

Fig. 2.6. Acoustic system of the composition based on two plane pressure waves in opposite directions

$$\begin{bmatrix} p^-_{\mathrm{suc}} \\ p^-_{\mathrm{dis}} \end{bmatrix} = [\mathbf{S}] \cdot \begin{bmatrix} p^+_{\mathrm{suc}} \\ p^+_{\mathrm{dis}} \end{bmatrix} = \begin{bmatrix} \mathrm{S}_{11} & \mathrm{S}_{21} \\ \mathrm{S}_{12} & \mathrm{S}_{22} \end{bmatrix} \cdot \begin{bmatrix} p^+_{\mathrm{suc}} \\ p^+_{\mathrm{dis}} \end{bmatrix} \tag{2.31}$$

where S_{11} and S_{22} represent the reflection coefficients of pump inlet and outlet ports respectively, S_{12} and S_{21} are the transmission coefficients of pump inlet and outlet ports respectively. These elements of scattering matrix are complex functions of the frequency.

According to the Eq. (2.31), the exiting pressure wave p^-_{suc} at the suction pipe of the centrifugal pump is the result of a linear superposition ($\mathrm{S}_{11} \cdot p^+_{\mathrm{suc}} + \mathrm{S}_{21} \cdot p^+_{\mathrm{dis}}$) of two plane acoustic wave components. When the entering wave p^+_{suc} transmitted to

the inlet port of the centrifugal pump, a part of it is reflected to form a pressure wave $S_{11} \cdot p_{\mathrm{suc}}^{+}$ due to the change of impedance. At the outlet port of the centrifugal pump, a portion of the entering wave p_{dis}^{+} is transmitted to the inlet port of the centrifugal pump and forms the sound pressure wave $S_{21} \cdot p_{\mathrm{dis}}^{+}$. Similarly, the exiting pressure wave p_{dis}^{-} at the discharge pipe of the centrifugal pump is also a linear superposition of two acoustic components $S_{12} \cdot p_{\mathrm{suc}}^{+}$ and $S_{22} \cdot p_{\mathrm{dis}}^{+}$. If the incident coefficient S_{12} and S_{21} equating to zero, there is no coupling relationship at the inlet and outlet ports of the centrifugal pump.

The signals obtained at different acoustic boundary conditions or different external excitation acoustic loads were processed by using Eq. (2.31) resulting in a large set of experimental data on travelling pressure waves under different frequencies. However, the elements of the scattering matrix are expected to remain constant for a given frequency, i.e., each single set of experimental data should verify Eq. (2.32) and Eq. (2.33). Therefore, the systematic application of Eq. (2.32) and Eq. (2.33) to all the *N* data groups results in two large systems of *N* independent equations, each with just two unknowns: the two elements of either the first or the second line of *S*.

$$p_{\mathrm{suc},j}^{-} = S_{11} p_{\mathrm{suc},j}^{+} + S_{21} p_{\mathrm{dis},j}^{+} \qquad (j = 1 \ldots N) \tag{2.32}$$

$$p_{\mathrm{dis},j}^{-} = S_{12} p_{\mathrm{suc},j}^{+} + S_{22} p_{\mathrm{dis},j}^{+} \qquad (j = 1 \ldots N) \tag{2.33}$$

where the subscripts “suc" and “dis” refer to the plane waves travelling along the suction and discharge pipes of the pump, respectively.

To reduce the influence of fluid-dynamic pressure fluctuations and to minimize experimental measurement errors, these two overdetermined systems of *N* independent equations can be solved by means of a least square error procedure, so that the errors E_1 and E_2 as defined by Eq. (2.34) and Eq. (2.35) become minima:

$$E_1 = \sum_{\mathrm{j}=1}^{\mathrm{N}} (S_{11} p_{\mathrm{suc},j}^{+} + S_{21} p_{\mathrm{dis},j}^{+} - p_{\mathrm{suc},j}^{-})^2 \tag{2.34}$$

$$\begin{aligned} \frac{\partial E_1}{\partial S_{11,\mathrm{r}}} = 2\{ & S_{11,\mathrm{r}} \cdot \sum_{j=1}^{\mathrm{N}} [(p_{\mathrm{suc},j,\mathrm{r}}^{+})^2 + (p_{\mathrm{suc},j,\mathrm{i}}^{+})^2] + S_{21,\mathrm{r}} \cdot \sum_{j=1}^{\mathrm{N}} (p_{\mathrm{dis},j,\mathrm{r}}^{+} \cdot p_{\mathrm{suc},j,\mathrm{r}}^{+} + \\ & p_{\mathrm{dis},j,\mathrm{i}}^{+} \cdot p_{\mathrm{suc},j,\mathrm{i}}^{+}) + S_{21,\mathrm{i}} \cdot \sum_{j=1}^{\mathrm{N}} (-p_{\mathrm{dis},j,\mathrm{i}}^{+} \cdot p_{\mathrm{suc},j,\mathrm{r}}^{+} + p_{\mathrm{dis},j,\mathrm{r}}^{+} \cdot p_{\mathrm{suc},j,\mathrm{i}}^{+}) + \\ & \sum_{j=1}^{\mathrm{N}} (-p_{\mathrm{suc},j,\mathrm{r}}^{-} \cdot p_{\mathrm{suc},j,\mathrm{r}}^{+} - p_{\mathrm{suc},j,i}^{-} \cdot p_{\mathrm{suc},j,\mathrm{i}}^{+})\} = 0 \end{aligned}$$

$$\frac{\partial E_1}{\partial S_{11,\mathrm{i}}} = 2\{S_{11,\mathrm{i}} \cdot \sum_{j=1}^{\mathrm{N}} [(p_{\mathrm{suc},j,\mathrm{r}}^{+})^2 + (p_{\mathrm{suc},j,\mathrm{i}}^{+})^2] + S_{21,\mathrm{r}} \cdot \sum_{j=1}^{\mathrm{N}} (-p_{\mathrm{dis},j,\mathrm{r}}^{+} \cdot p_{\mathrm{suc},j,\mathrm{i}}^{+} +$$

$$p^+_{\mathrm{dis},j,\mathrm{i}} \cdot p^+_{\mathrm{suc},j,\mathrm{r}}) + \mathrm{S}_{21,\mathrm{i}} \cdot \sum_{j=1}^{\mathrm{N}} (p^+_{\mathrm{dis},j,\mathrm{i}} \cdot p^+_{\mathrm{suc},j,\mathrm{i}} + p^+_{\mathrm{dis},j,\mathrm{r}} \cdot p^+_{\mathrm{suc},j,\mathrm{r}}) +$$

$$\sum_{j=1}^{\mathrm{N}} (p^-_{\mathrm{suc},j,\mathrm{r}} \cdot p^+_{\mathrm{suc},j,\mathrm{i}} - p^-_{\mathrm{suc},j,\mathrm{i}} \cdot p^+_{\mathrm{suc},j,\mathrm{r}})\} = 0$$

$$\frac{\partial E_1}{\partial \mathrm{S}_{21,\mathrm{r}}} = 2\{\mathrm{S}_{11,\mathrm{r}} \cdot \sum_{j=1}^{\mathrm{N}} (p^+_{\mathrm{suc},j,\mathrm{r}} \cdot p^+_{\mathrm{dis},j,\mathrm{r}} + p^+_{\mathrm{suc},j,\mathrm{i}} \cdot p^+_{\mathrm{dis},j,\mathrm{i}}) +$$

$$\mathrm{S}_{11,\mathrm{i}} \cdot \sum_{j=1}^{\mathrm{N}} (-p^+_{\mathrm{suc},j,\mathrm{i}} \cdot p^+_{\mathrm{dis},j,\mathrm{r}} + p^+_{\mathrm{suc},j,\mathrm{r}} \cdot p^+_{\mathrm{dis},j,\mathrm{i}}) + \mathrm{S}_{21,\mathrm{r}} \cdot \sum_{j=1}^{\mathrm{N}} [\left(p^+_{\mathrm{dis},j,\mathrm{r}}\right)^2 +$$

$$(p^+_{\mathrm{dis},j,\mathrm{i}})^2] + \sum_{j=1}^{\mathrm{N}} (-p^-_{\mathrm{suc},j,\mathrm{r}} \cdot p^+_{\mathrm{dis},j,\mathrm{r}} - p^-_{\mathrm{suc},j,\mathrm{i}} \cdot p^+_{\mathrm{dis},j,\mathrm{i}})\} = 0$$

$$\frac{\partial E_1}{\partial \mathrm{S}_{21,\mathrm{i}}} = 2\{\mathrm{S}_{11,\mathrm{r}} \cdot \sum_{j=1}^{\mathrm{N}} (-p^+_{\mathrm{suc},j,\mathrm{r}} \cdot p^+_{\mathrm{dis},j,\mathrm{i}} + p^+_{\mathrm{suc},j,\mathrm{i}} \cdot p^+_{\mathrm{dis},j,\mathrm{r}}) +$$

$$\mathrm{S}_{11,\mathrm{i}} \cdot \sum_{j=1}^{\mathrm{N}} (p^+_{\mathrm{suc},j,\mathrm{i}} \cdot p^+_{\mathrm{dis},j,\mathrm{i}} + p^+_{\mathrm{suc},j,\mathrm{r}} \cdot p^+_{\mathrm{dis},j,\mathrm{r}}) + \mathrm{S}_{21,\mathrm{i}} \cdot \sum_{j=1}^{\mathrm{N}} [\left(p^+_{\mathrm{dis},j,\mathrm{r}}\right)^2 +$$

$$\left(p^+_{\mathrm{dis},j,\mathrm{i}}\right)^2] + \sum_{j=1}^{\mathrm{N}} (p^-_{\mathrm{suc},j,\mathrm{r}} \cdot p^+_{\mathrm{dis},j,\mathrm{i}} - p^-_{\mathrm{suc},j,\mathrm{i}} \cdot p^+_{\mathrm{dis},j,\mathrm{r}})\} = 0$$

$$E_2 = \sum_{j=1}^{N} (\mathrm{S}_{12} p^+_{\mathrm{suc},j} + \mathrm{S}_{22} p^+_{\mathrm{dis},j} - p^-_{\mathrm{dis},j})^2 \tag{2.35}$$

$$\frac{\partial E_2}{\partial \mathrm{S}_{12,\mathrm{r}}} = 2\left\{\mathrm{S}_{12,\mathrm{r}} \cdot \sum_{j=1}^{\mathrm{N}} [\left(p^+_{\mathrm{suc},j,\mathrm{r}}\right)^2 + \left(p^+_{\mathrm{suc},j,\mathrm{i}}\right)^2\right] + \mathrm{S}_{22,\mathrm{r}} \cdot \sum_{j=1}^{\mathrm{N}} (p^+_{\mathrm{dis},j,\mathrm{r}} \cdot p^+_{\mathrm{suc},j,\mathrm{r}} +$$

$$p^+_{\mathrm{dis},j,\mathrm{i}} \cdot p^+_{\mathrm{suc},j,\mathrm{i}}) + \mathrm{S}_{22,\mathrm{i}} \cdot \sum_{j=1}^{\mathrm{N}} (-p^+_{\mathrm{dis},j,\mathrm{i}} \cdot p^+_{\mathrm{suc},j,\mathrm{r}} + p^+_{\mathrm{dis},j,\mathrm{r}} \cdot p^+_{\mathrm{suc},j,\mathrm{i}}) +$$

$$\sum_{j=1}^{\mathrm{N}} (-p^-_{\mathrm{dis},j,\mathrm{r}} \cdot p^+_{\mathrm{suc},j,\mathrm{r}} - p^-_{\mathrm{dis},j,i} \cdot p^+_{\mathrm{suc},j,\mathrm{i}})\} = 0$$

$$\frac{\partial E_2}{\partial \mathrm{S}_{12,\mathrm{i}}} = 2\{\mathrm{S}_{12,\mathrm{i}} \cdot \sum_{j=1}^{\mathrm{N}} [(p^+_{\mathrm{suc},j,\mathrm{r}})^2 + (p^+_{\mathrm{suc},j,\mathrm{i}})^2] + \mathrm{S}_{22,\mathrm{r}} \cdot \sum_{j=1}^{\mathrm{N}} (-p^+_{\mathrm{dis},j,\mathrm{r}} \cdot p^+_{\mathrm{suc},j,\mathrm{i}} +$$

$$p^+_{\mathrm{dis},j,\mathrm{i}} \cdot p^+_{\mathrm{suc},j,\mathrm{r}}) + \mathrm{S}_{22,\mathrm{i}} \cdot \sum_{j=1}^{\mathrm{N}} (p^+_{\mathrm{dis},j,\mathrm{i}} \cdot p^+_{\mathrm{suc},j,\mathrm{i}} + p^+_{\mathrm{dis},j,\mathrm{r}} \cdot p^+_{\mathrm{suc},j,\mathrm{r}}) +$$

$$\sum_{j=1}^{\mathrm{N}}(p_{\mathrm{dis},j,\mathrm{r}}^{-}\cdot p_{\mathrm{suc},j,\mathrm{i}}^{+}-p_{\mathrm{dis},j,\mathrm{i}}^{-}\cdot p_{\mathrm{suc},j,\mathrm{r}}^{+})\}=0$$

$$\frac{\partial E_2}{\partial \mathrm{S}_{22,\mathrm{r}}}=2\{\mathrm{S}_{12,\mathrm{r}}\cdot\sum_{j=1}^{\mathrm{N}}(p_{\mathrm{suc},j,\mathrm{r}}^{+}\cdot p_{\mathrm{dis},j,\mathrm{r}}^{+}+p_{\mathrm{suc},j,\mathrm{i}}^{+}\cdot p_{\mathrm{dis},j,\mathrm{i}}^{+})+\mathrm{S}_{12,\mathrm{i}}\cdot\sum_{j=1}^{\mathrm{N}}(-p_{\mathrm{suc},j,\mathrm{i}}^{+}\cdot p_{\mathrm{dis},j,\mathrm{r}}^{+}+p_{\mathrm{suc},j,\mathrm{r}}^{+}\cdot p_{\mathrm{dis},j,\mathrm{i}}^{+})+\mathrm{S}_{22,\mathrm{r}}\cdot\sum_{j=1}^{\mathrm{N}}[\left(p_{\mathrm{dis},j,\mathrm{r}}^{+}\right)^{2}+\left(p_{\mathrm{dis},j,\mathrm{i}}^{+}\right)^{2}]+\sum_{j=1}^{\mathrm{N}}(-p_{\mathrm{dis},j,\mathrm{r}}^{-}\cdot p_{\mathrm{dis},j,\mathrm{r}}^{+}-p_{\mathrm{dis},j,\mathrm{i}}^{-}\cdot p_{\mathrm{dis},j,\mathrm{i}}^{+})\}=0$$

$$\frac{\partial E_2}{\partial \mathrm{S}_{22,\mathrm{i}}}=2\{\mathrm{S}_{12,\mathrm{r}}\cdot\sum_{j=1}^{\mathrm{N}}(-p_{\mathrm{suc},j,\mathrm{r}}^{+}\cdot p_{\mathrm{dis},j,\mathrm{i}}^{+}+p_{\mathrm{suc},j,\mathrm{i}}^{+}\cdot p_{\mathrm{dis},j,\mathrm{r}}^{+})+\mathrm{S}_{12,\mathrm{i}}\cdot\sum_{j=1}^{\mathrm{N}}(p_{\mathrm{suc},j,\mathrm{i}}^{+}\cdot p_{\mathrm{dis},j,\mathrm{i}}^{+}+p_{\mathrm{suc},j,\mathrm{r}}^{+}\cdot p_{\mathrm{dis},j,\mathrm{r}}^{+})+\mathrm{S}_{22,\mathrm{i}}\cdot\sum_{j=1}^{\mathrm{N}}[\left(p_{\mathrm{dis},j,\mathrm{r}}^{+}\right)^{2}+\left(p_{\mathrm{dis},j,\mathrm{i}}^{+}\right)^{2}]+\sum_{j=1}^{\mathrm{N}}(p_{\mathrm{dis},j,\mathrm{r}}^{-}\cdot p_{\mathrm{dis},j,\mathrm{i}}^{+}-p_{\mathrm{dis},j,\mathrm{i}}^{-}\cdot p_{\mathrm{dis},j,\mathrm{r}}^{+})\}=0$$

where *i* and *r* denote imaginary part and real part of the physical variables, respectively.

To detect the solved elements of the scattering matrix and reduce the possible influence of the error, the determination coefficient R^2 is proposed. R^2 is a key output of regression analysis to evaluating the degree of compliance between the sound pressure predicted and actual values in this study. The value of determination coefficient ranges from 0 to 1, the closer to one the better fitting. The higher the R^2 coefficient can be considered satisfactory. Expressed as follows:

$$R^2=1-\frac{C_{res}}{C_{tot}} \tag{3.36}$$

where C_{res} is the sum of squares of residuals, C_{tot} is the total sum of squares. For the both overdetermined systems equation sets Eq. (2.34) and Eq. (2.35), the elements $C_{res(1)}, C_{tot(1)}$ and $C_{res(2)}, C_{tot(2)}$ are calculated as follows:

$$C_{res(1)}=\sum_{j=1}^{N}[p_{suc,j}^{-}-(S_{11}\cdot p_{suc,j}^{+}+S_{21}\cdot p_{dis,j}^{+})]^2 \tag{3.37}$$

$$C_{tot(1)}=\sum_{j=1}^{N}(p_{suc,j}^{-}-\frac{\sum_{j=1}^{N}p_{suc,j}^{-}}{N})^2 \tag{3.38}$$

$$C_{res(2)} = \sum_{j=1}^{N} [p_{dis,j}^{-} - (S_{12} \cdot p_{suc,j}^{+} + S_{22} \cdot p_{dis,j}^{+})]^2 \tag{3.39}$$

$$C_{tot(2)} = \sum_{j=1}^{N} (p_{dis,j}^{-} - \frac{\sum_{j=1}^{N} p_{dis,j}^{-}}{N})^2 \tag{3.40}$$

By solving the R^2 obtained, the elements of the scattering matrix that satisfy the requirements are selected for further analysis.

3 Experimental instruments and equipment

3.1 Pump facilities

In order to obtain the scattering matrix parameters of the test pump through the experimental method, the experimental analysis in this paper will use the auxiliary pump as the external sound source of the test pump. That is, the auxiliary pump is in the same pipeline system as the test pump, and the noise generated during the operation of the auxiliary pump is transmitted to the test pump through the pipeline. This is because the auxiliary pump, which could generate the different pressure pulsation amplitudes at the different shaft frequency and blade passing frequency (including their harmonics) by altering rotational speed, was used as an external sound source. The specific test operation will be described in detail in the following chapter.

3.1.1 Auxiliary pump

The auxiliary pump is a conventional single-stage single-suction centrifugal pump, which is mainly composed of an impeller with seven blades, a spiral volute and variable-frequency motor. The photograph of the auxiliary pump is shown in Fig. 3.1. During the experiment, the operating conditions of the auxiliary pump can be changed by adjusting the valve of the discharge pipeline and the frequency of the motor.

Fig. 3.1. Photograph of the auxiliary pump

3.1.2 Test pump

The test pump is a conventional single-stage single-suction centrifugal pump with seven 3D backward swept blades, a spiral volute and variable-frequency motor.

The shaft frequency of impeller is $f_S=n/60$ Hz and the blade passing frequency is $f_B=Z\times n/60$ Hz in which n represents the rotational speed of the impeller and Z is the number of blades. The detail geometric parameters of test pump are listed in Table 3.1. The photographs of the impeller and volute are shown in Fig. 3.2.

Table 3.1. The main geometry parameters of the test pump

Items	Value
Radius at impeller inlet, r_1 [mm]	28.5
Radius at impeller outlet, r_2 [mm]	105
Width at impeller outlet, b_2 [mm]	16
Number of blades, z_B	7
Outlet angle relative to tangent, β_2 [deg]	26
Radius at tongue tip, r_3 [mm]	116
Blade thickness at trailing edge, δ [mm]	7
Cross-sectional area at narrow side of the tongue, A_0 [cm^2]	11.3
Cross-sectional area at wide side of the tongue, $A_{2\pi}$ [cm^2]	34.6
Volute width, b_3 [mm]	40
Volute throttle cross-section, A_T [cm^2]	20
Length suction port to impeller eye, L_{SE} [mm]	90
Length throttle to discharge port, L_{TD} [mm]	240
Diameter of suction port, d_S [mm]	100
Diameter of discharge port, d_D [mm]	65
Non-dimensional specific speed, $n_s=Q^{0.5}/(gH)^{0.75}$	0.46

(a) Test pump (b) Impeller and volute casing (Barrio et al, 2010)

Fig. 3.2. Photograph of the test pump

3.2 Overview of the open test system

The conventional centrifugal pump is a kind of machinery with simple structure and is widely used in many fields to transfer various different media. However, the flow state inside the pump is very complicated three-dimensional unsteady turbulence. So far, the fluid-dynamic properties of centrifugal pump cannot be completely determined by means of analytically method, and the fluid-dynamic noise is more complicated (Ni et al. 2018, Zhang et al. 2019). Therefore, the test analysis is still an important means to investigate the fluid-dynamic noise of centrifugal pump. The fluid-dynamic excitation noise is main internal sound source of model pump in the water circulatory system formed together by the centrifugal pump and external ducts. According to acoustic theory (Munjal, 1987 and 2014) and previous research results (Parrondo et al. 2011), a test system capable of measuring the sound source characteristics of fluid-dynamic excitation noise in model pump was established, and the test pump researched in the present study was installed in the laboratory of the Department of Energy at the University of Oviedo.

Flow excitation noise test system of centrifugal pump is mainly composed of hydraulic circulatory system, operational control system and signal acquisition system. The mutual relationship of each system is shown in the Fig. 3.3.

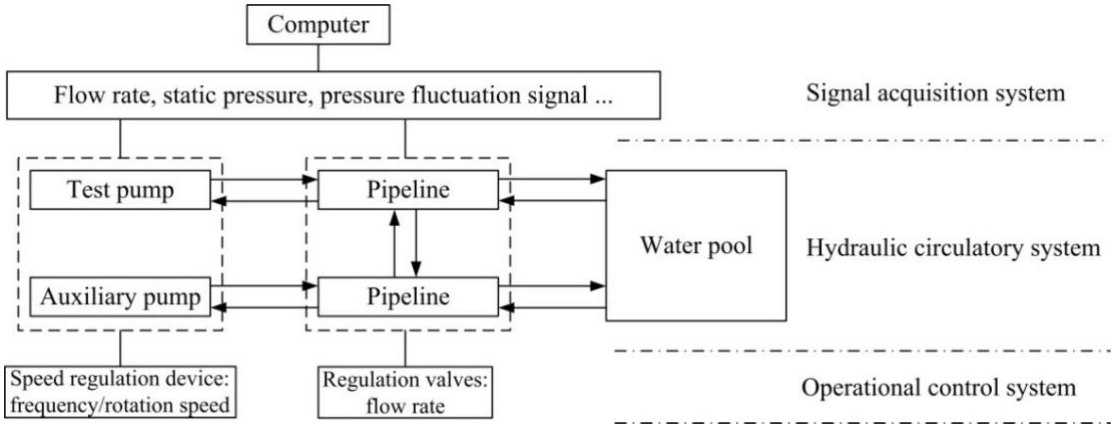

Fig. 3.3. Schematic view of the relationship between systems

3.2.1 Hydraulic circulatory system

The hydraulic circulatory system, as a testing platform for the study of fluid-dynamic excitation noise in centrifugal pump, is mainly composed of test pump, auxiliary pump, several pipelines, electromagnetic flow meter and water pool. The details of test rig are shown in Fig. 3.4. Both centrifugal pumps have variable-frequency drives to regulate their rotational speed based on needs.

During the operation of the hydraulic system, the operating conditions of the centrifugal pump need to be changed according to the experimental requirements.

Thus it requires the monitoring instrument to quantitatively display this change. An electromagnetic flowmeter (Krohne IFC 090) manufactured by the Krohne Group was installed to measure the water flow rate in the hydraulic circulatory system, as shown in Fig. 3.5. It can obtain steady and precise measurement results with steady or pulsating flows. The maximum measuring error is less than 0.5% of the measured value.

Fig. 3.4. Photograph of the hydraulic circulatory system

Fig. 3.5. Photograph of the electromagnetic flow meter

3.2.2 Operational control system

Operational control system is mainly composed of regulation valves and variable-frequency drive of a centrifugal pump. During the experiment, there are two ways to change operating conditions of centrifugal pumps: one is to control the opening degree of the regulation valve, and another is to alter the rotational speed of pump by means of variable-frequency drive. For the performance characteristics of centrifugal

pump, performance parameters (e.g. flow rate, head, efficiency…) were recorded by changing the operating conditions of regulation valve.

3.2.3 Signal acquisition system

External noise interference is an important source of measurement error, and its influence on measurement accuracy can not be ignored, especially in the case of weak signals. In the monitoring process of the signal, it is usually desirable that the sensitivity of the sensor is as high as possible. Because higher sensitivity means that the sensor is capable of perceiving the smaller amount of change, that is, the sensor has a larger output when the measured signal changes slightly. Meanwhile, it should be considered that when the sensitivity is higher, the external interference unrelated to the measurement signal is more easily to be mixed, thereby being amplified by the amplification device. At this time, it is necessary to consider that the sensor is able to detect small magnitude changes and to resist external interference. Therefore, it is often required that the signal-to-noise ratio of the sensor is as high as possible in the signal monitoring process, that is, the sensor itself is required to have low noise and is not easy to introduce interference from the outside.

To satisfy the experimental requirements for measuring the dynamic pressure signals of monitor points of centrifugal pump, fast response piezoelectric pressure sensors (model Type 701A) with high sensitivity (approximately -80 pC/bar) and with high signal-to-noise ratio manufactured by the Kistler Instrument Corp were adopted for the experiments. This sensor used to collect the sound pressure signal have the following characteristics: small size, wide frequency response range, wide dynamic range, low noise, omnidirectional response, relatively stable amplitude and phase. In addition, it has good dynamic pressure measurement capability and is capable of generating a charge signal proportional to the pulsating pressure by using the piezoelectric effect of the piezoelectric material. The linearity and hysteresis of the sensors were smaller than ±0.5%. The working field is 0~2.5 bar and the operating temperature range is -150~200 ℃. This pressure sensor was installed into the adapter through a mounting nut which was flush mounted on the internal surface of volute and piping system, as presented in Fig. 3.6.

(a) Photo of pressure sensor

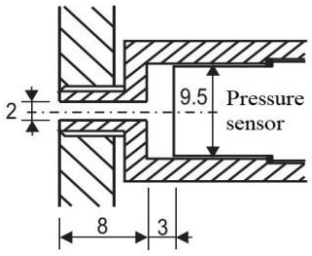

(b) Schematic view of pressure sensor casing (unites in mm) (J Keller, 2014)

Fig. 3.6. Fast response piezoelectric pressure sensor

In order to minimize the measurement error, the pressure sensor needs to be calibrated before measuring the dynamic pressure of the fluid in the pipeline. Based on the experimental measurement of the scattering matrix of the centrifugal pump, this research needs to arrange two piezoelectric pressure sensors at each suction pipe and discharge pipe of the centrifugal pump. Therefore, the arrangement method shown in Fig. 3.7 can be used to calibrate the pressure sensors. In the measurement process, if the amplitude and phase of the four pressure sensors are approximately the same, then these sensors can be considered usable. Otherwise, the test needs to replace the pressure sensor or use a corresponding pressure calibrator to calibrate the pressure sensor.

Based on highly sensitive piezoelectric pressure sensors and charge amplifiers, the expected accuracy (according to the manufacturer) is $<\pm 2\%$. The four pressure sensors are arranged on the same pipe cross-section in the radial direction. The calibration check obtained according to the test shows that the amplitude difference is less than 2% of the average value and the phase difference is less than 3 degrees of the average value. This satisfies the requirement that the sensors will be used for subsequent further tests.

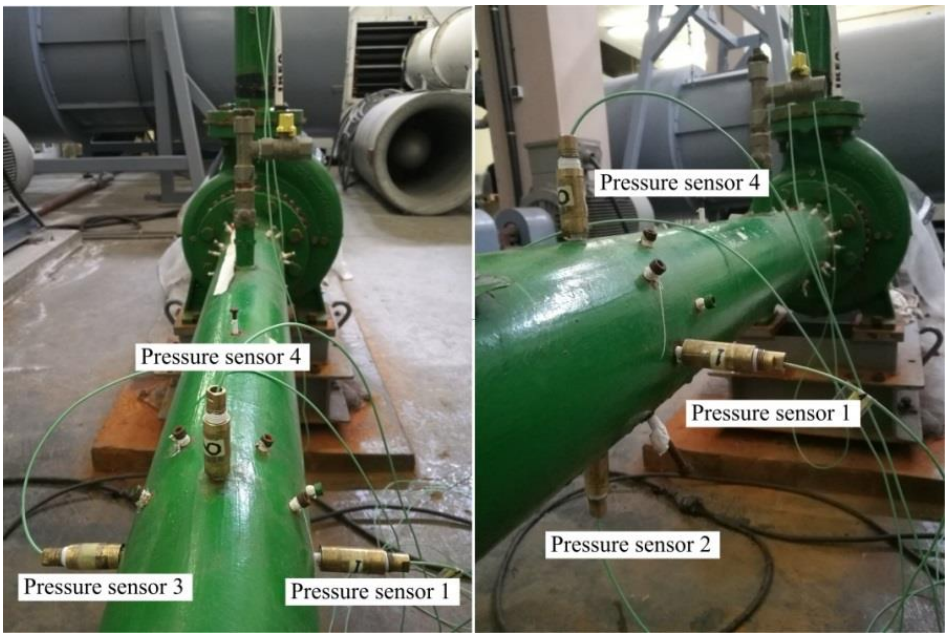

Fig. 3.7. Calibration of fast response piezoelectric pressure sensors

The fluid-dynamic noise of the centrifugal pump, which is mainly concerned with its low and medium frequency noise, is the main noise source in the hydraulic circulation system. To effectively avoid relatively large attenuation of the signal in low-frequency bands, the single-channel charge amplifier (Type 5018A, see Fig. 3.8) was employed for signal conditioning of each piezoelectric pressure sensor. The charge signals from the different measuring points into corresponding output signals were converted by means of the charge amplifier.

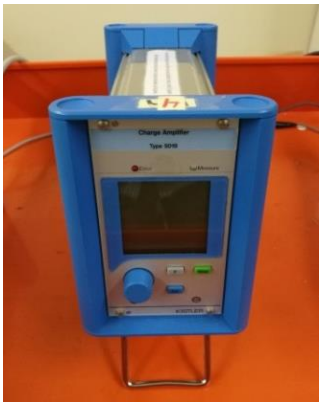

Fig. 3.8. Photograph of the charge amplifier

Table 3.2. Technical data of the charge amplifier Type 5018A

Specification	Value	Unit
Measuring range	±2 ... 2200000	pC
Frequency response	0 ... 200000	Hz
Output voltage	±2 ... ±10	V
Output current	2	mA
Accuracy	< ±0.5% ... < ±3%	/
Operating temp. range	0 ... 50	℃
Power	115/230 VAC	/

The data acquisition system mainly includes two parts: hardware and software, as shown in Fig. 3.9 and Fig. 3.10. The hardware part is the data acquisition channel, which is connected to the computer through the network cable and completes the data transmission. The software part is a data acquisition and processing module, which can display the collected data in real-time and complete the analysis and graphic processing of the data.

Fig. 3.9. Photograph of the measurement-hardware of data acquisition system

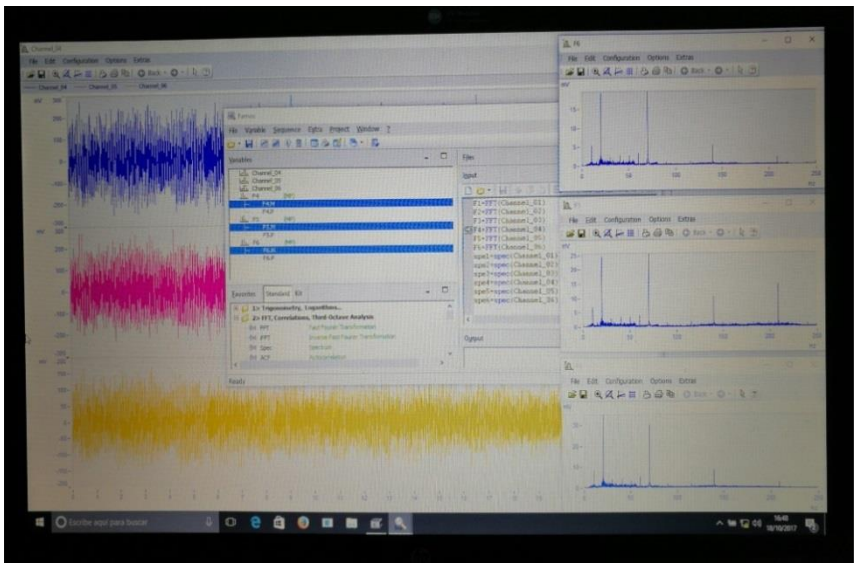

Fig. 3.10. Photograph of the measurement-software of data acquisition system

The portable collector of IMC in Germany is used for data acquisition, data pretreatment, and data transmission. IMC offers high-quality measurement-hardware (imc CRONOS-PL2) and measurement-software (imc FAMOS, namely Fast Analysis and Monitoring of Signals) for data acquisition solutions. This system has good sampling stability and strong anti-interference ability, and can monitor and process the sampled-data in real-time.

Measurement-hardware imc CRONOS-PL2 provides direct connection to multiple types of sensors and features powerful multi-channel data acquisition. It can ensure that each channel can be sampled simultaneously and performing analog-to-digital conversion simultaneously. In addition, it can collect the monitored signals in parallel and continuously, and has the characteristics of simple operation, high speed and high precision. Measurement-software imc FAMOS is a multi-channel signal acquisition and real-time analysis software based on the Windows operating system. It is able to process data recorded using an imc system and existing in the FAMOS data file format. The control analysis software matched with the digital acquisition not only has the regular data post-processing function but also can perform real-time online analysis and display of data. For example, this software provides a wide range of signal data processing functions, including FFT, spectrum analysis, waveform editing, digital filtering, etc.

3.3 Acoustic coupling effect in hydraulic piping system

For the single-stage single-suction centrifugal pumps, the pressure pulsation at the blade passing frequency, which can be attributed to the intermittent interaction between the impeller blades and the volute tongue, is the main excitation for the fluid-dynamic noise. In a hydraulic circulatory system consisting of centrifugal pump and pipelines, the fluid-dynamic noise propagates along the pipelines and is bound to

be affected by the pipe ports and other connection parts during the operation of the pump system. Therefore, the fluid-dynamic noise induced in a centrifugal pump need to take into account the impact of the system and can only be tested in the piping system during the process of conducting a test. In this section a test rig was carried out to determine the coupling effect of the different hydraulic piping systems on the pressure pulsations of the different monitor points in a centrifugal pump.

3.3.1 Test instrumentation and piping scheme configurations

The centrifugal pump, with a vaneless volute casing and an impeller of seven 3D backward swept blades, was chosen for this experiment. A schematic view describing the distribution of monitor points and the layout of experimental instrumentations is shown in Fig. 3.11. For these tests, three piezoelectric pressure sensors P_1~ P_3 (Kistler 701A) were flush-mounted on the wall of the centrifugal pump to capture the transient change of pressure fluctuation signals in different monitor positions. The monitor point P_1 was located at the volute casing and not far from the tongue region. The monitor points P_2 and P_3 were set up at the discharge pipe of the pump respectively, in which P_2 was closer to the outlet port of the pump. The transient pressure signal from each piezoelectric sensor was transmitted to the corresponding the charge amplifier (Kistler type 5018), then these signals were output through the processing and recording of the multi-channel device (IMC Cronos-PL2).

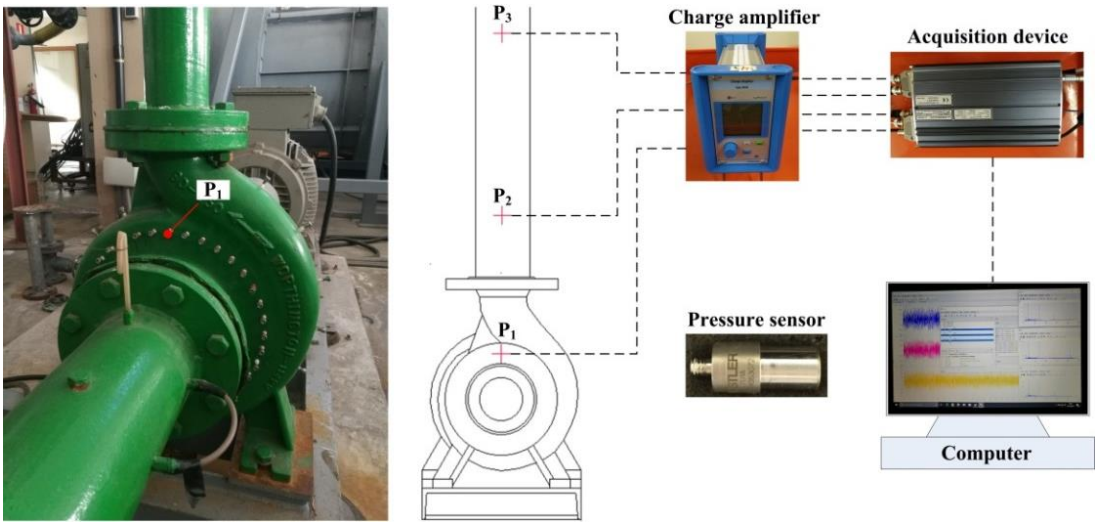

Fig. 3.11. Distribution of the monitor points and layout of the experimental instrumentations

Through the regulation of the different valve combinations, three different discharge piping schemes connected with the pump outlet were proposed in Fig. 3.12. The purpose of adopting different discharge piping schemes was to modify the acoustic boundary condition (namely acoustic impedance) of the port of the pump outlet.

For Scheme 1, the water flowing out from the pump outlet was only discharged from discharge pipe 1, that is, the valves 1, 2 and 3 were open and valve 4 was shut off. For Scheme 2, the valves 1, 2, 4 and 5 were open and the valves 3 and 6 were closed. For Scheme 3, the suction pipe of the pump and discharge pipe 3 formed a closed loop hydraulic piping system.

During the test, the rotational speed of the pump was operated to 900 rpm by means of a variable-frequency drive and only valves 3, 5 and 7 were used to regulate flow rate of the pump in different discharge piping configurations. To obtain a manifest pressure pulsation excitation, the flow rate of the centrifugal pump was operated to a very low flow rate (Q=9 m^3/h) capable of producing relatively high pressure pulsation at its blade passing frequency.

To ensure the consistency of the operational conditions between different test schemes, the rotational speed of the pump, flow rate, inlet and out pressure of the pump, valve opening of the circulatory piping system always remained unchanged under three different discharge piping schemes. In addition, the accuracies of the pressure sensors have been checked and calibrated before starting the experiments.

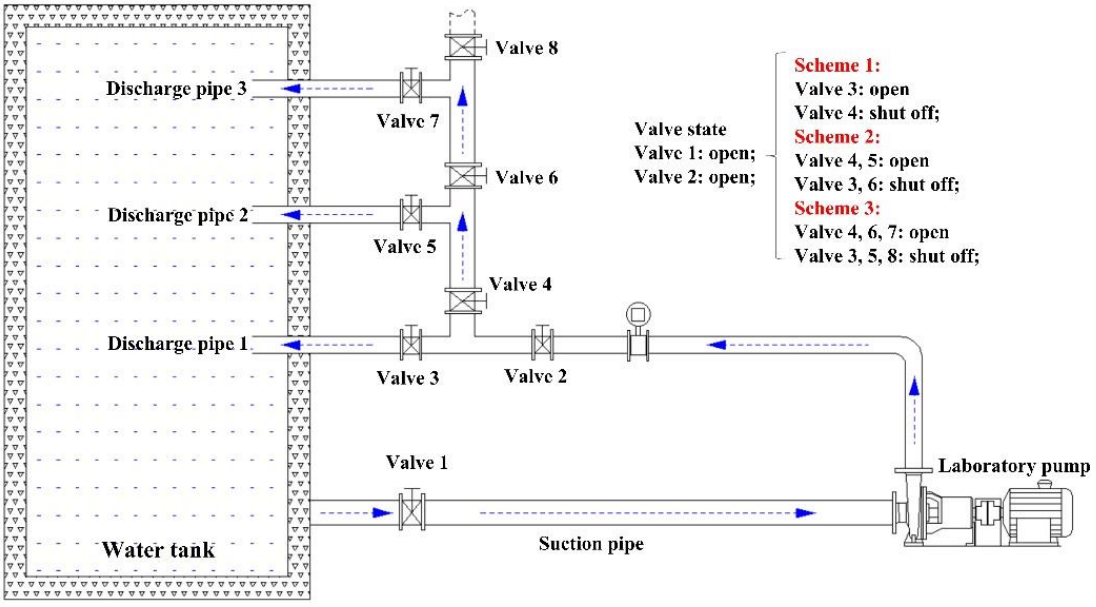

Fig. 3.12. Schematic view of the test rig for three different discharge piping schemes

3.3.2 Pressure pulsation comparison for three discharge piping schemes

Since the time domain of pressure fluctuation signal induced by the fluid-dynamic excitation just directly reflect a visualized pressure variation mode, more thorough information should be further received through the frequency-spectrum determination. For instance, noise reduction need to find the

sound source through the frequency domain, thereby performing the intervention during the process of sound generation, propagation and acceptance. In other words, the intensity of the specific frequency component is enhanced or weakened to achieve the objective of noise reduction.

In this section, frequency-spectrum analysis was carried out by means of the fast Fourier transform algorithm to account for variations of the pressure pulsations. In order to make the discrete signal obtained after continuous signal sampling can guarantee the main characteristics of the original signal, neither distortion nor interference, it is necessary to select a suitable sampling frequency. If the sampling frequency is set too low, the discrete time domain signal may not be able to reflect the waveform characteristics of the original continuous signal, causing frequency aliasing (once the signal is aliased, it cannot be separated and the original waveform cannot be reproduced.). If the sampling frequency is set too high, this means that excessive discrete data is collected for a certain long time waveform, which requires the large storage space and increases the operation time. In practical applications, the sampling frequency must be larger than the highest useful frequency of the signal. The main frequency of internal pressure pulsation and fluid-dynamic noise of the centrifugal pump is generally low-frequency noise. In order to fulfill the periodic requirements and avoid the aliasing and leakage errors as much as possible, pressure fluctuation signals were processed with the Hanning window function.

In order to verify the repeatability and reliability of the test results, the measurements of the experimental data were duplicated three times in the centrifugal pump for three different discharge piping schemes. Fig. 3.13 showed the amplitude variation of pressure pulsation at different monitor points for three discharge piping schemes. As expected, the variation of pressure pulsations is obvious due to the influence of the coupling between hydraulic piping system and fluid-dynamic excitation induced in the pump. Furthermore, the pressure pulsation at predominant frequency gradually decreases as the monitor point moving away from the tongue region of the volute.

For a more intuitive display of pressure amplitudes, the values and the average values of pressure pulsations obtained at the shaft frequency (f_S) and blade passing frequency (f_B) for the three sets of tests are shown in Table 1 and Table 2, respectively. The amplitudes of P_1 at f_S and f_B show a slight change while the variations of the other two monitor points are more intense under three different discharge piping schemes. The maximum deviations of the pressure pulsations at different monitor points even exceeded 20% at the blade passing frequency. This indicates that the monitor point close to the excitation source of the fluid-dynamic noise could be subject to a weak coupling relative to other two monitor points far from the volute tongue. That is, the monitor point away from the main excitation source is more susceptible to the influence of system coupling. Therefore, the direct measurement method of pressure pulsation in the pipeline of the pump does not directly reflect the acoustic properties of the pump itself. Due to the coupling effect of system, it might be even seriously misleading in some situations.

(a)

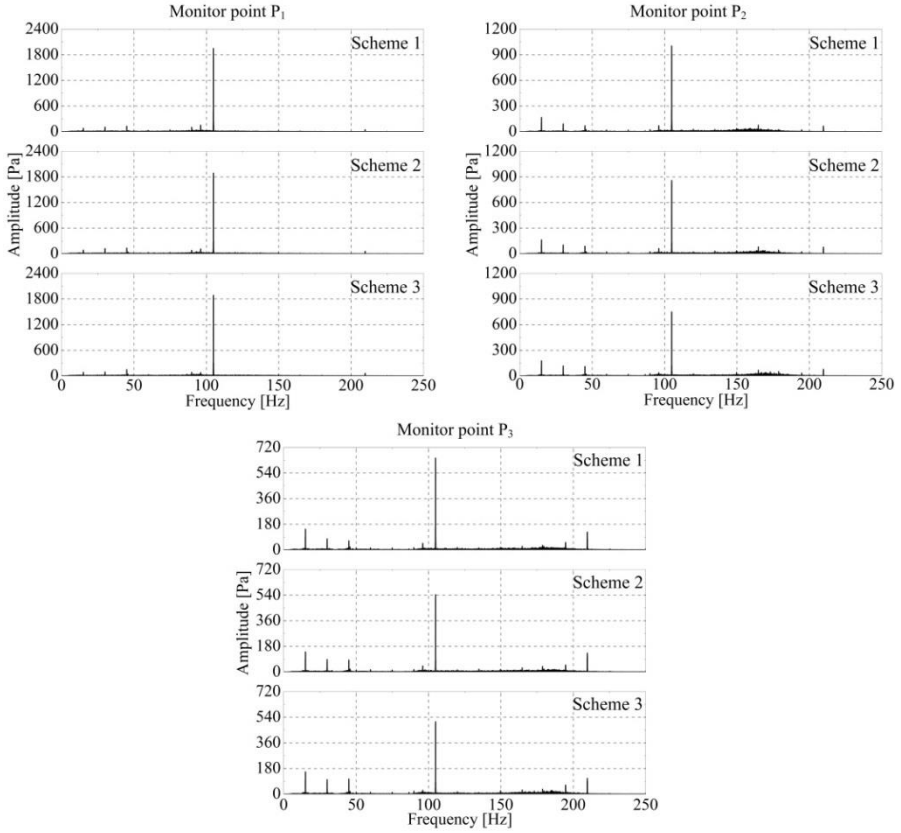
Monitor point P1
Monitor point P2
Monitor point P3
Scheme 1
Scheme 2
Scheme 3
Amplitude [Pa]
Frequency [Hz]

(b)

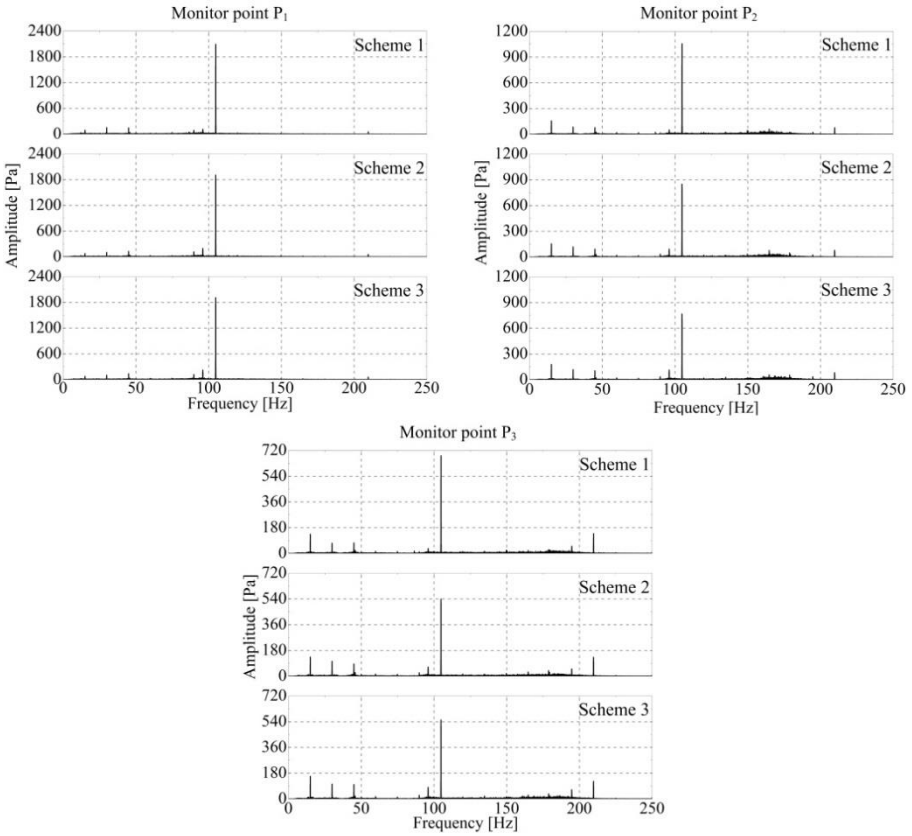
Monitor point P1
Monitor point P2
Monitor point P3
Scheme 1
Scheme 2
Scheme 3
Amplitude [Pa]
Frequency [Hz]

(c)

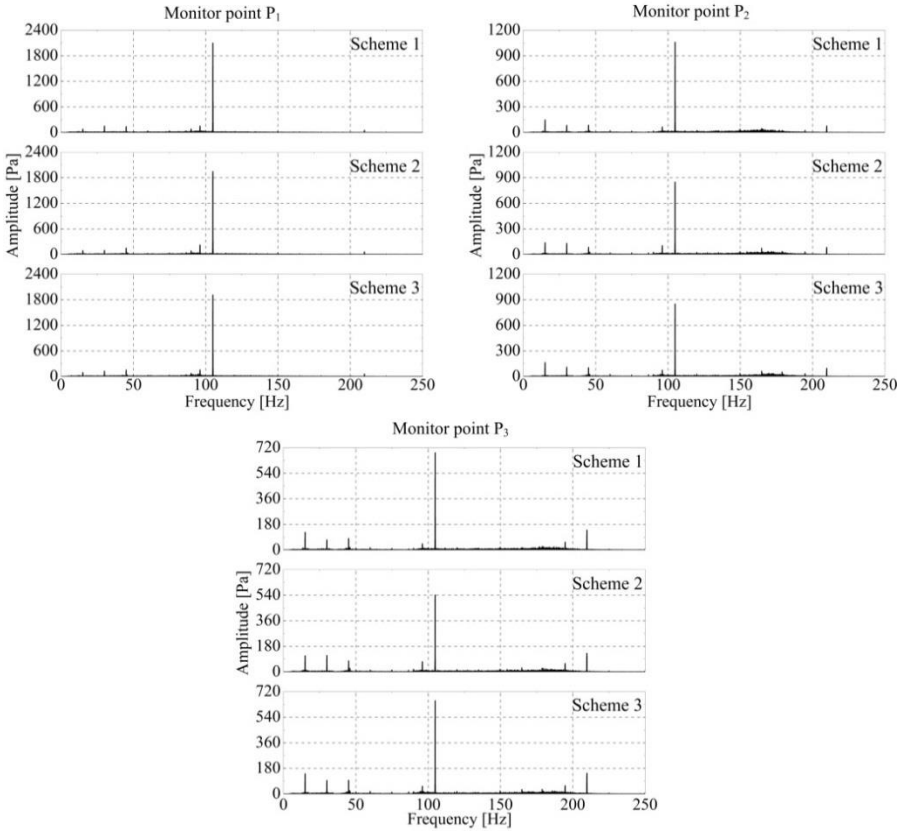

Fig. 3.13. The pressure pulsations of monitor points under three discharge piping schemes; (a) First test; (b) Second test; (c) Third test.

Table 3.3. Three sets of experimental data for three discharge piping schemes

Test/Scheme \ Point		Shaft frequency			Blade passing frequency		
		P_1 [Pa]	P_2 [Pa]	P_3 [Pa]	P_1 [Pa]	P_2 [Pa]	P_3 [Pa]
First Test	Scheme 1	82.8	166.4	145.5	1947.2	1003.4	644.7
	Scheme 2	86.3	163	140.7	1889.5	857.6	542.9
	Scheme 3	82.8	176.5	156.3	1889.3	749.9	508.4
Second Test	Scheme 1	89.5	156.6	133.8	2093.9	1055.3	683.2
	Scheme 2	76.9	154.2	134.2	1904.9	848.1	538.7
	Scheme 3	75.4	178.3	158.1	1910.7	767.6	552.8
Third Test	Scheme 1	80.4	146.8	124.2	2094.3	1057.6	683.7
	Scheme 2	88.8	138.1	113.3	1943.4	848.2	540.9
	Scheme 3	87.2	163.4	142.5	1910.3	849.8	655.5

Table 3.4. The average of three sets of experimental data for three piping schemes

Scheme \ Point	Shaft frequency			Blade passing frequency		
	P_1 [Pa]	P_2 [Pa]	P_3 [Pa]	P_1 [Pa]	P_2 [Pa]	P_3 [Pa]
Scheme 1	84.2	156.6	134.5	2045.1	1038.8	670.5
Scheme 2	84.0	151.8	129.4	1912.6	851.3	540.8
Scheme 3	81.8	172.7	152.3	1903.4	789.1	572.2

4 Acoustic model development

In order to estimate the transmission matrix, Stirnemann et al. (1987) used an electrical analogy to represent the pump as a series impedance Z_2, which connects the suction and discharge ports of the pump, plus two parallel admittances, Y_1 and Y_3, one at each port (Fig. 4.1).

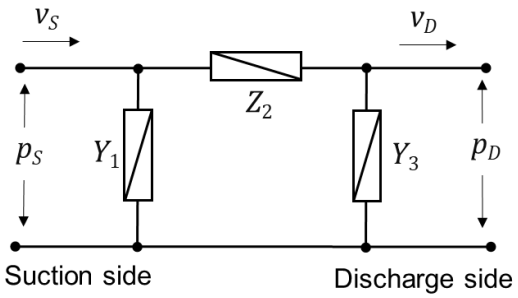

Fig. 4.1. Electrical analogy for pumps (Stirnemann et al. 1987)

According to that analogy, the transmission matrix **T** results to be:

$$\mathbf{T} = \begin{bmatrix} 1 + Z_2\, Y_3 & Z_2 \\ Y_1 + Y_3 + Y_1\, Z_2\, Y_3 & 1 + Z_2\, Y_1 \end{bmatrix} \tag{4.1}$$

Equation (4.1) gained some general use though the choice for the equivalent electrical parameters was not clear and varied among researchers. Rzentkowski and Zbroja (2000) suggested the following estimates for Y_1, Z_2 and Y_3:

$$\begin{cases} Z_2 = -g\dfrac{\partial H}{\partial Q} + i \cdot \omega \dfrac{V_{IMP}}{A_P^2} \\ Y_1 = Y_3 = i \cdot \omega \dfrac{V_{PUMP}}{2c^2} \end{cases} \tag{4.2}$$

where $\partial H/\partial Q$ represents the slope of the pump characteristic curve, V_{IMP} and V_{PUMP} are the volumes of the impeller and pump respectively and A_P is the average of the pump eye section and the throat section. However, they only recommended the application of that model for a low range of frequency. In general the order of magnitude of the entries T_{11} and T_{22} is 1, T_{12} is very large and T_{21} is very low. Despite this, Bardeleben and Weaver (2002), who conducted extensive tests on a laboratory pump, remarked the importance of not neglecting the entry T_{21} in order to improve the predictions of the scattering matrix. However, their experimental data exhibited a large dispersion and the study was not conclusive.

Indeed, obtaining reliable experimental data for the transmission or scattering matrices of pumps has proved to be a difficult task, due to the distorting effects of the pump induced noise, flow turbulence and pipe vibration. They can be partially circumvented by taking measurements with redundant sensors (Carta et al. 2000,

Bardeleben et al. 2002, Han et al. 2003), but even at pump-off conditions the results can be affected by trapped air bubbles or casing compliance (Carta et al. 2000 and 2002). Therefore, this paper designs a novel acoustic model, which aims to reproduce the internal sound distribution of centrifugal pumps under the presence of internal or external sources. This model can be used to determine the transmission matrix or the scattering matrix of a given pump.

4.1 Acoustic model design process

This research focuses on conventional centrifugal pumps with a shrouded impeller that can rotate in a vaneless volute casing (Fig. 4.2). The impeller takes the fluid in the axial direction from the suction port of the pump and drives it to the radial direction through passage channels defined by blades and shrouds. Around the impeller, the exiting fluid is collected by the volute, which has an increasing cross-section from a minimum (at tongue) until the throat. Then flow continues along a curved diffuser, until the discharge port of the pump.

There is substantial evidence from a number of previous experimental studies that the passive acoustic properties at low frequency noise for non-cavitating centrifugal pumps are little affected by the operating point (Bardeleben et al. 2002) or the rotation speed, up to the point of advising to conduct tests with pumps off (Carta et al. 2000 and 2002, Han et al. 2003). Hence, for the present study it was considered a non-rotating impeller with no flow across the pump.

For this pump model, the volute casing is represented as a chamber that is short in the axial direction, with most of the central part being occupied by the impeller. In that chamber, sound is assumed to propagate in plane wave mode along the volute (i.e. in the circumferential direction), while receiving and transmitting sound to the impeller channels. The exit of each impeller channel plus the throttle are considered as side ports of the volute chamber, allocated along the circular direction. The model assumes that the internal sound field can be reasonably described by establishing a network with a few nodes and transfer matrices that connect nodes of neighboring regions. In particular, the sound exchange between impeller channels and volute is assumed to take place only at one specific location or region for each impeller channel.

The regions considered inside the pump are (Fig. 4.2): pump inlet, impeller eye, volute sections next to the exit of each impeller channel, tongue-throttle zone and pump outlet. For instance, a pump with a 7-blade impeller would have 11 regions, labeled R_0 to R_{10} in Fig. 4.2. In case of assuming internal sound sources in the pump, another region should be assigned to each of them. The latter, however, is beyond the scope of this study, since the purpose is to check the capability of the model to estimate the passive acoustic properties in terms of transmission or scattering matrices. In consequence any sound source shall be external and sound is assumed to enter the pump only through the suction and discharge ports.

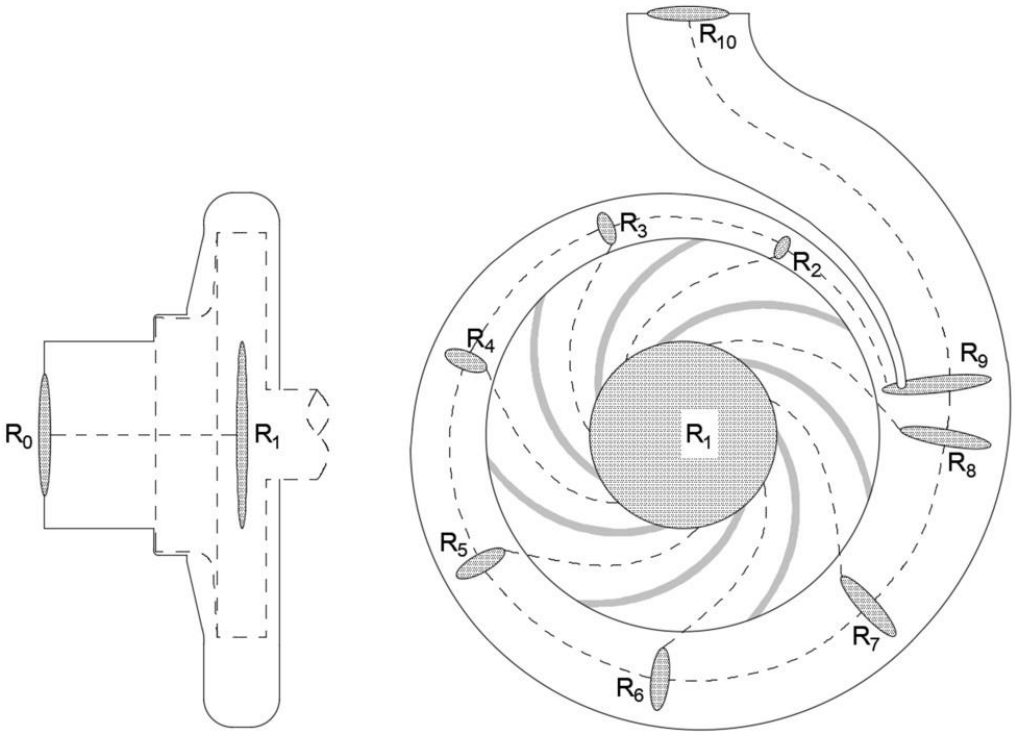

Fig. 4.2. Pump reference regions to characterize the internal sound transmission.

In this system, each region R_i contains one or more nodes n_{im}, which are positions with some local value of acoustic pressure p_{im} and acoustic mass flow velocity v_{im}. In particular, each region contains one node for every other connected region, as follows:

- Pump inlet region (R_0 in Fig. 4.2): one single node n_{00}, facing the impeller eye.
- Impeller eye region (R_1): one central node n_{10} facing the pump inlet, plus another z_B nodes, each at the inlet of an impeller channel (Fig. 4.3(a)).
- Regions along the volute: one node at the outlet of the corresponding impeller channel plus two other nodes facing the previous and subsequent volute regions (Fig. 4.3(b)).
- Tongue-throttle region (R_9 in Fig. 4.2): it has three nodes as well, two of them at both sides of the impeller-tongue gap facing the volute neighboring regions and the third one at the pump throttle facing the impeller outlet region (Fig. 4.3(c)).
- Pump outlet region (R_{10}): one single node (n_{100} for z_B =7) facing the throttle.

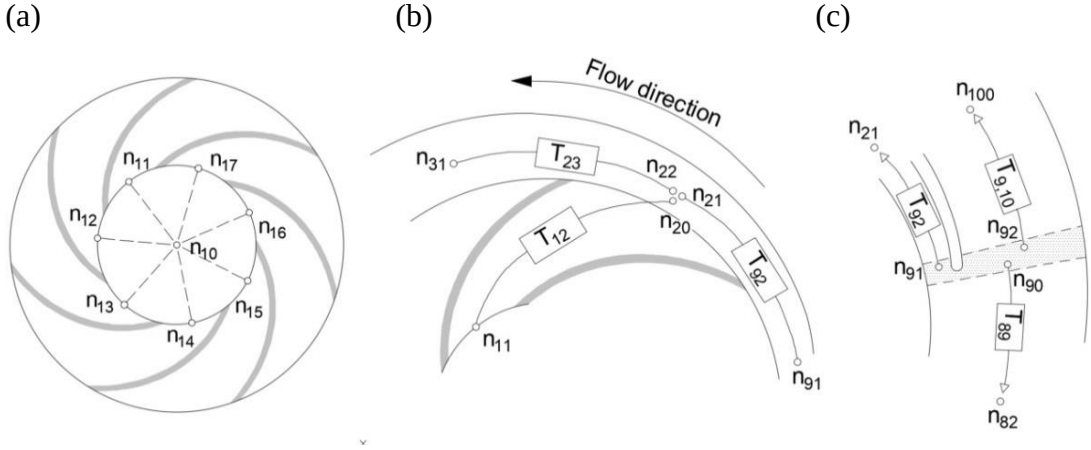

Fig. 4.3. Nodes at the impeller eye region (a), volute region (b) and tongue region (c).

Together, there would be 34 nodes for a pump with z_B= 7 blades, like the one shown in Fig. 4.2. The acoustic pressure p_{im} and mass flow velocity v_{im} at the nodes n_{im} of any internal region R_{i} are considered to verify:

- Uniform acoustic pressure:

$$p_{i0} = p_{i1} = \cdots = \mathrm{p_{im}} \tag{4.3}$$

- Mass flow continuity:

$$\sum_{m} v_{im} = 0 \tag{4.4}$$

In the case of the pump inlet and outlet regions, special boundary conditions are to be imposed depending on the external acoustic load applied on the pump.

Every node n_{im} in the domain, located in region R_{i}, must be connected to another node n_{jn} of a neighboring region R_{j} by means of a specific transfer matrix $\mathbf{T_{ij}}$ so that:

$$\begin{bmatrix} p_{im} \\ v_{im} \end{bmatrix} = \mathbf{T_{ij}} \begin{bmatrix} p_{jn} \\ v_{jn} \end{bmatrix} = \begin{bmatrix} T_{ij11} & T_{ij12} \\ T_{ij21} & T_{ij22} \end{bmatrix} \begin{bmatrix} p_{jn} \\ v_{jn} \end{bmatrix} \tag{4.5}$$

In order to determine these transfer matrices, it was assumed that the respective sound paths between connected nodes are equivalent to ducts with a cross-section that varies linearly from one end to the other. Each transfer matrix was calculated by means of a segmentation method with the *matrizant* approach (Mimani and Munjal 2010), which consists in (Fig. 4.4):

- i) divide each duct in *N* thin slices,

- ii) assign the transfer matrix to each slice as would correspond to an exponentially shaped duct with appropriate values of cross-section at the two sides depending on the slice position, and
- iii) multiply sequentially the transfer matrices of the *N* slices.

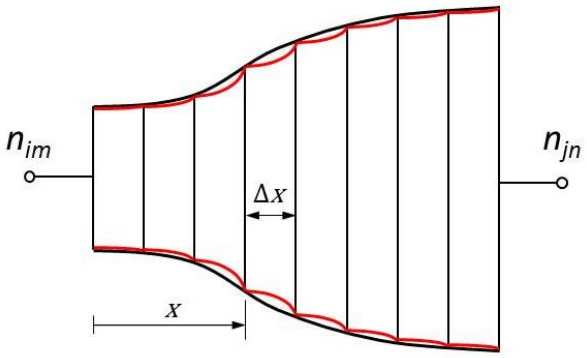

Fig. 4.4. Passage between two nodes n_{im} and n_{jn} as a succession of slices with cross-section varying exponentially.

For a slice of thickness Δx that starts at the longitudinal coordinate x and has an exponential shape between the known cross-sections $A(x)$ and $A(x+\Delta x)$, the transfer matrix can be defined as (Munjal 2014):

$$\begin{bmatrix} p_x \\ v_x \end{bmatrix} = \mathbf{T}_{S(x)} \begin{bmatrix} p_{x+\Delta x} \\ v_{x+\Delta x} \end{bmatrix} =$$

$$= \begin{bmatrix} e^{h\Delta x}\left(\cos\alpha - \dfrac{s}{k'}\sin\alpha\right) & j\, y_0\, e^{-h\Delta x}\, \dfrac{k_0}{k'}\sin\alpha \\ \dfrac{j}{y_0}\, e^{h\Delta x}\, \dfrac{k_0}{k'}\sin\alpha & e^{-h\Delta x}\left(\cos\alpha + \dfrac{s}{k'}\sin\alpha\right) \end{bmatrix} \begin{bmatrix} p_{x+\Delta x} \\ v_{x+\Delta x} \end{bmatrix} \tag{4.6}$$

where k_0 is the wave number at position x, $y_0 = c_0/A(x)$ is the characteristic impedance and:

$$h = \frac{1}{\Delta x}\ln\frac{A(x+\Delta x)}{A(x)} \tag{4.7}$$

$$k' = \sqrt{k_0^2 - h^2} \tag{4.8}$$

$$\alpha = k'\Delta x \tag{4.9}$$

In consequence, the transfer matrix $\mathbf{T}_{ij}$ between the nodes that connect regions R_{i} and R_{j} is calculated as:

$$\mathbf{T}_{ij} = \prod_{k=1}^{N} \mathbf{T}_{S(x_k)} = \prod_{k=1}^{N} \mathbf{T}_{S(k\cdot\Delta x)} \tag{4.10}$$

Some other special considerations were taken into account as follows:

i) End corrections were included for the transfer matrices that represent the impeller channels (both sides) and also the pump diffuser (only throttle side), by adding short pipes with equivalent lengths of 60% of the associated hydraulic radius (Munjal 2014).

ii) At the outlet of the impeller channels, sound is considered to expand abruptly to a cross-surface that covers an arc of a cylinder with the radius of the impeller outlet, the axial width of the volute and a peripheral extension that is proportional to that of the impeller channel by a factor $k_P \geq 1$ (Fig. 4.5(a)). Once in the volute, those curved sound waves are assumed to progress in the direction β_2 of the impeller blades up to a medium position *M* between impeller and volute surface (Fig. 4.5(b)). A new transfer matrix was determined for that short path across a fraction of the volute by means of the segmentation method described above. Then the previous transfer matrix of each impeller channel was multiplied by that new matrix.

iii) The transition between the exit area of the impeller channels (β_2 direction) and the volute (peripheral direction) is affected by sound reflection from the volute wall, in a fashion comparable to an extended-tube resonator of the reversal type (Fig. 4.5(b)). In order to take this effect into account, the transfer matrix of each impeller channel was multiplied by the matrix of a lumped shunt element (Munjal 2014), as defined in Eq. (4.11):

$$\mathbf{T}_{Sh} = \begin{bmatrix} 1 & 0 \\ 1/Z'_R & 1 \end{bmatrix} \tag{4.11}$$

In Eq. (4.11), Z'_R represents the impedance of a branch resonator. If $\mathbf{T}_R$ is the transfer matrix associated to the radial path between the central position in the volute (*M* in Fig. 4.5(b)) and the volute internal surface, which can be estimated by using the segmentation method again, the corresponding resonator impedance Z_R results to be:

$$Z'_R = \frac{T_{R11}}{T_{R21}} \tag{4.12}$$

iv) Subsequent sound propagation along the volute also covers the lateral areas between impeller and casing (Fig. 4.5(b)).

The transfer matrices that relate nodes along the volute depend on the local cross-section and so they are different for every pair of connected nodes. Moreover, they depend somewhat on the relative position of the impeller with respect to the tongue, as the latter determines the precise position of all the nodes in the volute. A similar dependence occurs for the transfer matrices of the impeller channels, because

the transition effects from impeller to volute depend too on the magnitude of the volute cross-section.

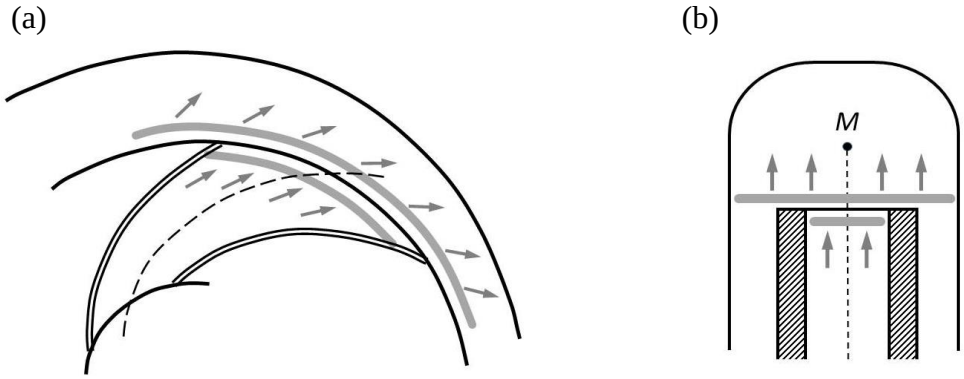

Fig. 4.5. Transition from an impeller channel to volute: a) frontal view; b) meridional view.

4.2 System resolution

In the acoustic model for centrifugal pumps described above, the acoustic pressure and mass velocity at all the nodes in the system constitute a finite number of unknown complex variables. They are to be determined according to the relationships established for the nodes in a given region (Eq. (4.3) and Eq. (4.4)) and by the transfer matrices between nodes of neighboring regions.

The number of nodes depends on z_B, the number of blades of the impeller, and so does the number of variables and equations. For the case of z_B=7 (Fig. 4.6) there are 34 nodes, i.e. 68 unknowns. Besides there are 17 transfer matrices each producing 2 equations, plus 23 pressure identity equations and 9 continuity equations by virtue of Eq. (4.3) and Eq. (4.4) respectively. This makes a total of 66 linear equations and hence two more equations are needed to obtain a closed system. These two additional equations correspond to boundary conditions at the suction and discharge ports of the pump, which, for z_B=7, are represented by nodes $n_S = n_{00}$ and $n_D = n_{100}$ respectively (Fig. 4.6). And those boundary conditions depend on the external acoustic load applied on the pump.

In order to determine the overall transmission matrix of a given pump, it is necessary to consider two situations with independent acoustic loads, hence with independent sets of boundary conditions. A convenient choice is summarized in Table 1. Once the system of equations is closed it can be solved by any method suitable for linear equation systems (Burden and Faires 2011). Direct methods are preferable since the expected number of variables and equations is low (68 complex unknowns and equations for z_B=7 blades). For the calculations reported below the classical method of

Gaussian elimination proved to be very effective when used with complete pivoting during the process.

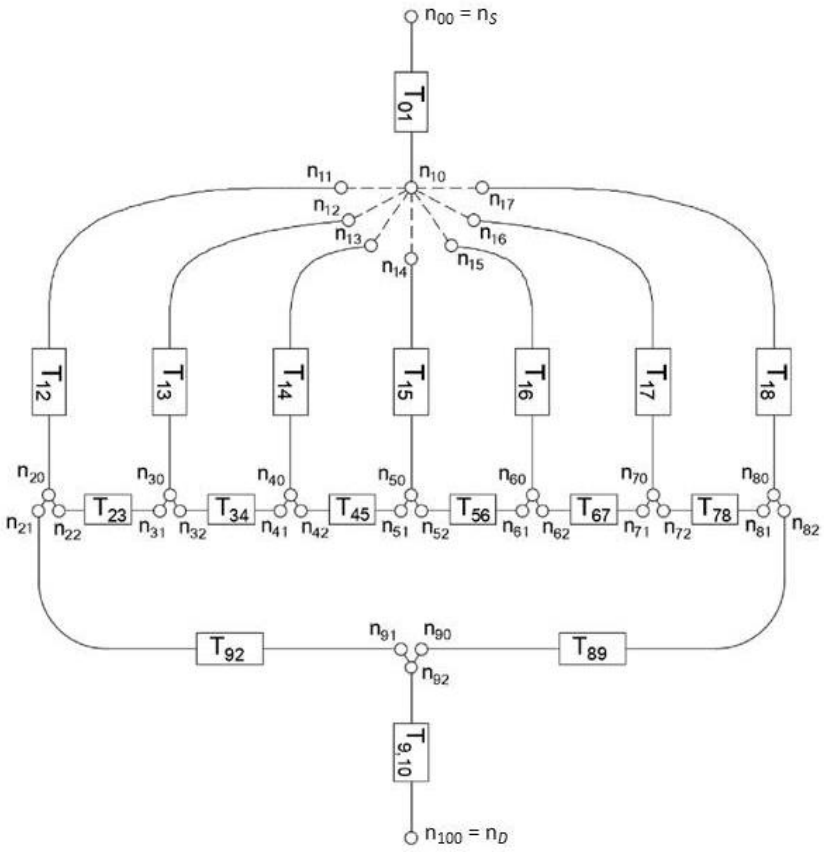

Fig. 4.6. Network of nodes and transfer matrices for a pump with a seven-blade impeller.

Table 4.1. Acoustic loads and boundary conditions to determine the pump transmission matrix. *S*=node at suction port (n_S=n_{00} in Fig. 4.6); *D*=node at discharge port (n_D=n_{100} in Fig. 4.6)

Load	Boundary condition	Description	Equation
I	BC-*I*-1	External source at suction pipe, inducing an incoming unitary pressure wave.	$p_S + y_S\, v_S = 2$ (4.13)
	BC-*I*-2	Discharge piping with anechoic end.	$p_D - y_D\, v_D = 0$ (4.14)
II	BC-*II*-1	Suction piping with anechoic end.	$p_S + y_S\, v_S = 0$ (4.15)
	BC-*II*-2	External source at discharge pipe, inducing an incoming unitary pressure wave.	$p_D - y_D\, v_D = 2$ (4.16)

The application of the whole procedure to form and solve the equation system results in the values of all the unknown variables, for each of the two acoustic loads considered. In particular, the overall transmission matrix of the pump **T** has to relate the acoustic pressure and mass velocity at the suction and discharge ports of the pump, i.e. at nodes n_S and n_D (Fig. 4.6), so that for both acoustic loads *I* and *II* it must be verified:

$$\begin{bmatrix} p_S \\ v_S \end{bmatrix}_{I-II} = \mathbf{T} \begin{bmatrix} p_D \\ v_D \end{bmatrix}_{I-II} = \begin{bmatrix} T_{11} & T_{12} \\ T_{21} & T_{22} \end{bmatrix} \begin{bmatrix} p_D \\ v_D \end{bmatrix}_{I-II} \tag{4.17}$$

Eq. (4.17) constitutes two pairs of equations, with each pair involving only the two entries of either the first or the second row of **T**. In consequence all the elements of **T** can be obtained easily.

Finally, the scattering matrix of the pump, **S**, can also be obtained from the elements of the transmission matrix, by using the following relationships (Bardeleben and Weaver 2002):

$$\begin{cases} S_{11} = \dfrac{1}{Den}\left(T_{11} - y_S\, T_{21} + \dfrac{T_{12}}{y_D} - \dfrac{y_S\, T_{22}}{y_D}\right) \\ S_{12} = \dfrac{2}{Den} \\ S_{21} = \dfrac{2}{Den}\left(T_{11}\, T_{22} - T_{12}\, T_{21}\right) \\ S_{22} = \dfrac{1}{Den}\left(-T_{11} - y_S\, T_{21} + \dfrac{T_{12}}{y_D} + \dfrac{y_S\, T_{22}}{y_D}\right) \\ Den = T_{11} + y_S\, T_{21} + \dfrac{T_{12}}{y_D} + \dfrac{y_S\, T_{22}}{y_D} \end{cases} \tag{4.18}$$

No acoustic dissipation has been included in the internal transfer matrices, as well as no effect of fluid velocity on the effective sound speed. In consequence the elements T_{11} and T_{22} of the pump transmission matrix only have real part, the elements T_{12} and T_{21} only have imaginary part and the determinant of **T** is equal to 1 (real part only), as corresponds to a reciprocal system (Brennen 2011). This would be also the case of the electrical model by Stirnemann et al. (1987) (Eq. 4.1) if the real part of the impedance Z_2 as given in Eq. (4.2) is negligible. Regarding the pump scattering matrix **S**, reciprocity brings about the same modulus for S_{11} and S_{22}, and the same argument for S_{12} and S_{21}, whereas the modulus of the determinant of **S** is equal to 1.

4.3 Effect of model parameters on predictions

The acoustic model was first put into practice on a reference pump with the main data shown in Table 4.2. The other model parameters are as follows:

Table 4.2. Other model parameters

Angular position of first blade (trailing edge) relative to tongue, φ_1 [deg]	30
Number of segments for passages with variable cross-section, N	25
Peripheral expansion factor at impeller outlet, k_P	2
Sound speed, c_0 [m/s]	1400

As described in Section 4.2, the sound field in the pump has to be computed twice, each under a different acoustic load, before determining the transmission matrix. An example of those computations is given in Fig. 4.7, which shows the modulus and phase of the pressure so obtained at four nodes, when the reference pump is subject to the acoustic load named *II* in Table 4.1. Calculations have covered a wide range of frequencies, from 0 to 400 Hz. The nodes selected are located at the suction and discharge ports of the pump (n_S and n_D), at the tongue region (n_{90}) and in the volute at the opposite side to the tongue (n_{50}). It is observed that, though differences between nodes increase with frequency, the three nodes from suction to tongue region exhibit a similar behavior, i.e. the acoustic pressure is relatively uniform in the chamber defined by the volute casing. Node n_D, however, shows a rather distinct trend, as corresponds to a position in a duct (the diffuser) at significant distance from the pump chamber.

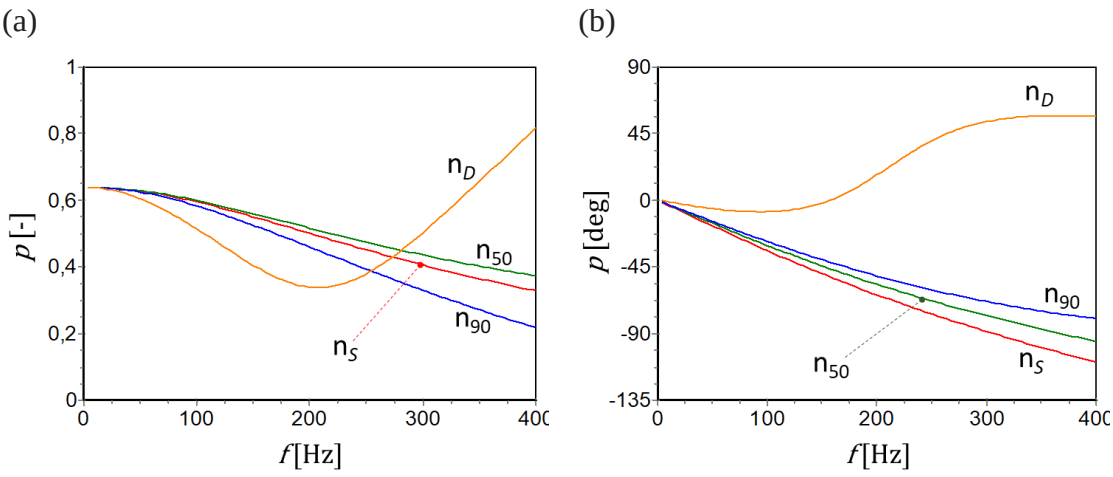

Fig. 4.7. Modulus (a) and phase (b) of the acoustic pressure at four nodes of the reference pump for the acoustic load II (Table 4.1). Nodes as in Fig. 4.6.

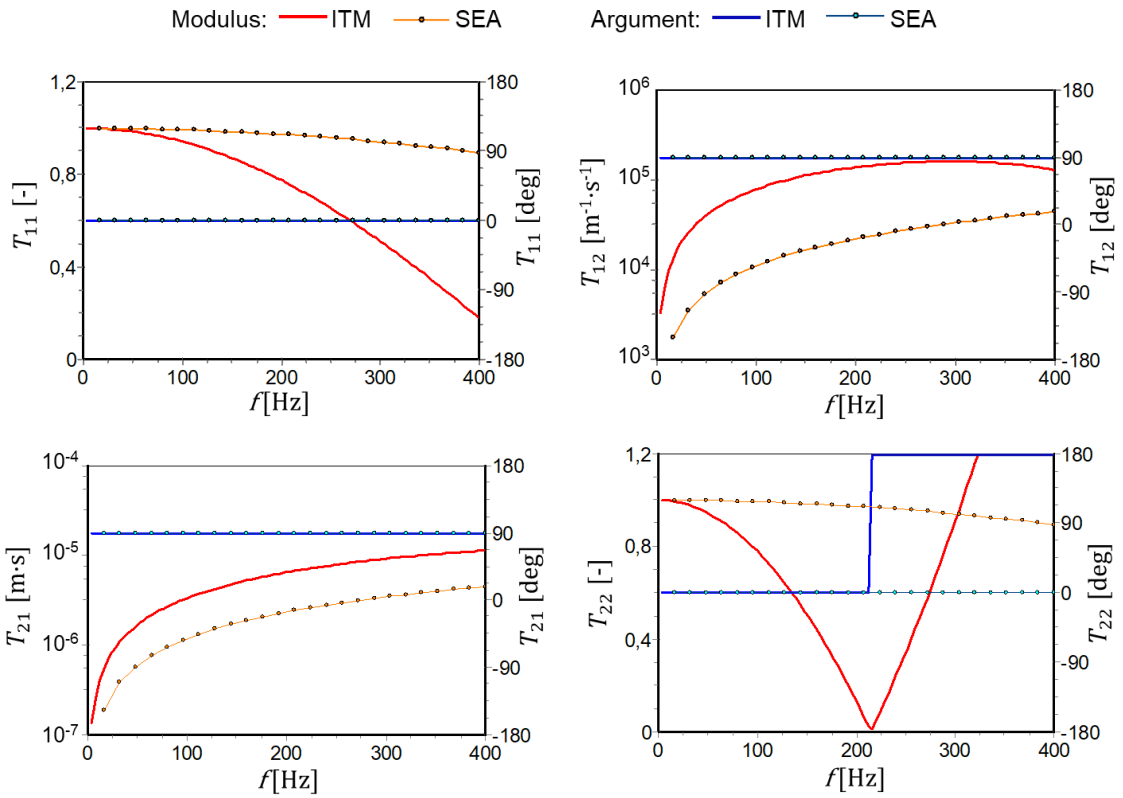

Fig. 4.8. Transfer matrix calculated for the reference pump. ITM= current internal transfer matrix model; SEA= Stirnemann's electrical analogy model, Eqs. (4.1-4.2).

Appropriate processing according to Eq. (4.17) of the acoustic pressure and mass velocity at nodes n_S and n_D for the two acoustic loads of Table 4.1 results in the transfer matrix for the reference pump. This is shown in Fig. 4.8, as well as the predictions from Stirnemann's electrical analogy (Stirnemann et al. 1987) as given by Eqs. (4.1-4.2) with $\mathrm{Re}(Z_2)$=0.

The two models predict that elements T_{11} and T_{22} only have real part whereas T_{12} and T_{21} only have imaginary part, as expected. Also, increasing the frequency makes the modulus of T_{11} and T_{22} decay from unity with both models, but according to Eqs. (4.1-4.2) the slope of the decay is very smooth whereas the current transfer matrix model gives a quick reduction of magnitude, up to the point of reaching T_{22}=0 and then reversing phase and growing above 215 Hz. Besides, the magnitudes of T_{12} and T_{21} as predicted with Eqs. (4.1-4.2) are significantly lower than the values obtained from the transfer matrix model. All this suggests that, compared to the model now proposed, the values estimated with Eq. (4.1-4.2) for the equivalent impedance and admittances are too low. This is in line with the observations by other researchers (Bardeleben et al. 2002) and it is further discussed in next section.

Once the transmission matrix is known the scattering matrix can be obtained by

using Eq. (4.18). A selection of results on the reference pump is given below to show the effect of some parameters of the acoustic model and also some pump parameters. Among the former, the most influential one is the peripheral expansion factor k_P, which accounts for the effect of the abrupt change in cross-section at the outlet of the impeller channels. The least possible value for k_P is 1, which actually means no peripheral expansion. As illustrated in Fig. 4.9 on element S_{11}, varying k_P from 1 to 2 and then to 3 accelerates the deviation of the variables when increasing frequency with respect to the values at 0 Hz. In particular, changing k_P from 1 to 2 gives a maximum relative change in the modulus of S_{11} of the order of 14% at about 200 Hz, whereas the argument reduces in 15 °. Other model parameters have much less impact on the predictions. For instance, the number of segments N considered to estimate the transfer matrix of channels with variable cross-section (Fig. 4.4) proved to have virtually no influence on the results as far as it is higher than about 15. All the computations presented in this section and in the next one correspond to N=25.

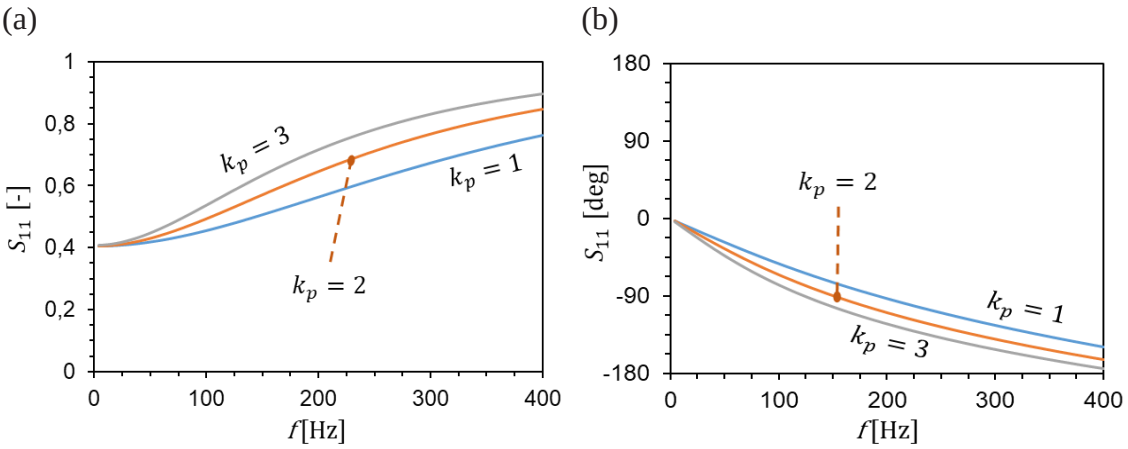

Fig. 4.9. Element S_{11} of the scattering matrix for the reference pump with peripheral expansion factors k_P=1, 2 and 3; (a) modulus; (b) argument.

With respect to the pump geometric parameters, the predictions of the scattering matrix show little dependence unless they are closely related to the global pump shape, i.e. to the pump specific speed. One example of parameters not dependent on specific speed is the angular position of the impeller, which is characterized by the angle φ_1 of the first blade (trailing edge) relative to tongue tip. In this case (Fig. 4.10), the maximum variation of the modulus of S_{11} for a range of φ_1 covering 360 °/z_B (z_B=number of blades) is about 2% of the average value, whereas the phase varies in 2.5 ° as highest. This little variation is consistent with the measurements reported by Carta et al. (2000) and supports dismissing the measure of that angle and even the rotation of the impeller for practical applications.

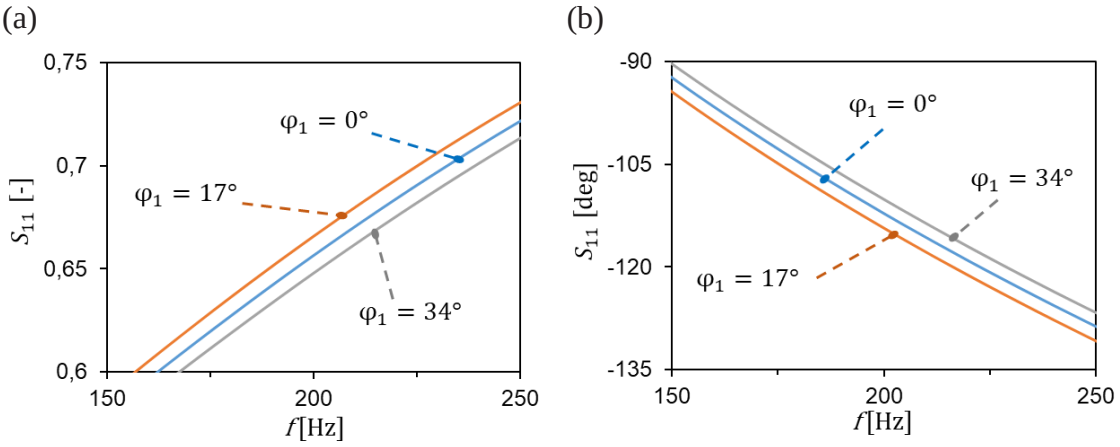

Fig. 4.10. Element S_{11} of the scattering matrix for the reference pump with impeller at angular positions φ_1= 0 °, 17 ° and 34 ° (φ_1= angle of first blade relative to tongue); (a) modulus; (b) argument.

Fig. 4.11 shows the effect of cutting the impeller to a smaller outlet radius r_2 while keeping the same volute casing, which is a common practice of pump manufacturers to extend the performance range of the pumps. Again, its effect on the acoustic properties is small: a reduction of r_2 from 105 to 80 mm (24%) just leads to an increment of 3 % in the modulus of S_{11} and a reduction of 8 ° in the argument at 200 Hz.

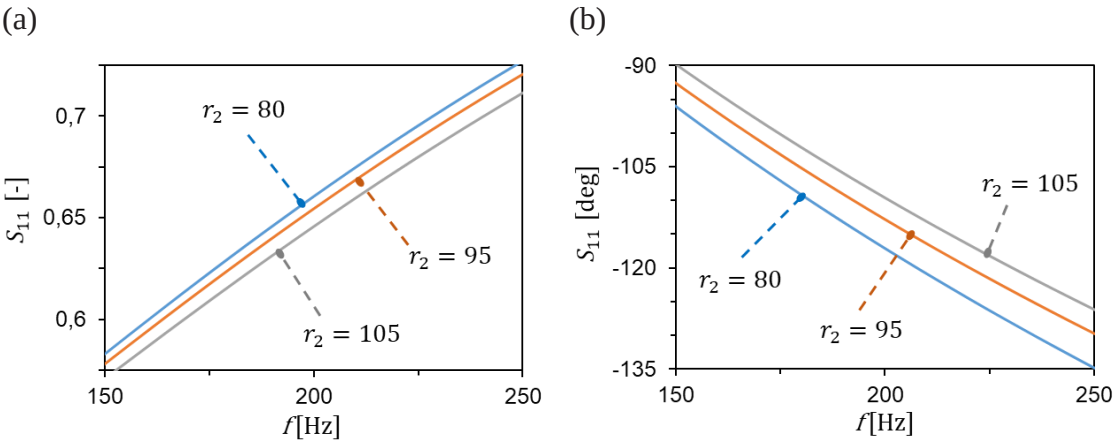

Fig. 4.11. Element S_{11} of the scattering matrix for the reference pump, with impeller outlet radius r_2 = 80, 95 and 105 mm; (a) modulus; (b) argument.

Another parameter with potential interest is the number of blades of the impeller, z_B, since it determines the number of nodes and internal transfer matrices involved in the pump acoustic model. However, Fig. 4.12 shows that varying z_B between 6 and 8 has little effect on the predicted modulus, and virtually no effect on the argument.

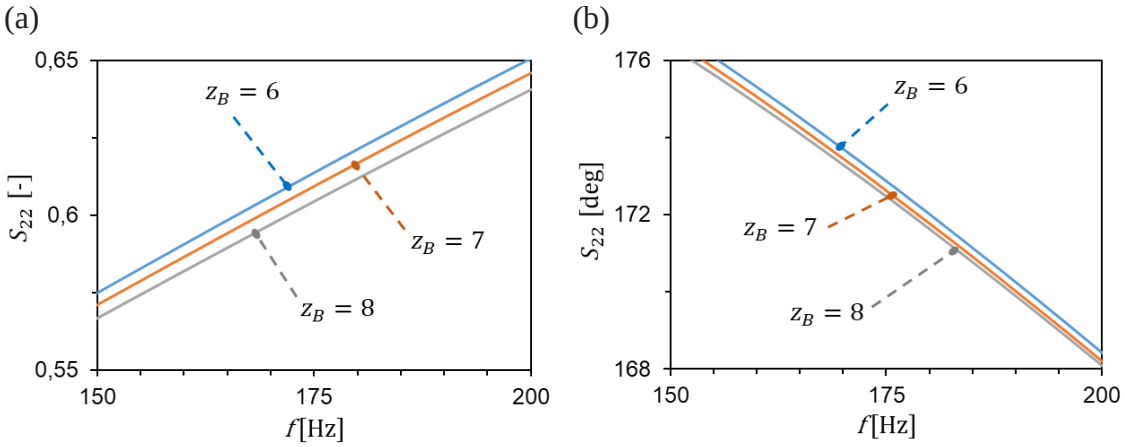

Fig. 4.12. Element S_{22} of the scattering matrix for the reference pump and impeller with z_B=6, 7 and 8 blades; (a) modulus; (b) argument

5 Contrast of predictions against experimental data

First, the experimental results obtained on the scattering matrix for the test pump are presented and compared to the predictions of the new internal transfer matrix model. Then, in order to evaluate its prediction capacity for pumps with different geometrical features, that contrast is then extended to several reference pumps tested by other researchers (Stirnemann et al. 1987, de Jong. 1996, Han et al. 2003, Bardeleben. 2005, Brümmer et al. 2019), so that a wide range of specific speeds is covered. A special quality parameter is defined to quantify how close are the predictions to the available experimental data, taking into account that in all cases the experimental data have a certain degree of dispersion. Additionally, the predictions for each pump from the new internal transfer matrix model are also compared and analyzed against the predictions from Stirnemann's classical model based on an electrical analogy.

5.1 Experimental data for the test pump and prediction contrast

5.1.1 Test rig and test facility

Fig. 5.1 shows a schematic representation of the hydraulic set-up and the instrumentation. The hydraulic circulatory system is composed of test pump, auxiliary pump, several pipelines and water tank. The auxiliary pump is a conventional single-stage single-suction centrifugal pump with 7 double-curved blades, a spiral volute and variable-frequency motor. The structure of the test pump is similar to that of the auxiliary pump. Its dimensionless specific speed is 0.46 and is calculated using the formulation $n_s=n\sqrt{Q}/(gH)^{0.75}$. The detailed geometrical parameters and the performance values of the test pump can be referred to Table 3.1 and the former study (Barrio et al. 2008). In this system, the test pump was installed in parallel with an auxiliary pump that acted as an external loudspeaker, because it was operated with a very low flow-rate and so it produced relatively high pressure pulsations at its blade-passage frequency. For the operational control system, there are three ways to modify the magnitude and frequency of the pressure pulsations induced at the measurement positions close to the test pump:

i) Control the opening degree of the regulation valve of the auxiliary pump. This modifies the pump operating point and in consequence it modifies the pressure pulsations generated at the auxiliary pump.

ii) Alter the rotation speed of the auxiliary pump by means of a variable-frequency drive. This also modifies the pressure pulsations generated at the auxiliary pump, since, for a given fraction of the best efficiency flow-rate, the

pressure amplitude is approximately proportional to the rotation speed squared.

iii) Adopt different pipeline configurations in the hydraulic system by opening/closing specific valves. This changes the acoustic transmission properties of the piping system, and in consequence the acoustic load on the test pump is modified too.

During each test, two pairs of fast response piezoelectric pressure sensors (Kistler type 701A) with high sensitivity installed separately in the suction and discharge pipelines were adopted to capture the unsteady pressure fluctuation signals of detection areas in test pump. These pressure sensors were fixed in a special casing which was flush-mounted on the internal surface of the volute and duct system. It's worth noting that the internal chamber between adapter outlet and sensor should be filled with water before installation to avoid the affecting of measurement accuracy from air bubbles, more detailed descriptions as shown in Parrondo et al. (2002). The pressure fluctuation signals were amplified and recorded by means of charge amplifiers (Kistler type 5018) and a multi-channel acquisition device (IMC Cronos-PL2), respectively. To fulfill the periodic requirements and avoid the aliasing and leakage errors as better as possible, pressure fluctuation signals were processed by means of the Hanning window function.

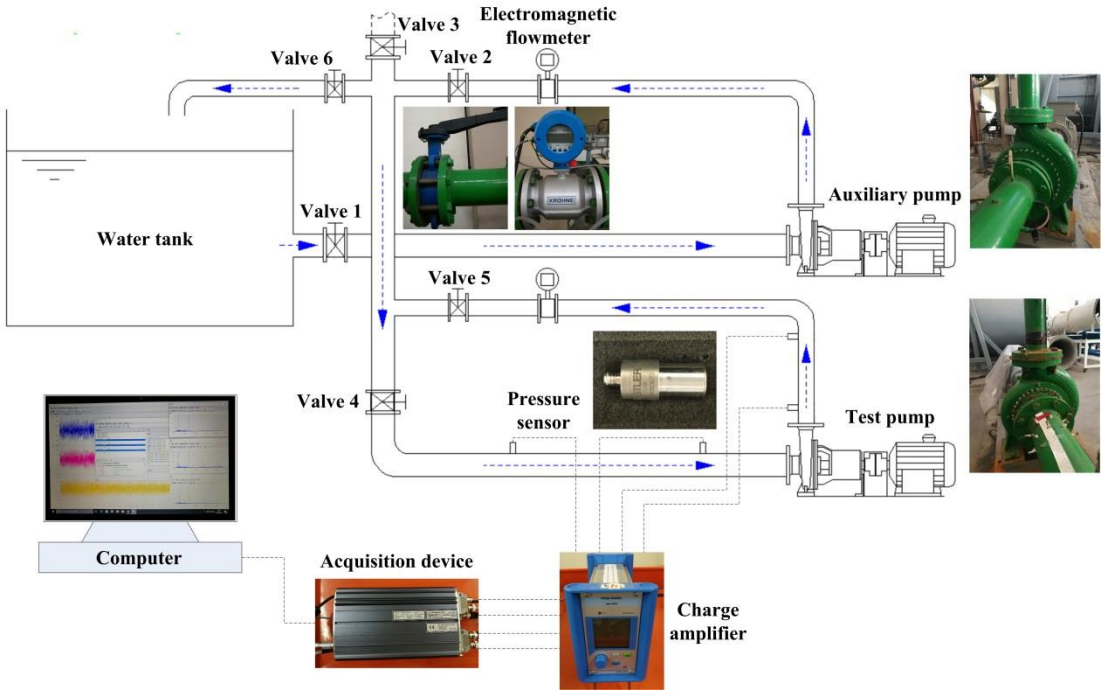

Fig. 5.1. Schematic view of the experimental facility

5.1.2 Test measurements based on different pipeline configurations

Fig. 5.2 shows the pressure spectra at four different positions (in Fig. 5.1) of the suction and discharge pipes of the test pump. During the test, the auxiliary pump was

operated at a very low flow-rate and the rotation speed was 1200 rpm. The test pump remained stationary to guarantee that the fluid-dynamic excitation noise induced by rotor-stator interaction cannot be generated inside its interior. The discharge pipe of the auxiliary pump was connected to the terminal of the hydraulic system and the suction pipe of the test pipe simultaneously. The valve 5 mounted in the discharge pipe of the test pump, valve 3 remained in the closed state and valve 1, 2 4 and 6 were open. As expected, the significant pressure pulsation amplitudes at shaft frequency f_S=20 Hz and blade passing frequency f_B=140 Hz were captured at all four monitoring points. This result clearly indicates that the inlet and outlet ports of the test pump are capable of receiving the acoustic pressure wave with sufficient energy radiated from the auxiliary pump.

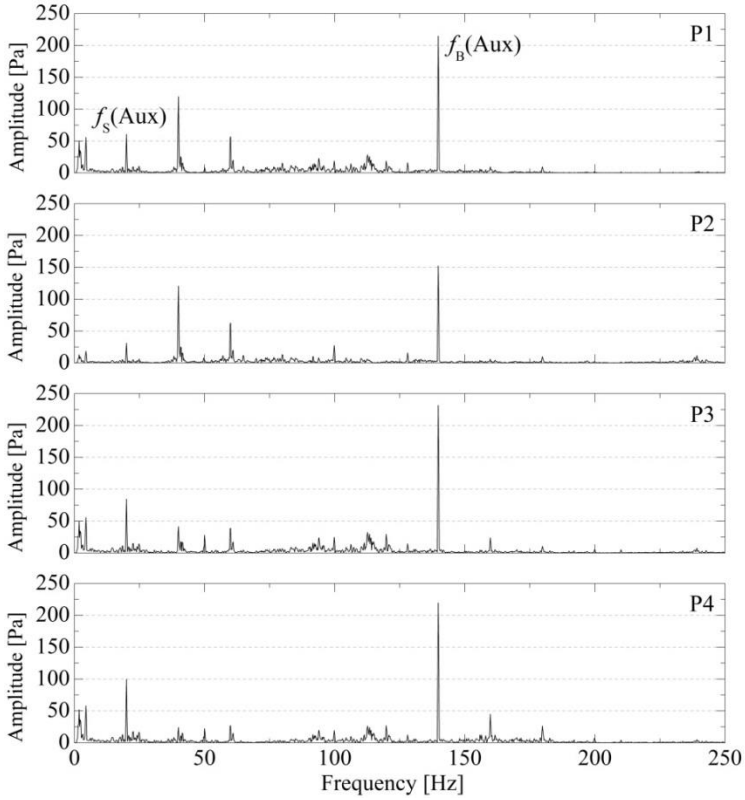

Fig. 5.2 Pressure spectra at four positions of the suction and discharge pipe of the test pump

For these tests, in order to extract the unknown elements of the scattering matrix based on the above Eqs. (2.34) and (2.35), redundant sets of tests by means of the above three different approaches were carried out to obtain the entering and exiting pressure wave amplitudes (p^+ and p^-) at the suction pipe (SP) and discharge pipe (DP) of the test pump. Fig. 5.3 compares the pressure amplitude and phase measured at f_S=20 Hz and f_B=140 Hz for different pipeline configurations while the auxiliary pump was operated at the same rotation speed and flow rate, i.e. the external sound source remained constant. The Conf. #1~4 represent the different duct configuration schemes, respectively, and detailed information (different valves either open or close)

is depicted in schematic views in Fig. 5.3. As expected from the experimental design, the effect of duct configurations on state variables at two-ports of the test pump is significant, so that the acoustic interaction between the auxiliary pump and the duct systems provides the basis and support for the subsequent solution of N independent Eqs (2.34) and (2.35). For example, the amplitudes (p^+ and p^-) and phases (φ^+ and φ^-) of Conf. #1 are similar to those of Conf. #3 at f_B and $2f_B$. When the pipeline system adopts Conf. #2 and Conf. #4, the amplitudes and phases at f_B and $2f_B$ produce a large variation, compared with Conf. #1 and Conf. #3, especially at DP (SP and DP denote the pressure amplitude at the suction and discharge pipes respectively). This is reasonable because the valve located at the discharge pipe of the test pump is open. Meanwhile, this phenomenon also indirectly reflects that the spectrum of the pressure pulsation measured directly in the pipeline of the centrifugal pump cannot be used to reflect the acoustic characteristic of the fluid-dynamic noise of the pump itself. Due to the coupling effect of the hydraulic system, in some situations, it might be even seriously misleading.

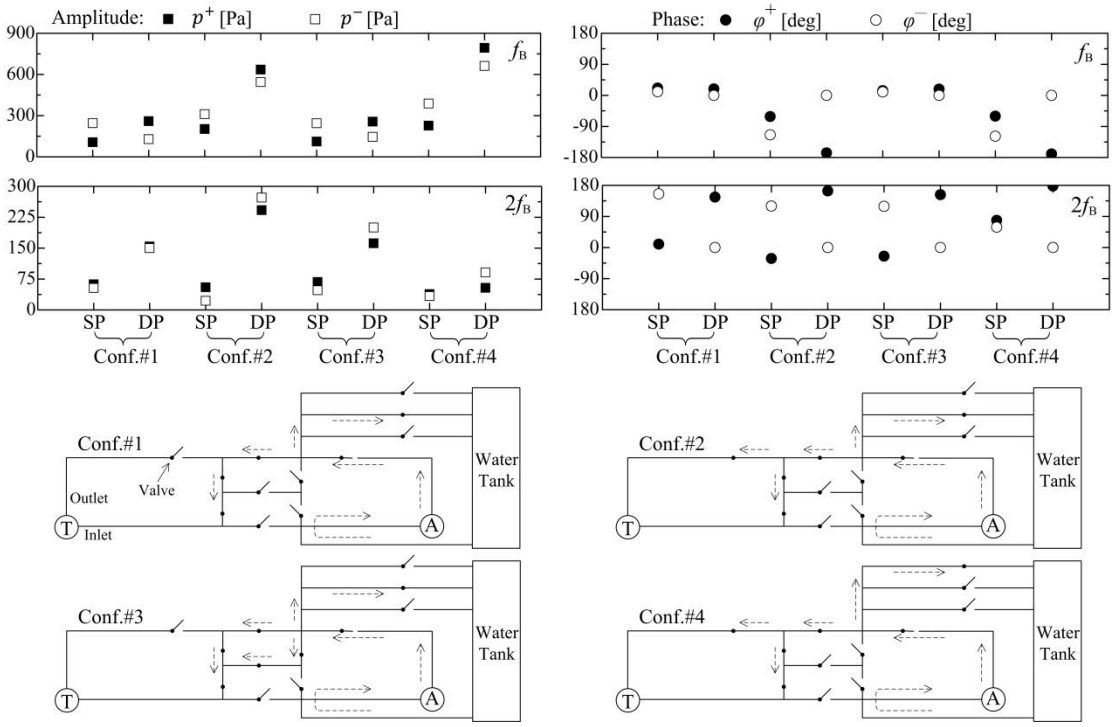

Fig. 5.3 Entering and exiting pressure waves from the test pump for different pipeline configuration (A and T denote the auxiliary pump and the test pump, respectively)

5.1.3 Results on the scattering matrix of the test pump

Fig. 5.4 presents the results obtained for the elements of the scattering matrix of the test pump from the measurements described above, as well as from the computations based on the ITM model of Chapter 4. The experimental data present a significant degree of dispersion, despite the efforts to perform accurate and repeatable

measurements. Though that dispersion may be partially attributed to measurement uncertainty, we believe there may be a considerable effect of vibration transmission from the auxiliary pump to the piping system. This would cause the pipes to vibrate with different vibration modes depending on the excitation frequency and the valve configuration. In any case the vibration amplitude would very low (virtually unperceivable), but, since the internal radiation surface of the pipes is large, those pipe vibrations still might be able to affect the travelling sound pressure waves. However, at present no action could be taken in the test set-up to avoid that possible vibration effect. In addition, the straight length of the discharge pipe of the test pump is short, which may cause the pressure values measured by the two pressure sensors located on it to be too similar to have good resolution at low frequency. This will have a certain degree of influence on the pressure wave decomposed at the discharge pipe, and further influence the elements of the scattering matrix obtained by the least square error procedure. Nevertheless, it is interesting that the data reported by other researchers on the scattering matrix or the transmission matrix measured for other pumps usually exhibit dispersion degrees similar to that of the current research, as shown in the following sections.

Despite the dispersion of the experimental data, the values determined for the scattering matrix elements denote clear trends. To begin with, at low frequency the modulus of the two coefficients S_{11} and S_{22} are seen to approach the value of the reflection coefficient k_{R} that corresponds to a change in cross-section between the suction and discharge pipes: $k_{\mathrm{R}} = \frac{A_S - A_D}{A_S + A_D} = 0.454$. Besides, when reducing the frequency down to zero the modulus of S_{12} and S_{21} are seen to tend to the values of the transmission coefficient for that same change in cross-section from pump inlet to outlet: $k_{\mathrm{TS}} = \frac{2A_S}{A_S + A_D} = 0.546$ and $k_{\mathrm{TD}} = \frac{2A_D}{A_S + A_D} = 1.454$. Finally, the arguments of S_{11} and S_{22} tend to 0 and 180 degrees respectively when reducing frequency to zero, while the arguments of S_{12} and S_{21} tend both to zero. All this suggests that, at very low frequency, the pump cavity is not really relevant in the transmission of sound trough the pump.

However increasing the frequency makes that all the values change considerably. In particular, the modulus of S_{11} and S_{22} are seen to increase progressively towards 1, but without exceeding that value, whereas the modulus of S_{12} and S_{21} are seen to reduce steadily. All this is consistent with energy considerations. In consequence, increasing the frequency produces that most of the on-coming sound to either the suction or the discharge ports becomes reflected back, i.e. the acoustic coupling between the two ports of the pump becomes progressively weaker.

On the other hand, increasing the frequency brings about a progressive reduction in the argument of the four scattering matrix elements. That reduction is approximately linear with frequency. This is consistent with the fact that, for sound waves travelling a given distance at constant speed, the phase delay induced is proportional to frequency.

Table 5.1 shows the coefficient of determination obtained by linear fitting of different elements of the scattering matrix for the test pump. The fitting function used in this test data is linear fitting, because the effect of other more complex fitting functions did not really increase the R^2 coefficient significantly. The results show that the R^2 of each element of the scattering matrix is not close to unity, which would be the ideal value. This is because of the high degree of dispersion of the test data. In any case, the trends defined by the linear fits of the data can be considered reasonable and acceptable since, as discussed above, at low frequency they represent a change in cross-section between the suction and discharge pipes while increasing the frequency rises up the effects of the pump chamber, resulting in a progressive disconnection between the two ports.

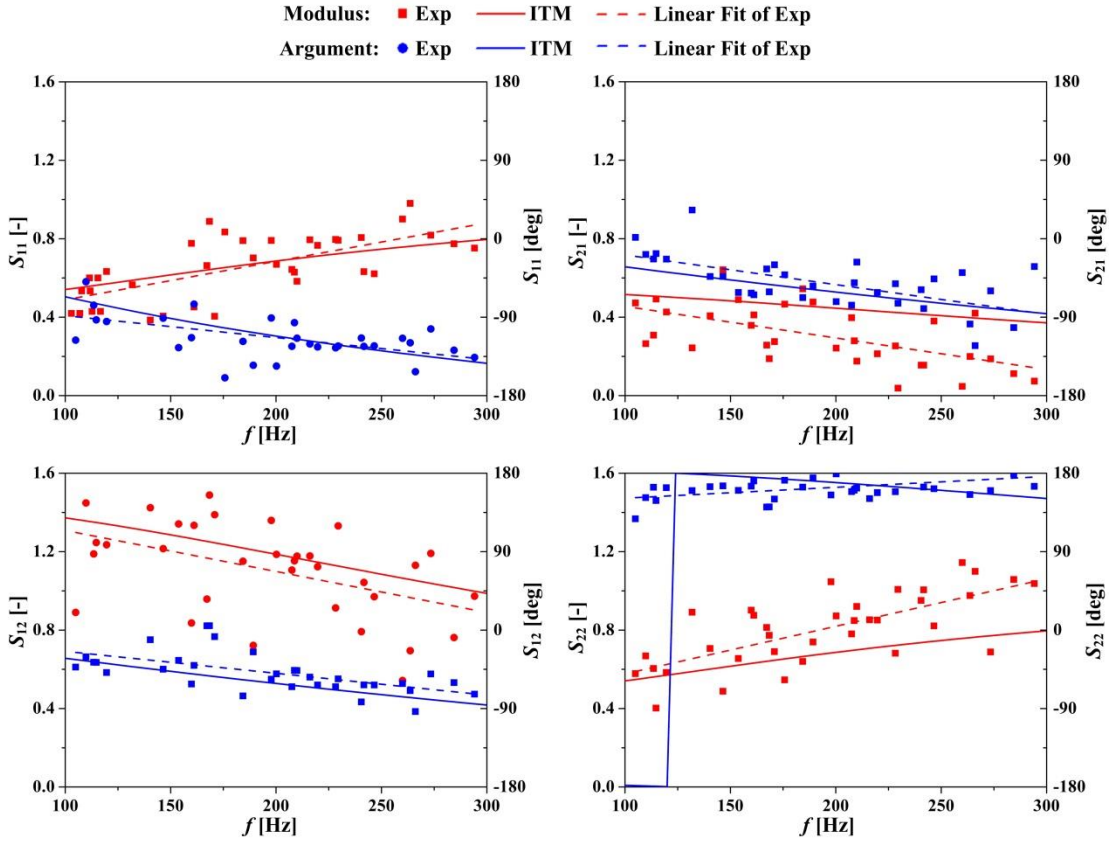

Fig. 5.4. Measurement and prediction for the scattering matrix of the test pump. ITM= current internal transfer matrix model

Table 5.1. Coefficient of determination for different elements of the scattering matrix (subscript ‘m’ represents modulus, subscript ‘a’ indicates argument)

Elements / Linear fit	$S_{11.\mathrm{m}}$	$S_{11.\mathrm{a}}$	$S_{12.\mathrm{m}}$	$S_{12.\mathrm{a}}$	$S_{21.\mathrm{m}}$	$S_{21.\mathrm{a}}$	$S_{22.\mathrm{m}}$	$S_{22.\mathrm{a}}$
R^2	0.410	0.273	0.344	0.393	0.227	0.352	0.505	0.233

5.2 Contrast against the experimental data reported by Stirnemann

In order to evaluate the prediction capacity of the internal transfer matrix model, it was applied on a centrifugal pump tested by Stirnemann et al. (1987), who conducted laboratory measurements in standstill conditions to determine its transmission matrix. The specific speed and main geometrical data reported for that pump are shown in Table 5.2. Other data reported were the flow rate with highest efficiency at 2900 rpm, which was $Q_{\mathrm{BEP}} = 162\ \mathrm{m}^2/\mathrm{h}$, and the maximum ratio between pipe diameter and wavelength, which was 0.009. The latter ensured that only plane wave propagation could take place in the piping.

Table 5.2. Main data reported for the pumps tested by Stirnemann et al. (1987)

Pump designation	Value
Specific speed (non-dimensional), n_s	0.95
Number of blades, z_B	6
Radius at impeller outlet, r_2 [mm]	84.5

The acoustic model operates with other non-reported input data, so they were estimated according to the pump specific speed and the corresponding general shape. Table 5.3 lists the main data assumed. Other model parameters were taken as constant for the pump model, including: sound speed c_0=1450 m/s (based on Stirnemann et al. 1987), peripheral expansion factor k_P =2 and first blade angular position φ_1=30 °.

Table 5.3. Additional geometric data for the pumps tested by Stirnemann et al. (1987)

ump designation	Value
Diameter of suction port, d_S [mm]	125
Diameter of discharge port, d_D [mm]	100
Radius at tongue tip, r_3 [mm]	90
Width at impeller outlet, b_2 [mm]	20
Outlet blade angle relative to tangent, β_2 [deg]	60
Volute width, b_3 [mm]	80
Throttle cross-section, A_T [cm^2]	35
Length suction port to impeller eye, L_{SE} [mm]	60
Length throttle to discharge port, L_{TD} [mm]	270

Stirnemann et al. (1987) reported the transmission matrix data of their pump at a series of frequencies between 20 Hz and 100 Hz. According to Eq. (4.18), the scattering matrix **S** of the pump can be obtained from the elements of the transmission matrix (Bardeleben and Weaver 2002). Fig. 5.5 shows the experimental data corresponding to the scattering matrix of the pump together with the predictions derived from the new internal transfer matrix model (ITM) as well as from Stirnemann's electrical analogy (SEA) as formulated in Eqs. (4.1) and (4.2). It can be seen that ITM and SEA have similar trends in the prediction of the four elements of the scattering matrix. The trends of the parameters predicted (modulus and argument) with the ITM and SEA model for increasing frequency are similar to those of the experimental data, but the rate of variation of both modulus of $S_{21}$with frequency is slightly slower. In addition, the comparison found that ITM has better prediction results than the SEA model in predicting arguments as the frequency increases. In summary, though the experimental data shows a certain degree of dispersion, both ITM and SEA model can be considered in reasonable agreement with the measurements of the scattering matrix.

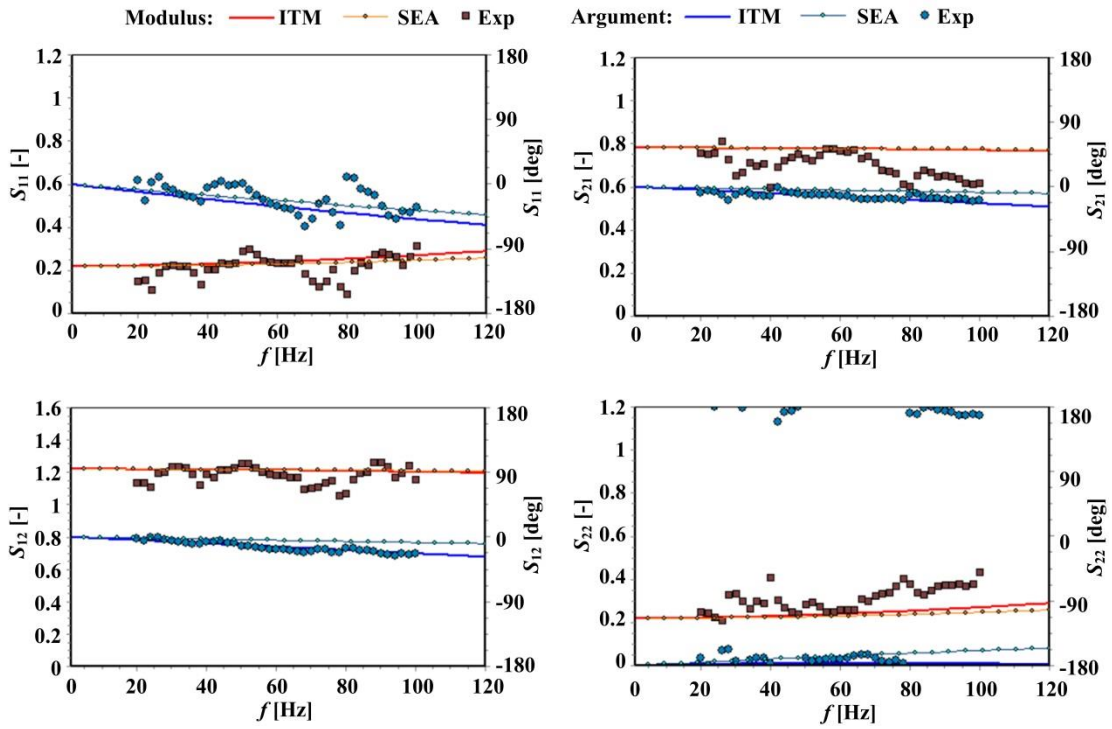

Fig. 5.5. Elements of the scattering matrix determined for the reference pump. ITM= internal transfer matrix model, SEA= Stirnemann's electrical analogy, Exp= data by Stirnemann et al. (1987)

Fig. 5.6 shows the experimental data of the transmission matrix determined for the pump together with the predictions derived from the new internal transfer matrix model (ITM) as well as from Stirnemann's electrical analogy (SEA) as formulated in Eqs. (4.1) and (4.2). According to the calculation results, the modulus and argument of the elements T_{11} and T_{12} of the transmission matrix predicted by ITM are in

good agreement with the corresponding experimental measurements. The experimental data of modulus and argument of the element T_{21} shows a certain degree of dispersion, but the ITM predictions can be considered in reasonable agreement with the measurements. For element T_{22}, as the frequency increases, the modulus change based on ITM prediction becomes slower, but the argument prediction is still quite satisfactory. Overall, the ITM has a relatively good prediction for the scattering matrix of the centrifugal pump tested by Stirnemann et al. (1987). Again, the SEA predictions diverge significantly from measurements when increasing the frequency, especially regarding the modulus of T_{12} and T_{22}.

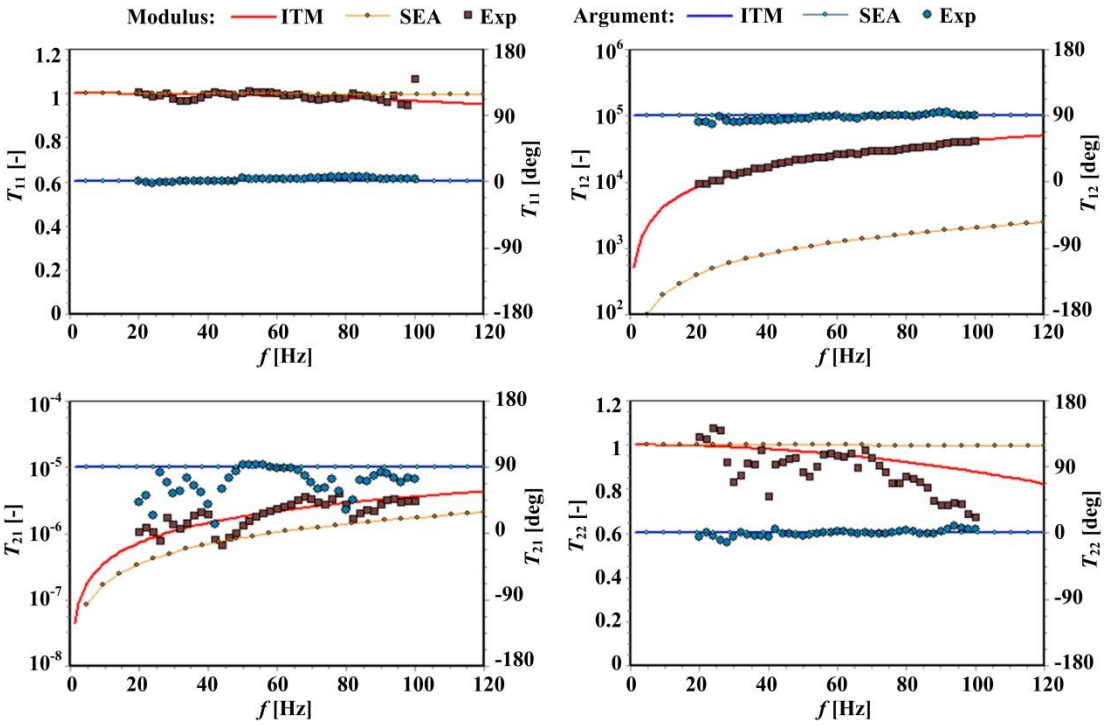

Fig. 5.6. Elements of the transmission matrix determined for the reference pump. ITM= internal transfer matrix model, SEA= Stirnemann's electrical analogy, Exp= data by Stirnemann et al. (1987)

5.3 Contrast against the experimental data reported by de Jong

The third pump considered to contrast the predictions of the internal transfer matrix model was the one tested by de Jong (1996). Like Stirnemann's, this is a centrifugal pump with a high specific speed (n_s =1.03), but measurements were taken on a much broader frequency range (up to 400 Hz). The data reported by De Jong for this pump include a nominal electrical power of 7.5 kW, a nominal speed of n=2870 rpm, a nominal head of H=18 m and a nominal flow rate of 96 m^3/h, as well as the main geometrical data shown in Table 5.4.

Table 5.4. Main data reported for the pumps tested by de Jong (1996)

Pump designation	Value
Specific speed (non-dimensional), n_s	1.03
Diameter of suction port, d_S [mm]	100
Diameter of discharge port, d_D [mm]	100
Number of blades, z_B	6
Radius at impeller outlet, r_2 [mm]	67
Width at impeller outlet, b_2 [mm]	22

Since the acoustic model operates with other non-reported input data, they were estimated according to the pump specific speed and the corresponding general shape. Table 5.5 lists the main data assumed. Other model parameters were taken as constant for the pump model, including: sound speed c_0=1450 m/s (based on de Jong 1996), peripheral expansion factor k_P =2 and first blade angular position φ_1=30 °.

Table 5.5. Additional geometric data for the pump tested by de Jong (1996)

Pump designation	Value
Radius at tongue tip, r_3 [mm]	75
Outlet blade angle relative to tangent, β_2 [deg]	34
Volute width, b_3 [mm]	60
Throttle cross-section, A_T [cm^2]	35
Length suction port to impeller eye, L_{SE} [mm]	140
Length throttle to discharge port, L_{TD} [mm]	235

De Jong (1996) conducted tests to determine the pump transmission matrix both at standstill and running conditions. Data under running conditions presented a higher degree of dispersion, but the average trends were very similar to those under standstill conditions. In consequence, the data selected for the present contrast corresponds to standstill.

Figs. 5.7 and 5.8 show the experimental data that correspond respectively to the scattering matrix and the transmission matrix of the pump together with the predictions derived from the ITM model as well as from the SEA model. As expected, the experimental data on the transmission matrix show that the modulus of elements T_{11} and T_{22} are equal to 1 at 0 Hz and then reduce progressively when increasing the frequency, whereas the argument remains close to 0 degrees. At the same time, T_{12} and T_{21} show a progressive increment in modulus from a very low value at 0 Hz, with the respective arguments being constant and equal to 90 degrees.

In the case of T_{22}, however, the reduction rate is high enough to reach zero within the frequency range of the measurements, in particular at about 335 Hz. Above that frequency the modulus is seen to increase again; now the dispersion of the data is significant but some kind of resonant effect is suggested at about 370 Hz. Besides, there is an obvious change in the argument, which now takes values close to 180 degrees, with a minimum of about 90 degrees at that resonance frequency of 370 Hz. Considering the initial decaying trend of the modulus of T_{11}, this element might also have another switching frequency somewhere around 450 Hz. However, possibly because of the resonance phenomena at 370 Hz mentioned above, the modulus becomes zero much earlier, at about 350 Hz, and then increases abruptly, while the argument is seen to increase and then reduce sharply down to zero again. Indeed this is in line with the possible presence of resonance phenomena, though the degree of dispersion gets too high for adequate interpretation of the data.

The values of the experimental transmission matrix of de Jong's pump were processed to determine the corresponding scattering matrix elements, which are shown in Fig. 5.7. For this pump the modulus of S_{11} and S_{22} at 0 Hz are equal to zero, whereas the modulus of S_{12} and S_{21} are equal to 1. This is because in this case the diameters of the inlet and outlet pipes are identical, and so no reflection is to be expected at the pump ports at 0 Hz, i.e. all the incoming sound is transmitted through the pump. Therefore, the acoustic behavior of the pump is only governed by the internal cavity geometry of the pump, with arguments for S_{12} and S_{21} that start at 0 degrees at 0 Hz whereas the arguments of S_{11} and S_{22} start at -90 degrees. As expected, increasing the frequency makes the modulus of S_{11} and S_{22} increase and the modulus of S_{12} and S_{21} decrease, while the arguments of the four elements reduce progressively. However the trends of the data exhibit significant perturbations above 300 Hz, which are to be attributed to the resonance phenomena suggested above.

Both Figs. 5.7 and 5.8 show that the predictions obtained with the new ITM model are in good qualitative and quantitative agreement with the experimental data. In particular the ITM model gives a prediction for the switching frequency of the element T_{22} of about 340 Hz, which is just 1.5 % higher than the experimental value of 335 Hz. At that frequency, the predicted argument is seen to switch from 0 to 180 degrees more sharply than the experimental data, because predictions are not affected by any other external resonance phenomena. Analogously, predictions from the ITM model for the element T_{11} suggest a switching frequency slightly above 450 Hz, which is consistent with the initial trend of the experimental data as discussed above. Besides, the predictions for the elements of the scattering matrix follow reasonably close the average trending lines of the measurements, especially for the arguments, for frequencies up to about 300 Hz. For higher frequencies the mismatch degree becomes higher since the experimental data exhibit sudden behavior changes as well as increasing dispersion, but as a whole predictions can be considered satisfactory.

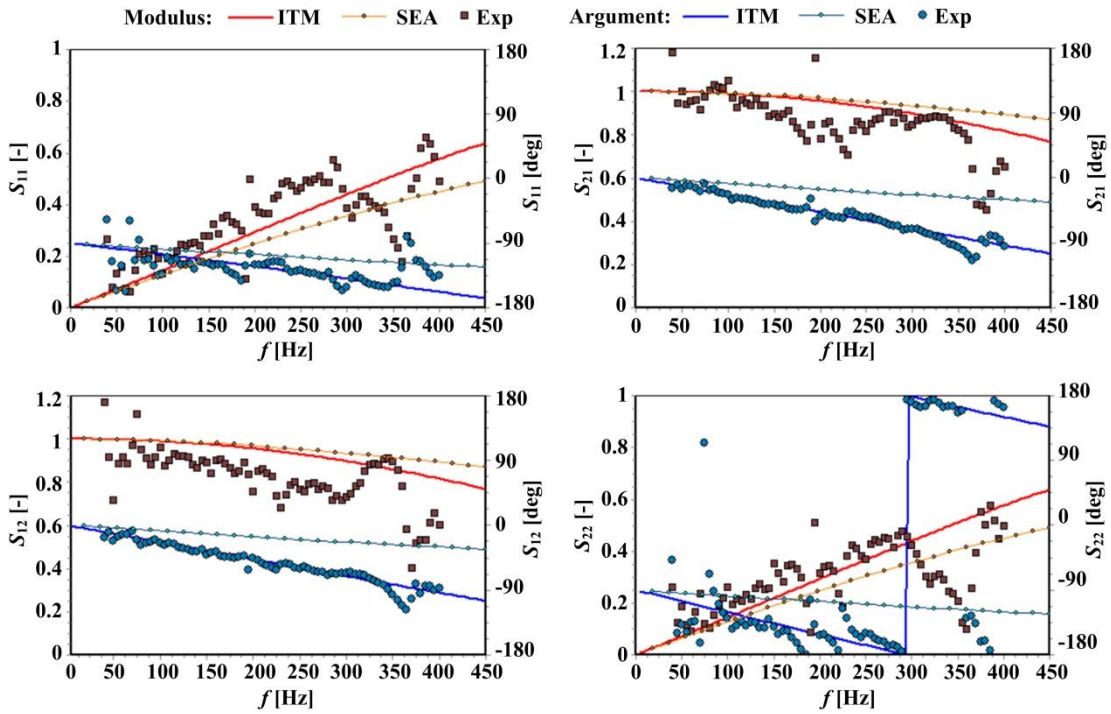

Fig. 5.7. Elements of the scattering matrix determined for the reference pump. ITM= internal transfer matrix model, SEA= Stirnemann's electrical analogy, Exp= data by de Jong (1996)

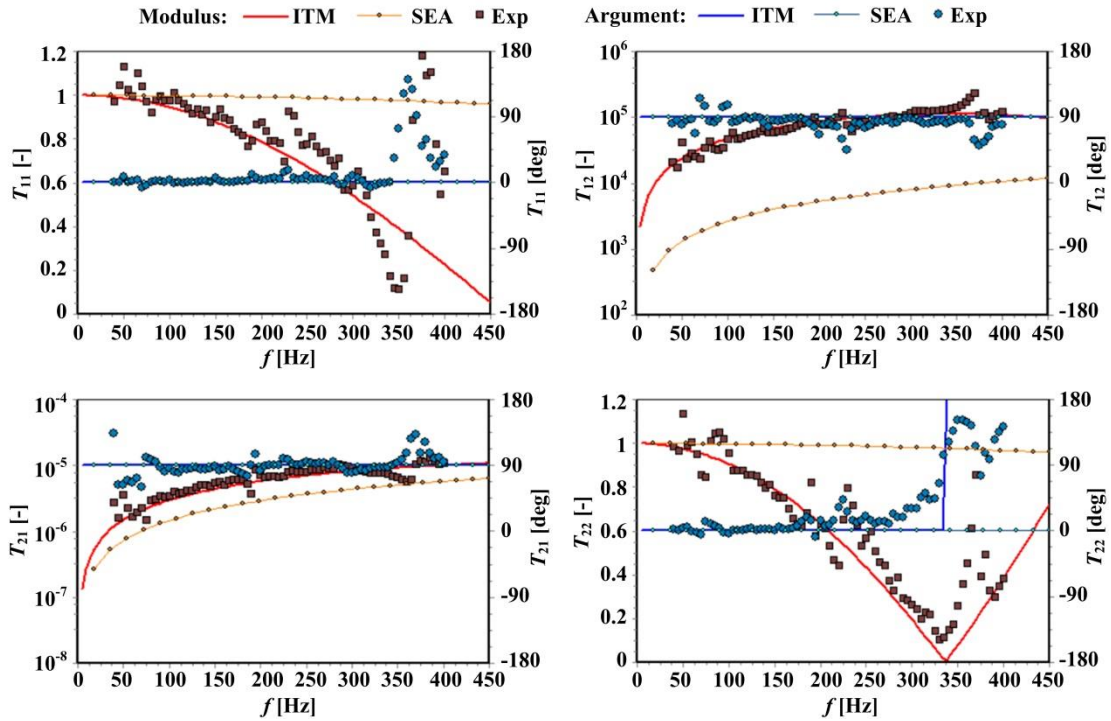

Fig. 5.8. Elements of the transmission matrix determined for the reference pump. ITM= internal transfer matrix model, SEA= Stirnemann's electrical analogy, Exp= data by de Jong (1996)

Finally, the predictions obtained from the Stirnemann's electric analogy model can be seen to be in good agreement with measurements only at the very low frequency range, for both transmission and scattering matrix. Increasing the frequency makes the SEA predictions to increase or reduce according to the variations observed in the measurements. However the rate of change of the SEA predictions with frequency happens to be very small, whereas the measurements (as well as the ITM predictions) show a strong frequency dependence, including the existence of a switching frequency for T_{22}. So, the correlation between SEA predictions and experimental data is poor, especially for the transmission matrix elements.

5.4 Contrast against the experimental data reported by Han

Han et al. (2003) provide a test method that can accurately estimate the pump acoustic transmission matrix. At the same time, it is obtained through experimental comparison that the transmission matrix of the pump is similar regardless of whether the pump is running or not. This shows that a relatively weak external sound source and a pump circuit system without cavitation can be used to determine the full-scale pump transmission matrix with the pump in standstill conditions. In this section, the experimental results of de Jong (1996) will be used to evaluate the predictive capacity of the internal transfer matrix model. The specific speed and main geometrical data reported for the pumps tested by Han et al. (2003) are shown in Table 5.6.

Table 5.6. Main data reported for the pumps tested by Han et al. (2003)

Pump designation	Value
Specific speed (non-dimensional), n_s	0.25
Diameter of suction port, d_S [mm]	89
Diameter of discharge port, d_D [mm]	48
Number of blades, z_B	4
Radius at impeller outlet, r_2 [mm]	114.5

The acoustic model operates with other non-reported input data, so they were estimated according to the pump specific speed and the corresponding general shape. Table 5.7 lists the main data assumed. Other model parameters were taken as constant for the reference pump model, including: sound speed c_0=1450 m/s (based on Han et al. 2003), peripheral expansion factor k_P =2 and first blade angular position φ_1=30 °.

Table 5.7. Additional geometric data for the pumps tested by Han et al. (2003)

Pump designation	Value
Radius at tongue tip, r_3 [mm]	130

Width at impeller outlet, b_2 [mm]	8
Outlet blade angle relative to tangent, β_2 [deg]	25
Volute width, b_3 [mm]	32
Throttle cross-section, A_T [cm^2]	8
Length suction port to impeller eye, L_{SE} [mm]	60
Length throttle to discharge port, L_{TD} [mm]	115

Figure 5.9 presents the comparison between the experimental data and the prediction data (derived from the ITM model and the SEA model respectively) of the scattering matrix of the pump. For the modulus of T_{22}, the change rate of ITM prediction results with frequency is slightly smaller than the change rate of measurement results with frequency. For the rest elements of the scattering matrix, the prediction results of adopting ITM are quite satisfactory. The increasing trends of the elements predicted by the SEA model with frequency are similar to those of the measurement data, but the change rate of modulus and argument with frequency is obviously too slow. Therefore, it can be considered that the ITM predictions are reasonably consistent with the measurements, especially regarding the argument.

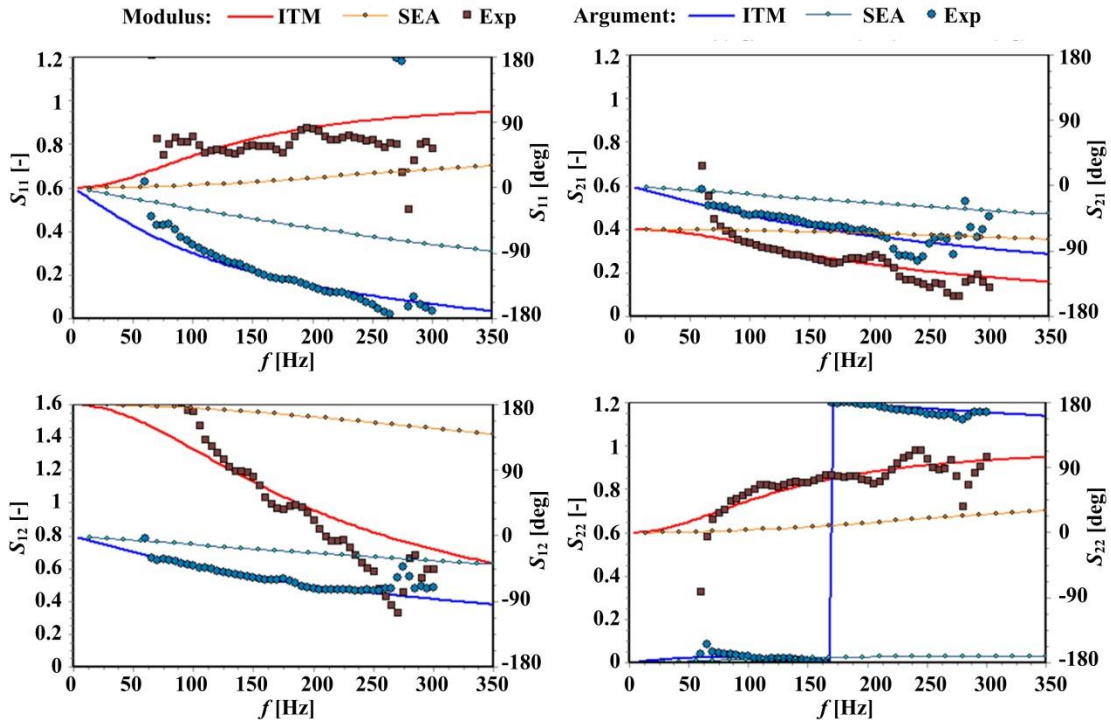

Fig. 5.9. Elements of the scattering matrix determined for the reference pump. ITM= internal transfer matrix model, SEA= Stirnemann's electrical analogy, Exp= data by Han et al. (2003)

Figure 5.10 presents the comparison between the experimental data and the prediction data (derived from the ITM model and the SEA model respectively) of the

scattering matrix of the pump. According to the comparison with the measurement results, it can be seen that the adoption of the ITM has a fairly good prediction for the elements of the pump transmission matrix reported by Han et al. (2003). It is worth noting that the prediction of the argument of T_{22} occurs a monotonic change around the frequency of 200 Hz, which is consistent with the change in the measurement result, whereas the prediction of the SEA model has poor correlation with experimental data.

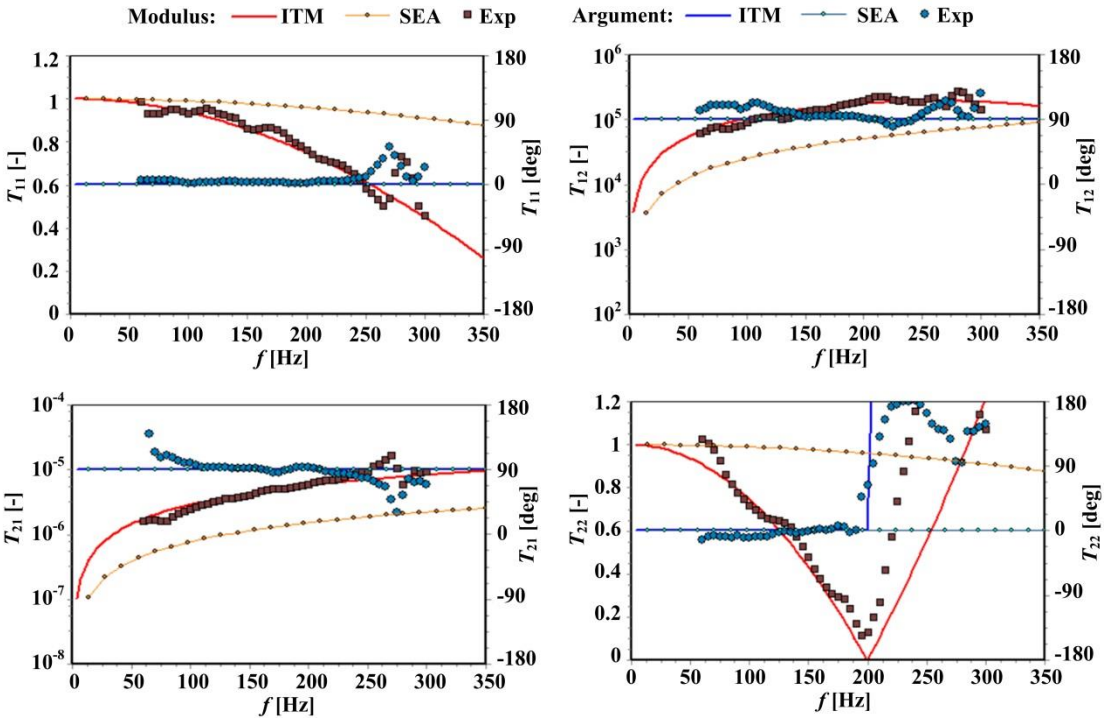

Fig. 5.10. Elements of the transmission matrix determined for the reference pump. ITM= internal transfer matrix model, SEA= Stirnemann's electrical analogy, Exp= data by Han et al. (2003)

5.5 Contrast against the experimental data reported by Bardeleben

Bardeleben (2005) obtained the scattering matrix of a centrifugal pump with a non-dimensional specific speed of 0.312 through the experimental method. Based on the internal transfer matrix model, the prediction of the scattering matrix and transmission matrix of the low specific speed centrifugal pump helps to further realize the application range of the novel model. The main geometrical data reported for the pumps tested by Bardeleben (2005) are shown in Table 5.8.

Table 5.8. Main data reported for the pumps tested by Bardeleben (2005)

Pump designation	Value
Specific speed (non-dimensional), n_s	0.312
Diameter of suction port, d_S [mm]	101.6
Diameter of discharge port, d_D [mm]	76.2
Number of blades, z_B	5
Radius at impeller outlet, r_2 [mm]	172.5
Radius at tongue tip, r_3 [mm]	182
Width at impeller outlet, b_2 [mm]	9
Outlet blade angle relative to tangent, β_2 [deg]	28
Volute width, b_3 [mm]	40
Throttle cross-section, A_T [cm^2]	32
Length suction port to impeller eye, L_{SE} [mm]	115
Length throttle to discharge port, L_{TD} [mm]	110

Fig. 5.11 shows the correspondence between the experimental data and the prediction data (derived from the ITM model and the SEA model respectively) of the pump scattering matrix. In the experiment process, it is difficult to avoid the experimental data showing a certain degree of dispersion. Therefore, comparing the predictions of the ITM and the SEA, the predictions of the ITM can in general be considered satisfactory with the measurement results, especially in terms of arguments. But the predictions of the SEA model in modulus and argument have poor correlated with experimental data. In other words, the SEA model does not apply to the prediction of the scattering matrix in the pump reported by Bardeleben (2005).

Fig. 5.12 shows the correspondence between the experimental data and the prediction data (derived from the ITM model and the SEA model respectively) of the pump transmission matrix. It can be seen that the measurement data of T_{12} and T_{11} show relatively serious dispersion. But within the test frequency range, the ITM prediction data is still located within a series of experimental points. In addition, the ITM has quite satisfactory predictions against the elements T_{11} and T_{21}, so it can be considered that the ITM is suitable for the transmission matrix prediction in the pump reported by Bardeleben (2005). However, the SEA model failed to effectively predict the elements of the transmission matrix in the measurement results, especially for modulus in T_{11} and T_{22}.

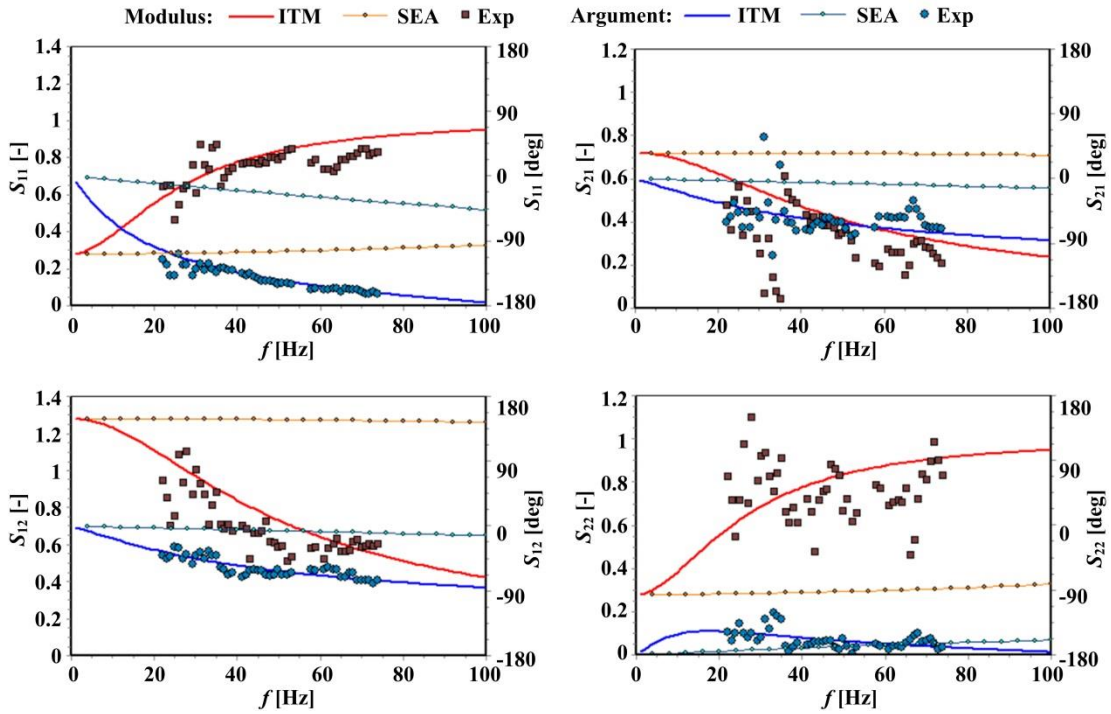

Fig. 5.11. Elements of the scattering matrix determined for the reference pump. ITM= internal transfer matrix model, SEA= Stirnemann's electrical analogy, Exp= data by Bardeleben (2005)

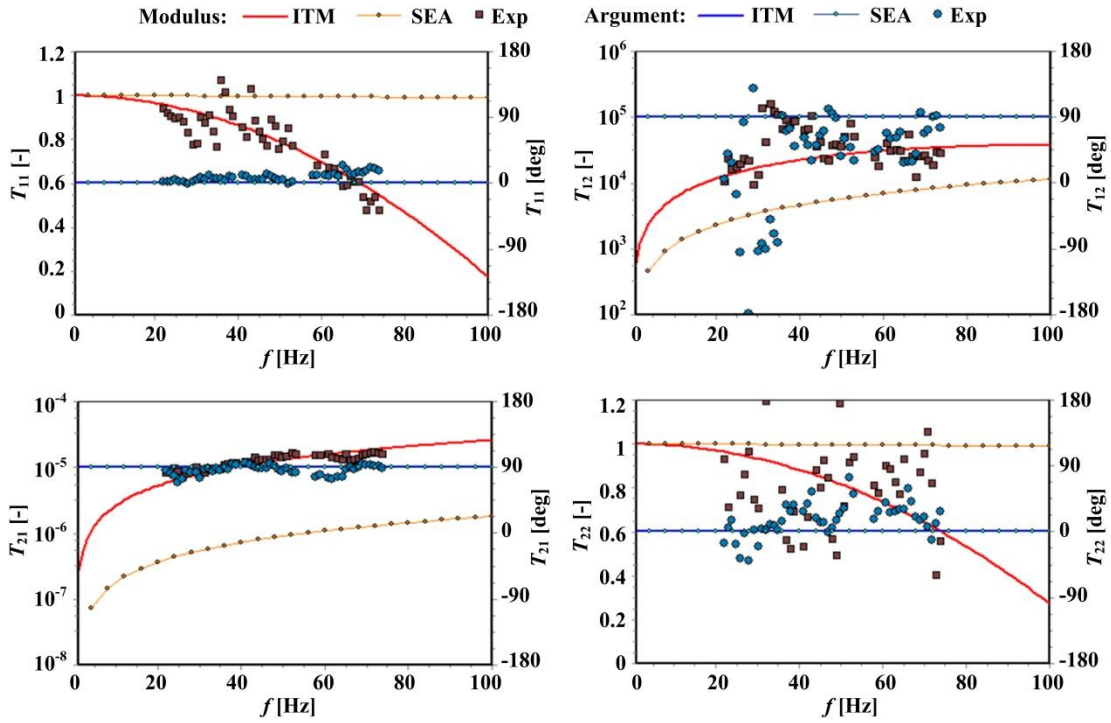

Fig. 5.12. Elements of the transmission matrix determined for the reference pump. ITM= internal transfer matrix model, SEA= Stirnemann's electrical analogy, Exp= data by Bardeleben (2005)

5.6 Contrast against the experimental data reported by Brümmer

The specific speed and main geometrical data reported for the pumps tested by Brümmer et al. (2019) are shown in Table 5.9. Pumps #1, #2 and #3 have the same inlet and outlet diameters, but their specific speed increases by a factor above 2. This indicates that the nominal flow-rate at a given rotational speed is in the same range for the three pumps, while the nominal head reduces to almost half. In consequence the size of the internal cross-section passages should be similar for the three pumps, whereas the external diameter of the impeller as well as the radial size of the casing reduce progressively from pump #1 to pump #3. Pump #4 has the same specific speed of pump #1 but its size is larger. Since the optimal geometry of fluid machinery depends basically on the specific speed, it is to be expected that pumps #1 and #4 are geometrically similar, with an approximate length scale factor of 100/65. Finally, pump #5 is identical to pump #1 except that the impeller was trimmed to an outside radius r_2 = 82.5 mm.

Table 5.9. Main data reported for the pumps tested by Brümmer et al. (2019)

Pump designation	#1 (#5)	#2	#3	#4
Specific speed (non-dimensional), n_s	0.46 (0.63)	0.70	0.99	0.46
Diameter of suction port, d_S [mm]	80	80	80	125
Diameter of discharge port, d_D [mm]	65	65	65	100
Number of blades, z_B	6	6	6	6
Radius at impeller outlet, r_2 [mm]	109.5 (82.5)	87.0	70.5	168.0
Radius at tongue tip, r_3 [mm]	117.6	96.6	78.8	180.5

The acoustic model operates with other non-reported input data, so they were estimated according to the pump specific speeds and the corresponding general shapes that manufactures use for each specific speed. Table 5.10 lists the main data assumed. Other model parameters were taken as constant for the five pump models, including: sound speed c_0=1350 m/s (based on Brümmer et al. 2019), peripheral expansion factor k_P =2 and first blade angular position φ_1=30 °.

Table 5.10. Additional geometric data for the pumps tested by Brümmer et al. (2019)

Pump designation	#1 (#5)	#2	#3	#4
Width at impeller outlet, b_2 [mm]	7.5	9.5	13	12
Outlet blade angle relative to tangent, β_2 [deg]	32	35	38	22
Volute width, b_3 [mm]	50	45	40	85
Throttle cross-section, A_T [cm^2]	18	18	18	40

Length suction port to impeller eye, L_{SE} [mm]	80	80	80	150
Length throttle to discharge port, L_{TD} [mm]	200	135	100	300

Brümmer et al. (2019) reported the scattering matrix data at seven specific frequencies between 150 Hz and 290 Hz for all the pumps but pump #4, for which data refers to 10 frequencies between 95 and 190 Hz. As an example, Fig. 5.13 shows the experimental data corresponding to pump #4 together with the predictions derived from the ITM as well as from the SEA. Though the experimental data exhibit some dispersion, the ITM predictions can be considered in reasonable agreement with the measurements, especially regarding the argument. On the other hand, the trends of the parameters predicted with the SEA model for increasing frequency are similar to those of the experimental data, but the rate of variation of both modulus and argument with frequency is clearly too slow. This is consistent with the comparison in Fig. 4.8 between the modulus of the transmission matrix elements predicted from both models.

Reciprocity relationships are readily apparent when comparing the data for the four elements of the scattering matrix in Fig. 5.13. For instance, the predicted moduli of the elements S_{11} and S_{22} at any given frequency are identical, and the corresponding experimental values are also very similar. The same happens regarding the argument of elements S_{12} and S_{21}.

Pump #4:

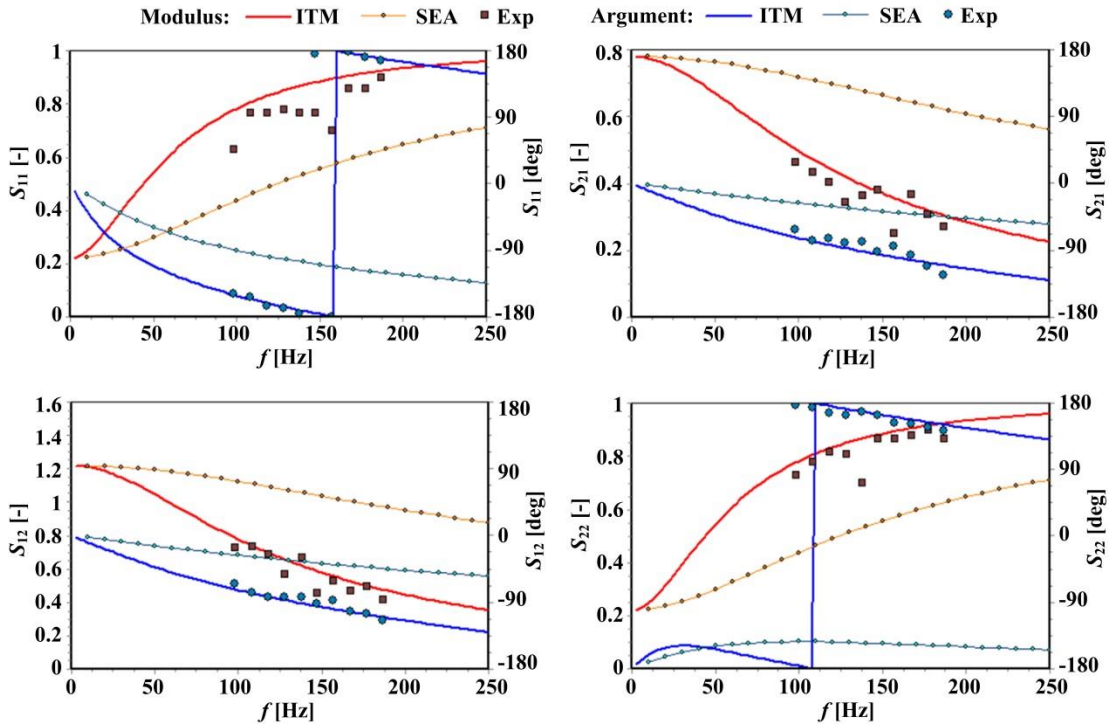

Fig. 5.13. Elements of the scattering matrix determined for Pump #4. ITM= internal transfer matrix model, SEA= Stirnemann's electrical analogy, Exp= data by Brümmer et al. (2019)

Fig. 5.14 presents the experimental data and predictions corresponding to elements S_{21} and S_{22} for the rest of the pumps. Again, accordance with measurements can in general be considered fairly satisfactory with respect to the ITM predictions, whereas the SEA predictions diverge significantly from measurements when increasing the frequency.

Comparing the results for pumps #1, #2 and #3, it is readily observed that all of them present the same values at very low frequency, as correspond to machines that have input and output ports with the same cross-sections. On the other hand, the effect of frequency is qualitatively similar to that of an intermediate expansion chamber, whose volume changes from one pump to another. Among the three of them, pump #1 appears as the most sensitive one with respect to frequency, which is to be attributed to the larger size of its volute casing in the radial direction in order to allocate the impeller with the highest diameter. However the internal geometry of the pumps is indeed more complex than just having an expansion chamber with the volume of the pump casing. In fact, that volume is explicitly assumed in the SEA model (Eq. (4.2)), but the predictions are poorly correlated with the experimental data, as further discussed below.

The sensitivity to frequency still augments somewhat when considering pump #5 instead of pump #1, because the trimming of the impeller brings about a slight increment in the effective volume of the casing chamber. Nonetheless, the impact of impeller trimming on the pump scattering matrix is very small, as already observed for the pump in Fig. 4.11.

Pump #1:

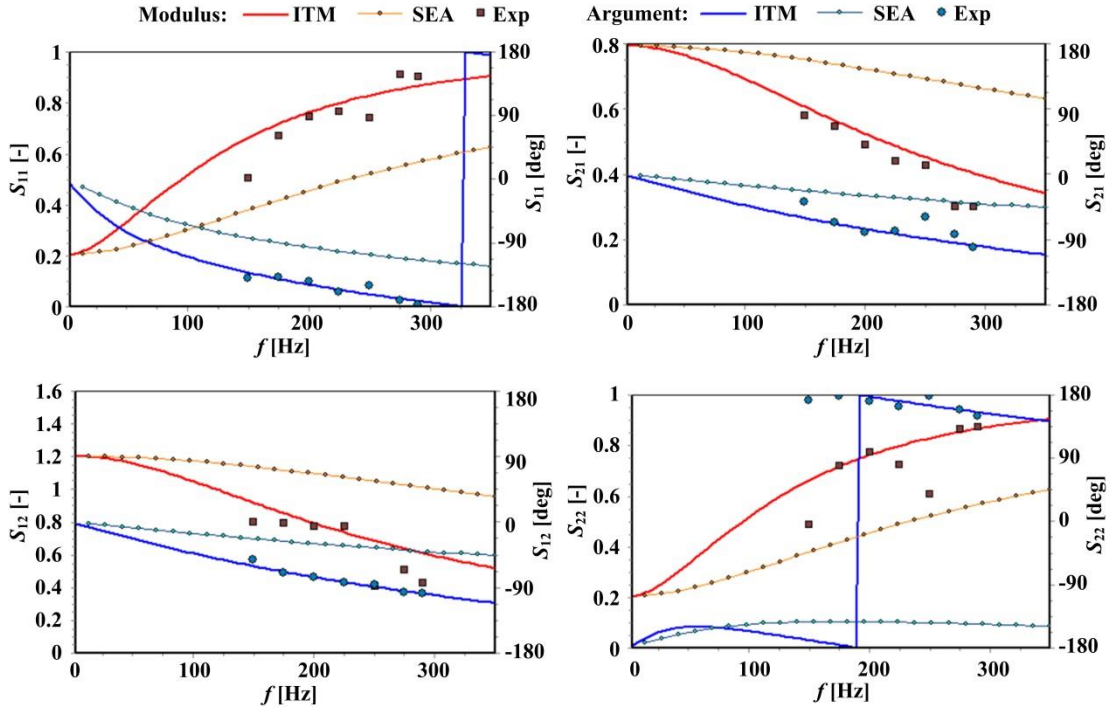

Pump #2:

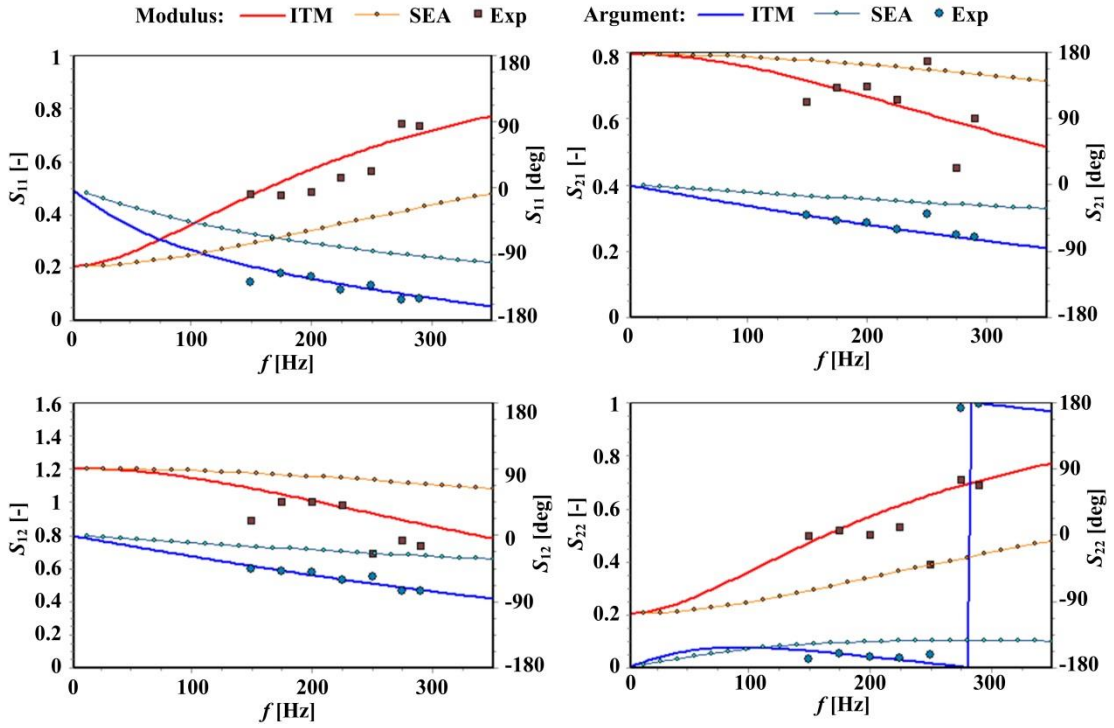
Modulus: ITM SEA Exp
Argument: ITM SEA Exp
S11 [-]
S11 [deg]
S21 [-]
S21 [deg]
S12 [-]
S12 [deg]
S22 [-]
S22 [deg]
f [Hz]

Pump #3:

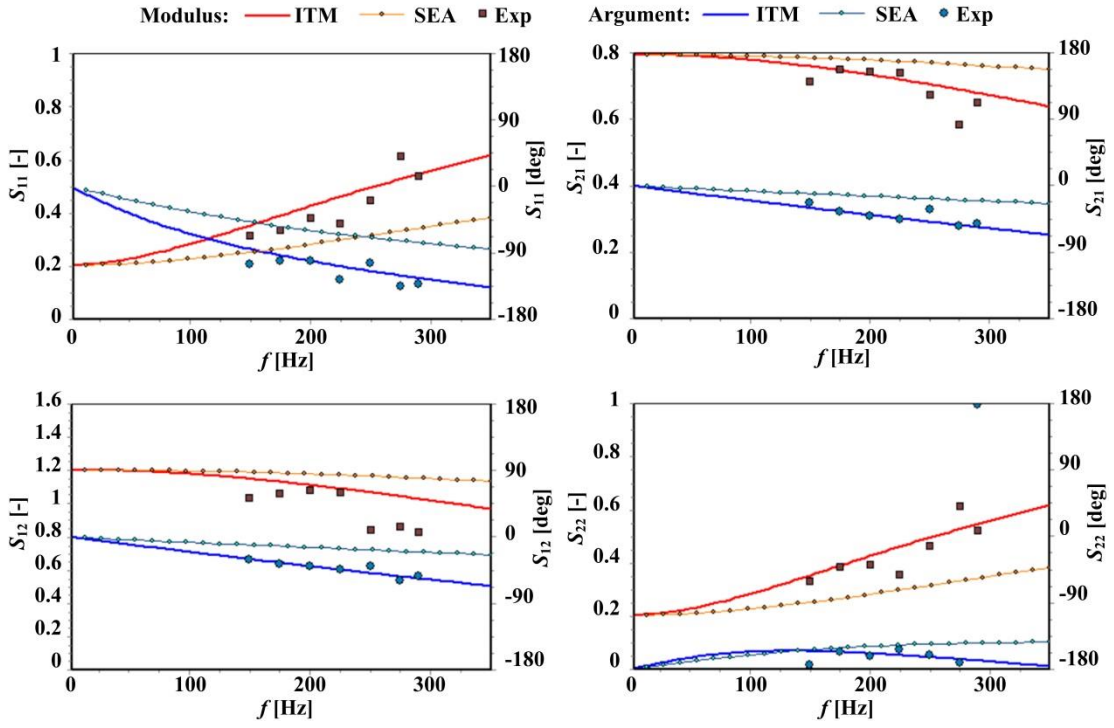
Modulus: ITM SEA Exp
Argument: ITM SEA Exp
S11 [-]
S11 [deg]
S21 [-]
S21 [deg]
S12 [-]
S12 [deg]
S22 [-]
S22 [deg]
f [Hz]

Pump #5:

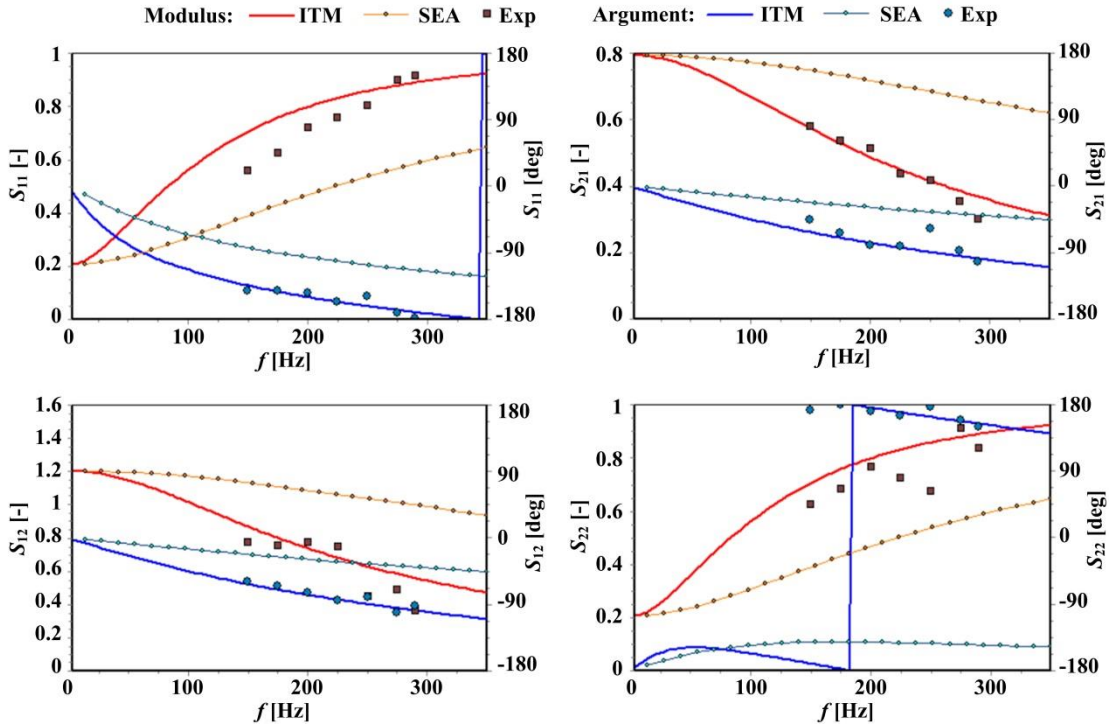

Fig. 5.14. Elements of the scattering matrix determined for several pumps. ITM= internal transfer matrix model, SEA= Stirnemann's electrical analogy, Exp= data by Brümmer et al. (2019)

Finally, it is interesting to compare the data for pumps #1 (Fig. 5.14) and #4 (Fig. 5.13). As expected for geometrically similar pumps with different size, the respective curves of the scattering parameters appear to be shifted in the frequency scale by an amount approximately equal to the length scale factor. This has already been shown by Brümmer et al. (2019) by using a Helmholtz number to scale the frequency axis.

Fig. 5.15 presents the experimental data and predictions corresponding to modulus and argument of transmission matrix elements for the several pumps. For the four elements of the transmission matrix, it can be clearly found that the T_{12} and T_{21} modulus predictions derived from the ITM and the SEA of the rest pump have relatively similar trends with the measurement results except for Pump #4. But the predictions derived from the SEA model still have a large deviation from the measurement results. That is, the predictions derived from the ITM are better. Regarding the prediction of T_{11} and T_{22} modulus, though the experimental data shows a certain degree of dispersion, the ITM predictions can be considered in reasonable agreement with the measurements, whereas the SEA predictions diverge significantly from measurements.

Pump #1:

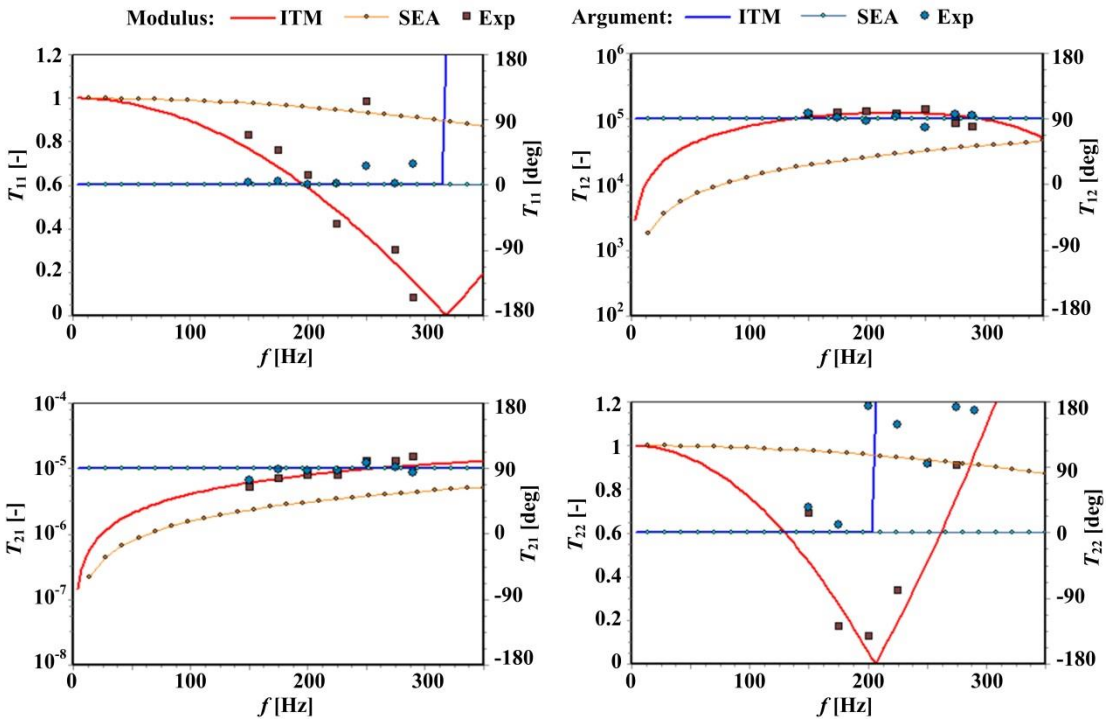
Modulus: ITM SEA Exp
Argument: ITM SEA Exp
T_{11} [-]
T_{11} [deg]
T_{12} [-]
T_{12} [deg]
T_{21} [-]
T_{21} [deg]
T_{22} [-]
T_{22} [deg]
f [Hz]

Pump #2:

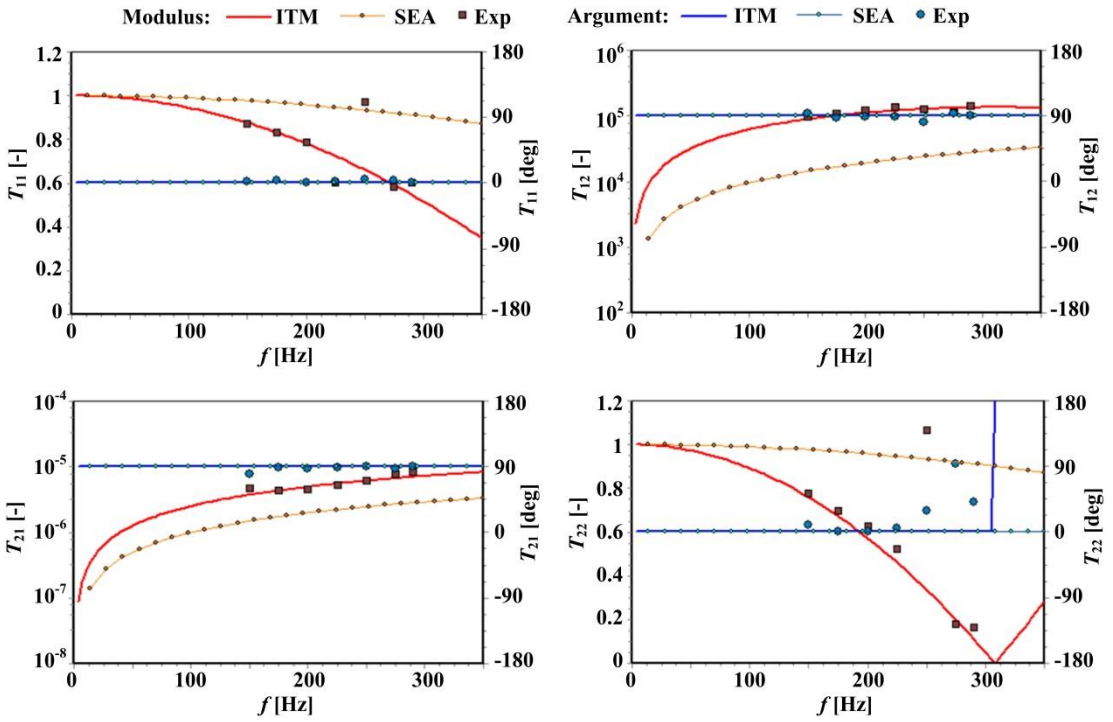
Modulus: ITM SEA Exp
Argument: ITM SEA Exp
T_{11} [-]
T_{11} [deg]
T_{12} [-]
T_{12} [deg]
T_{21} [-]
T_{21} [deg]
T_{22} [-]
T_{22} [deg]
f [Hz]

Pump #3:

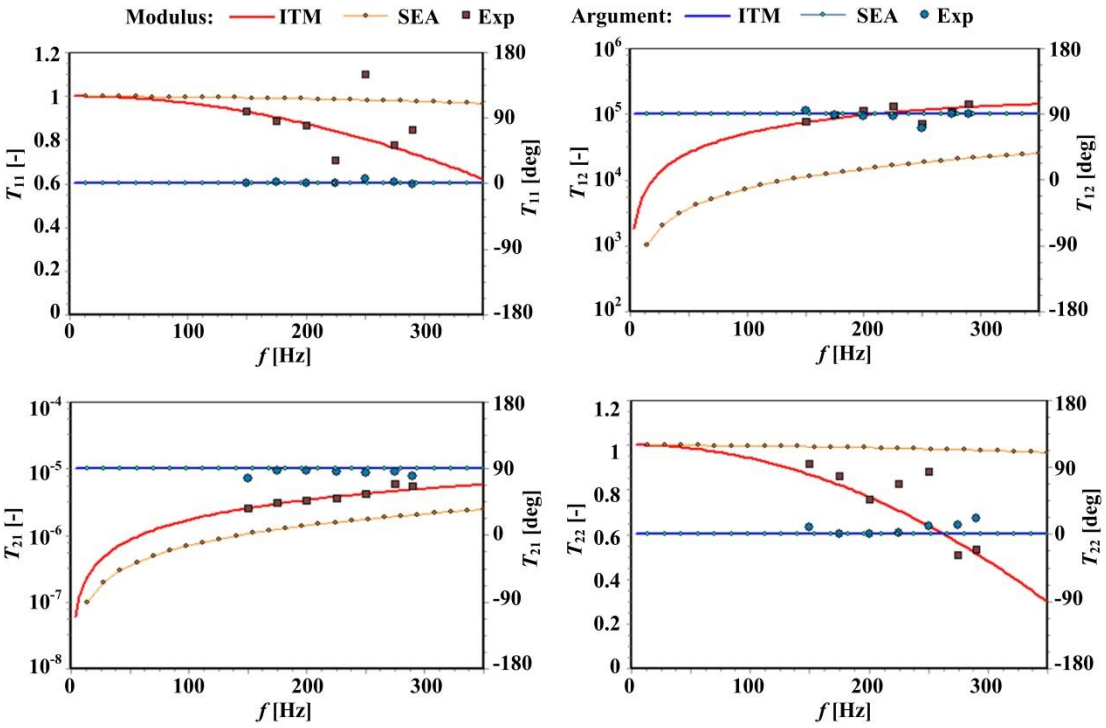
Modulus: ITM SEA Exp
Argument: ITM SEA Exp
T_{11} [-]
T_{11} [deg]
T_{12} [-]
T_{12} [deg]
T_{21} [-]
T_{21} [deg]
T_{22} [-]
T_{22} [deg]
f [Hz]

Pump #4:

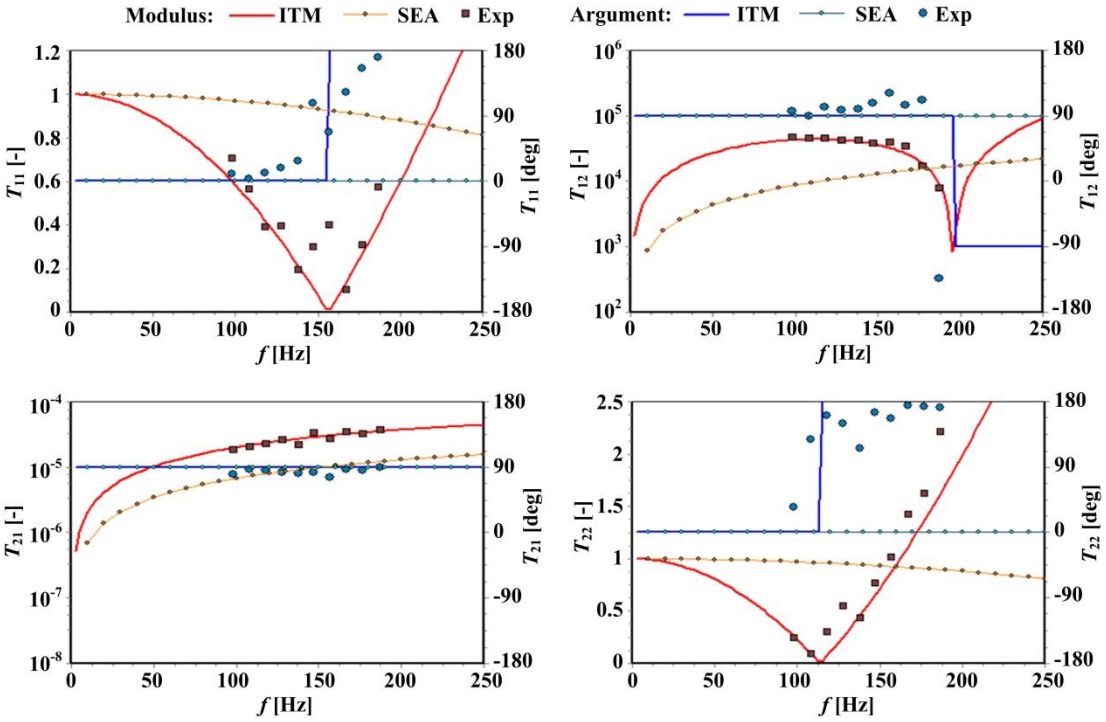
Modulus: ITM SEA Exp
Argument: ITM SEA Exp
T_{11} [-]
T_{11} [deg]
T_{12} [-]
T_{12} [deg]
T_{21} [-]
T_{21} [deg]
T_{22} [-]
T_{22} [deg]
f [Hz]

Pump #5:

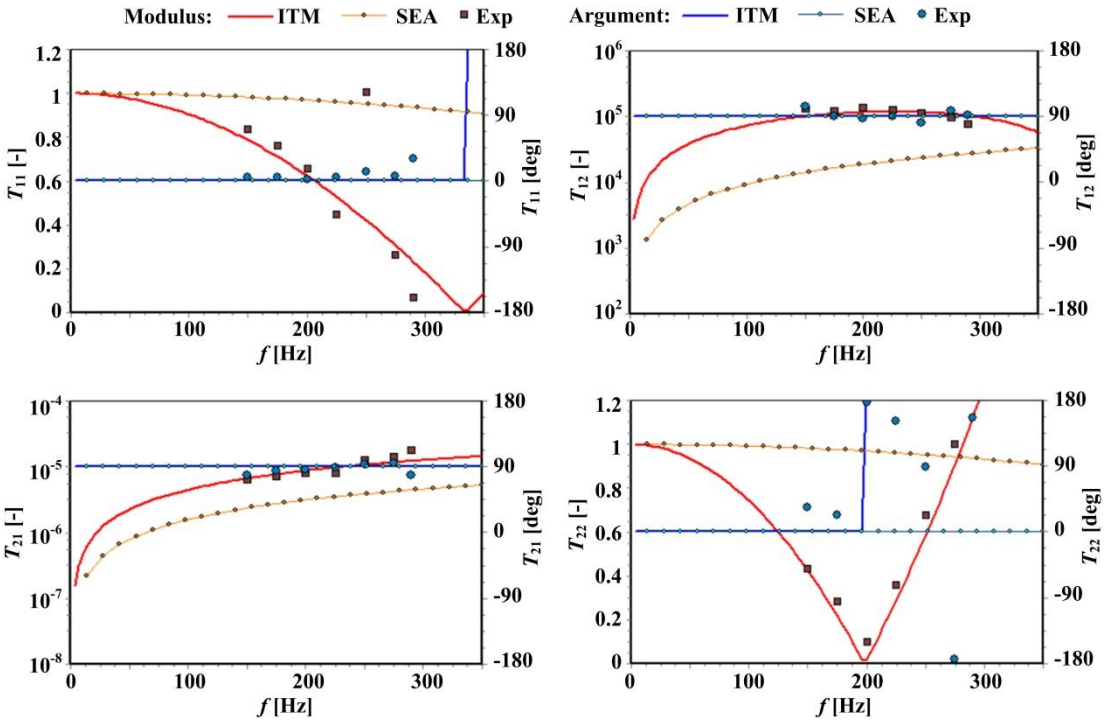

Fig. 5.15. Elements of the transmission matrix determined for several pumps. ITM= internal transfer matrix model, SEA= Stirnemann's electrical analogy, Exp= data by Brümmer et al. (2019)

5.7 Variance ratio of predictions for each pump

At some point, it is very necessary that we needed to quantify how close or far were our predictions from the experimental data, i.e., the prediction error. However, that error parameter should also take into account that the experimental data we have usually present a very high degree of scatter. Therefore, an especial quality parameter was defined in order to quantify how close or far are predictions from the available experimental data, while taking into account that the experimental data can present some dispersion. The parameter used has been a variance ratio, VR, defined as the variance of the predictions relative to the experimental data (i.e., the mean squared error) divided by the variance of the experimental data relative to their average value. In particular, the variance ratio VR that corresponds to any of the four elements s of the pump scattering matrix has been calculated by means of Eq. (5.1):

$$\mathrm{VR}(s) = \frac{\sum_{i=1}^{n}[(s_{PRi} - s_{ERi})^2 + (s_{PIi} - s_{EIi})^2]}{\sum_{i=1}^{n}[(s_{ERi} - \overline{s_{ER}})^2 + (s_{EIi} - \overline{s_{EI}})^2]} \tag{5.1}$$

where s is any of the four elements of the pump scattering matrix, n is the number of experimental data available, subscripts E and P denote experimental or predicted values at the same frequency and subscripts R and I denote real or imaginary

components. According to the definition, this variance ratio parameter can only take positive values, the closer VR to zero, the better the predictions.

This VR parameter is adequate to quantify and compare the goodness of the predictions for a given set of experimental data when geometry or calculation parameters are modified in the program. And it can also be used to compare the goodness of the predictions for different pumps, though in this case comparison can be affected by having experimental data with different variance values.

Fig. 5.16 shows the VR parameters so obtained for each element of the scattering matrix and for the five pumps tested by Brümmer et al. (2019). The predictions derived from the new internal transfer matrix model (ITM) give VR parameters always below 0.85, the lowest one usually associated to the suction reflection element S_{11}. The average VR for each pump lies in the range 0.5-0.6 except for pump #4, which takes a somewhat lower value, about 0.35, possibly because of having more experimental data available for that pump. Therefore, it may be concluded that the ITM model performs similarly and reasonably well regardless the pump specific speed, i.e., it does not really show a shape dependence. And the results for pump #4 suggest that there is no size dependence either.

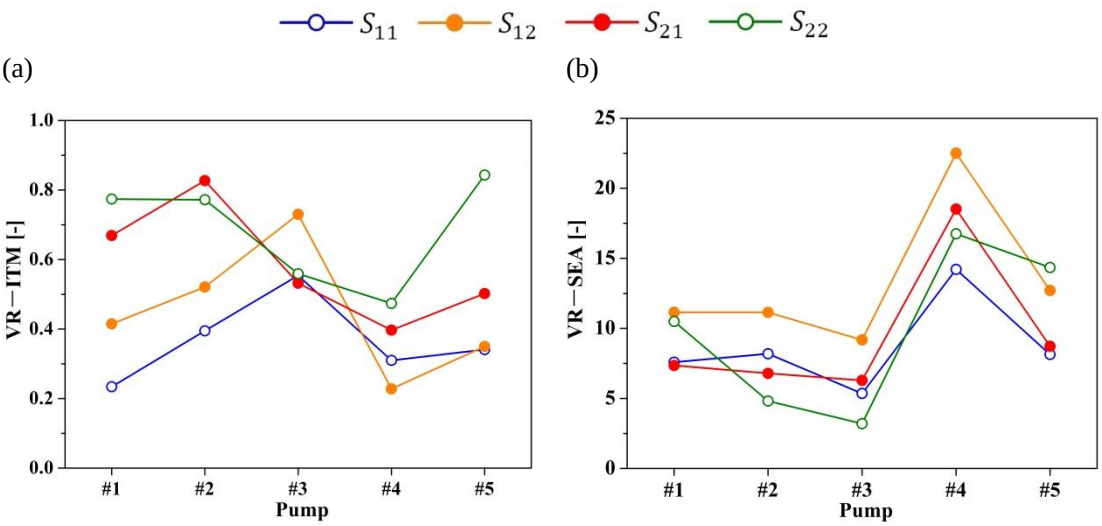

Fig. 5.16. Variance ratio parameter for the elements of the scattering matrix of five pumps tested by Brümmer et al. (2019). Predictions from (a) internal transfer matrix model and (b) Stirnemann's electrical analogy

In comparison, the VR values corresponding to the predictions from Stirnemann´s electrical analogy (SEA) with Eqs. (4.1-4.2) are at least one order of magnitude larger. Predictions are especially poor for pump #4 and even worse for pump #5. Considering that discrepancies between measurements and SEA predictions arise because the latter change too little with frequency (as seen in Figs. 5.13 and 5.14, it may be concluded that Eq. (4.2) systematically underpredicts the equivalent impedance and admittances of the pump. That becomes more evident

when the volume of the volute casing increases in the radial direction with respect to the impeller, either because the entire pump is bigger (pump #4) or because the impeller is shorter (pump #5). The latter is also supported by the slight reduction of the average VR that exhibits Fig. 5.16 (b) when going from pump #1 to #2 and #3, i.e., when increasing the specific speed.

Table. 5.11 lists the VR parameters so obtained for each element of the scattering matrix and for the pumps tested by different researchers. For the pump tested by de Jong (1996), the VR values of S_{11} and S_{22} of the predictions from ITM model are larger relative to those of S_{12} and S_{21}, which is related to significant perturbations in the experimental data trends above 300 Hz, as shown in Fig. 5.7. Similar situation also appears in the VR values of predicted data S_{21} and S_{22} for Bardeleben (2005), which is caused by the dispersion of experimental data (Fig. 5.11). For the pump tested by Han et al. (2003), the VR values of the elements of the scattering matrix derived from the ITM model are all lower than 0.35, so it may be concluded that the ITM model shows a relatively good predictive ability. In the pumps tested by this paper and Stirnemann et al. (1987), the predictions derived from the ITM model give VR parameters always lower than those from the SEA model. This further shows that the ITM model can better predict the elements of the scattering matrix of the reference pumps.

Table 5.11. Variance ratio parameter for the elements of the scattering matrix of the pumps tested by different researchers

Elements / Researchers	VR－ITM [-]				
	S_{11}	S_{12}	S_{21}	S_{22}	Average
Stirnemann et al. (1987)	1.208	0.296	2.001	1.603	1.277
de Jong (1996)	0.942	0.235	0.162	1.044	0.59575
Han et al. (2003)	0.294	0.303	0.337	0.269	0.30075
Bardeleben (2005)	0.388	0.557	1.81	1.127	0.9705
Test pump (this paper)	0.945	1.01	1.348	1.417	1.18
Elements / Researchers	VR－SEA [-]				
	S_{11}	S_{12}	S_{21}	S_{22}	Average
Stirnemann et al. (1987)	0.885	2.367	3.097	2.722	2.26775
de Jong (1996)	1.119	2.625	2.244	2.862	2.2125
Han et al. (2003)	2.323	2.916	2.802	2.535	2.644
Bardeleben (2005)	21.383	20.517	15.533	5.517	15.7375
Test pump (this paper)	4.667	2.946	3.399	3.209	3.55525

Chapter 6 Conclusions

6.1 Experimental procedure and method

In order to study experimentally the passive acoustic properties of the test pump, it is necessary to impose external acoustic loads on that pump while measuring pressure fluctuations at several positions along the connected pipes. In this research, the external acoustic loads were accomplished by having another auxiliary pump operating in the same hydraulic system to play the role of an external speaker. The main conclusions obtained are as follows:

1. The auxiliary pump proved to be a very effective generator of pressure pulsations at its blade-passage frequency, which could be modified by varying the pump speed, as far as the pump was operated at a low flow-rate by partially closing a regulation valve. This procedure allowed to get pressure fluctuations at the pump discharge pipe with typical amplitudes ranging between 500 Pa and 3 kPa at the blade-passing frequency.

2. The pressure fluctuations generated by the auxiliary pump were transmitted through the pipe system until the zone of test pump, inducing pressure fluctuations at the suction and discharge pipes of the test pump with amplitude ranging typically between 200 Pa to 1 kPa at the frequency excited by the auxiliary pump. In consequence the pulsations received at the test pump were high enough to be detected and measured with sensitive transducers as the piezoelectric pressure sensors used in this research.

3. The experimental facility demonstrated to give a good control capability of the external acoustic load on the test pump, by means of
   i) changing the rotation speed of the auxiliary pump,
   ii) controlling the opening of the regulation valve of the auxiliary pump and
   iii) opening or closing valves at branch pipes which result in pipeline configurations with different acoustic impedance.

4. Calibration checks conducted with four pressure sensors located radially at the same pipe cross-section indicated that the amplitude differences were less than 2% of the average value and the phase differences were less than 3 degrees with respect to the average value. These differences were considered reasonably low as to validate the measurement chain and, besides, it was demonstrated that pressure perturbations propagate in plane wave mode along the pipes of interest.

5. In order to reduce the dispersion of the final data on the scattering matrix as much as possible, the procedure was extended to include measurements under a variety of external acoustic loads instead of just two. Because of this, the decomposed pressure waves at the suction and discharge pipes of the test

pump bring about an overdetermined system of equations that can be solved by means of a least square error procedure.

6. The experimental results finally obtained for the scattering matrix of the test pump still denote a high dispersion degree, which is line with the results reported by other researchers. In the present case, possible reasons are:

   i) Some vibration is transmitted from the auxiliary pump to the piping system; though the vibration amplitude is very low the internal radiation surface of the pipes is high and so it might be able to affect the traveling sound pressure waves because of different vibration modes excited depending on the auxiliary pump frequency.

   ii) The straight length of the discharge pipe is short, which may cause the pressure values measured by the two pressure sensors on it to be too similar, so that good resolution cannot be obtained at low frequencies. This will have a certain degree of influence on the pressure wave decomposed at the discharge pipe, and further influence the elements of the scattering matrix obtained by the least square error procedure.

6.2 Acoustic model

In order to simulate the internal sound field in centrifugal pumps at low frequency (plane wave mode), a new model has been developed based on a selection of internal nodes connected by means of local transfer matrices, which are dependent on the pump geometry. In general, those local transfer matrices correspond to passages with variable cross-section, and so they were estimated by means of segmentation with the matrizant approach. This internal transfer matrix model has been used in a procedure to estimate either the global transfer matrix or the scattering matrix of a given pump as a function of frequency. The main conclusions obtained are:

1. The model defines a number of internal nodes that depends on the number of impeller blades, but is below 50 for the cases of interest. Continuity and transfer matrix relations between nodes plus boundary conditions results in a closed linear system of up to 100 equations with complex terms, i.e. with real and imaginary components. This system can be solved efficiently for the pressure and mass velocity fluctuations at every node by means of the classical Gauss decomposition method, though double pivoting is necessary.

2. The method of double imposition of external acoustic loads proved to be efficient to determine first the transmission matrix of a pump, and then the scattering matrix, for each frequency.

3. The low computational cost needed for the resolution of linear system that links the internal acoustic variables allows a fast computation of the pump scattering matrix for a range of frequencies even with a conventional

computer.

4. In relation with the segmentation approach used to establish the internal transfer matrices for passages with varying cross-section between nodes, it was concluded that more than 20 segments per transfer matrix did not virtually affect the final predictions.

5. The main acoustic events that determine the characteristics of the sound transmission through pumps are related to the volume and shape of the casing chamber, and, in particular, to the changes in cross-section that the waves encounter i) between the outlet of the impeller channels and the volute region and ii) at the throat between the volute region and the pump diffuser. Another influential event is the close location of the volute wall with respect to the outlet of the impeller channels, which behaves as an extended-tube resonator of the reversal type.

6. In particular, predictions happen to be somewhat sensitive to the parameter denoted as *peripheral expansion factor*, which is a model parameter that measures the expansion of the sound waves across the outlet of the impeller channels. A value in the range 2-2.5 is suggested for that factor, the higher the higher the number of impeller blades.

7. Predictions are sensitive too with respect to the outlet angle of the impeller blades, since sound is assumed to continue travelling along that direction when exiting the impeller channels.

8. In general the predictions obtained for a reference pump show that they are little sensitive to geometrical parameters that are not closely related to the pump specific speed or size. In particular, the number of blades has little effect for more than 5 blades. The diameter of the impeller, which may vary in practice in case of trimmed impellers while keeping the same casing, has little effect as well.

9. Since the model assumes that the impeller is not rotating, the angular position of the impeller blades relative to the tongue becomes another geometrical parameter of the pump. However, the effect of that angular position proved to be very small for the reference pump. This result is consistent with the empirical results reported by Carta et al. (2002), who measured the transmission matrix for a stopped pump with the impeller fixed at different angular positions.

6.3 Transmission properties of centrifugal pumps

The following conclusions have been obtained:

1. The transmission matrices predicted by the acoustic model contain reflection elements (main diagonal) that only have real part (argument equal to 0

degrees) and a value of 1 at zero frequency that reduces progressively while frequency is increased. On the other hand, the transmission elements only possess imaginary part and their value increase quickly with frequency. This is consistent with the model hypothesis and with the empirical data available from the literature.

2. The experimental results obtained for the pump tested in laboratory as well as the predictions derived from the new acoustic model indicate that, at very low frequency, the pump behaves as an element with an abrupt change in cross-section between the suction and the discharge ports, so that the modulus and phase of the elements of the scattering matrix can be obtained from the cross-section ratio.

3. Increasing the frequency up to 300 Hz brings about an increasing influence from the casing chamber of the pump, so that the reflection elements of the scattering matrix grow towards unity while the transmission elements decrease towards zero. Besides, the argument of the four elements of the scattering matrix reduce proportionally to frequency, which is consistent with constant equivalent internal distances and constant speed of sound.

4. The set of empirical data collected from the literature on the scattering matrix for nine different pumps (with non-dimensional specific speeds ranging from 0.25 to 1.03) indicates the same trends described above for the laboratory pump, with a higher dependence on frequency for higher sizes and lower specific speeds. This is because both factors indicate longer internal paths for the sound waves transmitted.

5. In order to quantify the degree of agreement between predictions and experimental data, a special variance ratio parameter was established, which represents the sum of square errors between predictions and measurements normalized by the variance of the empirical data relative to the average value.

6. For the case of the predictions obtained from the new internal matrix model, the variance ratio parameter gives values for most of the ten pumps considered that are well below 1 and close to 0. This indicates that the new model gives predictions of either the transmission or the scattering matrix that are reasonably close to the experimental data independently of the pump specific speed or size.

7. The experimental data collected was also compared to the predictions derived from Stirnemann's classical model (Stirnemann et al. 1987) based on an electrical analogy. While the predictions from this model indicate similar trends to the experimental data, the effect of frequency appears to be systematically underestimated, i.e., the values predicted for the elements of the scattering or the transmission matrix when increasing the frequency deviate very little from the values corresponding to zero frequency. The

corresponding variance ratio parameter is systematically greater than 1 and even greater than 10 in many cases, denoting large differences between predictions and measurements.

8. The discrepancies between empirical data and the predictions from the classical electric analogy model are higher for pumps with large size or low specific speed. It has been inferred that the values of the equivalent impedance and admittances considered in that model are systematically under-estimated, which is more obvious for pumps with large volute casing.

9. On the contrary, the new internal transfer matrix model has given predictions of the four elements of the scattering matrix and the transmission matrix, both in modulus and phase, that are in reasonable quantitative agreement with the experimental data, regardless the pump size or specific speed. As frequency is increased, its prediction capability clearly outperforms that of the electrical analogy model in all cases. In summary, the new model can be considered validated and an adequate tool to predict the passive acoustic features of centrifugal pumps.

6.4 Future work

The following research lines are suggested:

1. It is suggested to further investigate on the procedure to experimentally determine the scattering matrix of a test pump in laboratory, with a primary objective of reducing the degree of scatter of the results, possibly by preventing vibration transmission between elements of the hydraulic network. Also, the discharge pipe should be longer than in the present study. Reducing the dispersion of the data should result in higher accuracy and reliability, which is necessary for the next study suggested.

2. Once a more accurate experimental procedure is available, it might be put in practice on pump running under different conditions. In particular, the transmission properties of pumps can be expected to vary significantly in case of internal trapped air, due to the changes in net sound speed. Since that would also happen in case of cavitation, it opens another possible area of application for the measurement of the transmission or scattering matrix of pumps, which is the detection of cavitation at an early stage.

3. The new acoustic model for centrifugal pumps can be considered validated after the satisfactory contrast between its predictions and the experimental data for a variety of pumps. All this supports a possible future use of this new model complemented with internal acoustic sources as a tool to characterize the noise distribution inside pumps as would correspond to different noise excitation mechanisms at low frequency, such as the excitation associated to blade passing in front of the volute tongue.

Cap. 6 Conclusiones

6.1 Metodología experimental

A fin de estudiar experimentalmente las propiedades acústicas pasivas de la bomba de ensayo, es necesario poder imponer cargas acústicas externas sobre la bomba a la vez que se recogen señales de fluctuaciones de presión en varias posiciones a lo largo de las tuberías de aspiración e impulsión. En esta investigación, las cargas acústicas externas se generaron mediante otra bomba auxiliar que operaba en el mismo sistema hidráulico, y que realizaba una función de altavoz. Las principales conclusiones obtenidas son:

1. La bomba auxiliar resultó ser un generador muy efectivo de pulsaciones de presión a su frecuencia de paso de álabes, las cuales, además, podían ser fácilmente modificadas mediante la variación de la velocidad de rotación de esa bomba auxiliar, a condición de que operase con un caudal muy pequeño. Esto se conseguía mediante una válvula reguladora parcialmente cerrada. Este procedimiento permitió obtener fluctuaciones de presión en la descarga de esa bomba auxiliar con amplitudes típicas de entre 500 Pa y 3 kPa a la frecuencia de paso de álabes.
2. Las fluctuaciones de presión generadas por la bomba auxiliar se transmitían por el sistema de tuberías hasta la zona de la bomba de ensayo, induciéndose fluctuaciones de presión en sus conductos de aspiración y descarga con amplitudes típicas de entre 200 Pa y 1 kPa a la frecuencia excitada por la bomba auxiliar. En consecuencia, las pulsaciones recibidas en la bomba de ensayo eran suficientemente altas como para ser detectadas y medidas con los transductores piezoeléctricos de presión de alta sensibilidad como los empleados en esta investigación.
3. El banco de pruebas demostró poseer una buena capacidad de control de las cargas acústicas externas aplicadas sobre la bomba de ensayo, mediante:
   i) cambiando la velocidad de rotación de la bomba auxiliar,
   ii) controlando la apertura de la válvula de regulación de la bomba auxiliar y
   iii) abriendo o cerrando válvulas de paso de ramas en derivación, lo que permitía definir configuraciones de tuberías con diferentes impedancias acústicas asociadas.
4. Las pruebas de calibración que se llevaron a cabo con cuatro sensores de presión dispuestos radialmente en una misma sección transversal de una tubería arrojaron diferencias de amplitud menores del 2% del valor medio y diferencias de fase de menos de 3 grados también respecto al valor medio. Se consideró que estas diferencias eran suficientemente pequeñas como para suponer validada a la cadena de medida. Además, esas medidas sirvieron para demostrar que las perturbaciones de presión se propagan en modo de onda plana a lo largo de las tuberías de interés.
5. A fin de reducir en lo posible el esparcimiento de los datos finales sobre las matrices de dispersión de la bomba, se extendió la aplicación del procedimiento para incluir medidas bajo un alto número de cargas acústicas externas en vez de solamente dos. Esto hacía que las ondas de presión resultantes en cada frecuencia por las tuberías de aspiración e impulsión de la bomba de ensayo acabaran originando un sistema sobredeterminado de

ecuaciones lineales, que se resolvía mediante un procedimiento de errores cuadráticos mínimos.

6. Los resultados experimentales finalmente obtenidos para las matrices de dispersión de la bomba de ensayo denotan un alto grado de esparcimiento, curiosamente de modo similar a los resultados publicados por otros investigadores. En el presente caso, las razones para ese esparcimiento podrían ser:

   i) Desde la bomba auxiliar se transmite cierto nivel de vibración al sistema de tuberías. El nivel de amplitud de vibración es muy bajo, pero la superficie interna de las tuberías, que actúa como radiante, es muy grande. Cabe esperar que se exciten distintos modos de vibración de las tuberías según la frecuencia de la bomba auxiliar, con lo que el efecto sobre las medidas de las perturbaciones acústicas transmitidas puede ser distinto en cada caso.

   ii) El tramo recto del conducto de impulsión desde la bomba de ensayo es bastante corto, con lo que los valores de presión registrados en dos sensores a lo largo de ese tramo pueden ser muy parecidos sobre todo a baja frecuencia, reduciendo pues la resolución de la medida. En consecuencia, esto puede afectar a la descomposición de ondas de presión en la tubería de impulsión y puede por tanto acabar afectando a la precisión de los elementos de la matriz de dispersión de la bomba obtenidos mediante el procedimiento de mínimos cuadrados.

6.2 Modelo acústico

A fin de simular el campo sonoro a baja frecuencia (modo de onda plana) en el interior de bombas centrífugas, se ha desarrollado un nuevo modelo que se basa en la selección de un cierto número de nodos internos que están conectados mediante matrices de transferencia locales, dependientes de la geometría de las bombas. En general, esas matrices de transferencia locales corresponden a canales de paso con sección transversal variable, con lo que se estimaron mediante segmentación del tipo matrizante. El modelo de matrices de transferencia internas se ha empleado en un procedimiento diseñado para estimar las matrices de dispersión y de transmisión acústica de la bomba en función de la frecuencia. Las principales conclusiones obtenidas son:

1. El modelo define un número de nodos internos que, aunque depende del número de álabes del rodete, es menor de 50 para los casos de interés. Las relaciones de continuidad y las funciones de transferencia interna entre nodos, más las condiciones de contorno en los puertos de entrada y salida de la bomba, dan lugar a un sistema lineal de hasta 100 ecuaciones con términos complejos, es decir, con componentes real e imaginaria. Este sistema se puede resolver de forma eficiente y obtener las fluctuaciones de presión y flujo másico en todos los nodos mediante el método de descomposición clásica de Gauss, a condición de que se emplee doble pivote.
2. El método de doble imposición de cargas acústicas externas demostró ser eficiente para determinar las matrices de dispersión de la bomba para cada frecuencia.
3. El coste computacional necesario para la resolución del sistema lineal de

ecuaciones que gobiernan las variables acústicas internas es relativamente bajo, con lo que se puede calcular la matriz de dispersión acústica de las bombas para un amplio rango de frecuencias en un tiempo reducido (segundos) incluso con un ordenador convencional.

4. En relación con el método de segmentación empleado para establecer las matrices de transferencia internas para canales de paso entre nodos con sección transversal variable, se concluyó que con más de 20 segmentos para cada matriz de transferencia ya no se apreciaban diferencias en las predicciones finales.

5. Los principales eventos acústicos que determinan las características de la transmisión acústica a través de las bombas están relacionados con el volumen y forma de la cámara delimitada por la carcasa, y, en particular, con los cambios abruptos de sección transversal que los frentes de onda encuentran i) entre la salida de los canales del rodete y la región de la voluta y ii) en la garganta que separa la voluta del difusor de salida. Otro factor relevante es la proximidad de la pared de la voluta respecto a la salida de los canales del rodete, que se comporta como un resonador de tubo extendido de tipo reverso.

6. En particular, las predicciones resultan ser bastante sensibles respecto al parámetro denominado *factor de expansión periférica*, que es un parámetro del modelo que mide la expansión de las ondas sonoras al cruzar la salida de los canales del rodete. Se sugiere un valor para dicho factor dentro del rango 2-2.5, mayor cuantos más álabes tiene el rodete.

7. Las predicciones también son sensibles respecto al ángulo de salida de los álabes del rodete, ya que el modelo asume que el sonido continúa propagándose en la dirección de los álabes tras salir de los canales del rodete.

8. En general, las predicciones obtenidas para una bomba de referencia muestran que son poco sensibles respecto a parámetros geométricos que no estén directamente relacionados con la velocidad específica o el tamaño de la bomba. En particular, el número de álabes del rodete tiene poco efecto a partir de 5 álabes. El diámetro del rodete, que en la práctica puede variar sin que cambie la carcasa en el caso de rodetes recortados, también influye relativamente poco.

9. Dado que el modelo asume que el rodete no está girando, la posición angular de los álabes del rodete respecto a la lengüeta pasa a ser otro parámetro geométrico de la bomba. Sin embargo, el efecto de esa posición angular demostró ser muy pequeño para el caso de la bomba de referencia. Este resultado es consistente con los resultados empíricos de Carta et al. (2002), quienes midieron la matriz de transmisión acústica para una bomba parada con el rodete situado en distintas posiciones angulares.

6.3 Propiedades de transmisión acústica de las bombas centrífugas

Se han obtenido las siguientes conclusiones:

1. Las matrices de transmisión predichas por el modelo acústico contienen elementos de reflexión (diagonal principal) que solo poseen parte real (argumento igual a 0 grados) y un valor de amplitud que es igual a 1 a frecuencia nula y que se reduce progresivamente al subir la frecuencia. Esto es consistente con las hipótesis del modelo y con los datos empíricos disponibles en la literatura.

2. Los resultados experimentales obtenidos para la bomba ensayada en laboratorio, así como las predicciones derivadas del nuevo modelo acústico, indican que, a muy baja frecuencia, la bomba se comporta como un elemento de conducto con un cambio abrupto de sección transversal entre los puertos de aspiración y descarga, de modo que el módulo y la fase de los elementos de la matriz de dispersión se pueden obtener a partir de la relación entre ambas secciones.

3. A medida que se va subiendo la frecuencia (al menos hasta 300 Hz) se tiene cada vez más influencia de la cámara delimitada por la carcasa de la bomba, de modo que el módulo de los elementos reflexivos de la matriz de dispersión crece hacia la unidad mientras el de los elementos transmisivos se reduce hacia cero. Además, el argumento de los cuatro elementos de la matriz de dispersión se reduce proporcionalmente a la frecuencia, lo que es consistente con distancias de propagación internas constantes junto a velocidad del sonido también constante.

4. El conjunto de datos empíricos recopilado de la literatura sobre la matriz de dispersión para nueve bombas distintas (con velocidades específicas adimensionales en el rango de 0.25 a 1.03) indica el mismo tipo de tendencias antes descrito para la bomba de laboratorio. En particular la dependencia de los elementos respecto a la frecuencia resulta más acusada al aumentar el tamaño de las bombas y al reducir su velocidad específica. Esto es así porque ambos factores se corresponden con distancias de paso internas más largas para las ondas sonoras transmitidas.

5. A fin de cuantificar el grado de acuerdo entre las predicciones y los datos experimentales, se estableció un parámetro de relación de varianza, que representa la suma de los errores cuadráticos entre predicciones y medidas normalizados por la varianza de los datos empíricos relativa a su valor medio.

6. Para el caso de las predicciones obtenidas mediante el nuevo modelo de matrices internas, el parámetro de relación de varianza toma valores para la mayoría de las diez bombas consideradas que están bien por debajo de 1 y bastante próximas a 0. Esto indica que el nuevo modelo da predicciones bien de la matriz de transmisión o bien de la matriz de dispersión que están razonablemente próximas a los datos experimentales con independencia de la velocidad específica o del tamaño de la bomba.

7. Los datos experimentales recopilados también se compararon con las predicciones del modelo clásico de Stirnemann (Stirnemann et al. 1987), que está basado en una analogía eléctrica. Si bien las predicciones de este modelo indican tendencias similares a los datos experimentales, el efecto de la frecuencia en el modelo resulta siempre demasiado bajo, es decir, los valores predichos para los elementos de las matrices de dispersión y de transmisión al subir la frecuencia se desvían demasiado poco respecto a los valores correspondientes a frecuencia cero. En consecuencia, el parámetro de relación de varianza es sistemáticamente mayor de 1, y es incluso mayor de 10 en muchos casos, lo que denota que las diferencias entre predicciones y medidas son muy considerables.

8. Las discrepancias entre los datos empíricos y las predicciones del modelo clásico de analogía eléctrica son mayores para bombas de gran tamaño y de baja velocidad específica. Se ha inferido que los valores de impedancia y

admitancia equivalentes considerados en ese modelo son sistemáticamente demasiados bajos, lo que es particularmente obvio para bombas con voluta de gran tamaño.

9. Por el contrario, el nuevo modelo de matrices de transferencia internas ha dado predicciones para los cuatro elementos de las matrices de dispersión y de transmisión de las bombas, tanto en módulo como en fase, que guardan un razonable acuerdo cuantitativo con los datos experimentales, con independencia de la velocidad específica o del tamaño de la bomba. Al subir la frecuencia, la capacidad de predicción del nuevo modelo supera claramente a la del modelo de analogía eléctrica en todos los casos. En resumen, el modelo puede considerarse validado y adecuado como instrumento de predicción de las propiedades acústicas pasivas de las bombas centrífugas.

6.4 Trabajos futuros

Se sugieren las siguientes líneas de trabajo como continuación de esta investigación:

1. Se sugiere profundizar más en el desarrollo de un procedimiento experimental de determinación de la matriz de dispersión de una bomba de laboratorio, con el objetivo primario de reducir el grado de esparcimiento de los resultados, posiblemente mediante la instalación de elementos de aislamiento vibratorio para impedir la transmisión de vibración entre componentes del sistema hidráulico. Además, la tubería de descarga debería ser más larga que en el presente estudio. La reducción del grado de esparcimiento debería repercutir en una mayor precisión y fiabilidad, que son necesarias para el siguiente estudio sugerido.
2. Una vez se disponga de un procedimiento experimental de mayor precisión, se podría poner en práctica sobre una bomba de laboratorio operando bajo distintas condiciones. En particular, se puede esperar que las propiedades de transmisión de las bombas varíen significativamente en caso de aire atrapado internamente, debido a los cambios en velocidad neta del sonido. Dado que eso es lo que ocurre cuando hay cavitación, se abre otra posible área de aplicación de la medida de las matrices de transmisión y dispersión de bombas, que es la detección de cavitación en fase temprana.
3. Puede considerarse que el nuevo modelo acústico para bombas centrífugas ha quedado validado tras un satisfactorio contraste entre predicciones y datos experimentales para un conjunto de bombas con un amplio abanico de características. Ello supone una buena base para un posible uso futuro del nuevo modelo complementándolo con fuentes acústicas internas como instrumento de caracterización de la distribución del ruido dentro de las bombas tal como correspondería a diferentes mecanismos de excitación de baja frecuencia, entre los que se incluye la excitación asociada al paso de álabe frente a la lengüeta de la voluta.

References

Åbom, M. (1991). Measurement of the scattering-matrix of acoustical two-ports. *Mechanical Systems and Signal Processing*, 5(2): 89-104.

Alfayez, L. and Mba, D. (2005). Detection of incipient cavitation and determination of the best efficiency point for centrifugal pumps using acoustic emission. *Journal of Process Mechanical Engineering*, 219(4): 327-344.

Al Thobiani, F. (2011). The non-intrusive detection of incipient cavitation in centrifugal pumps. University of Huddersfield, UK. Doctoral Thesis.

Bardeleben, M. J. R. and Weaver, D. S. (2002). Estimation of the acoustic scattering matrix for a centrifugal pump. International Mechanical Engineering Congress and Exposition. *American Society of Mechanical Engineers*, 2002, 809-819.

Bardeleben, M. J. R. (2005). Acoustic characterization of a centrifugal pump using a two-port model. Hamilton, McMaster University.

Barron, R. F. (2003). Industrial noise control and acoustics. Marcel Dekker, New York.

Byskov, R. K., Jacobsen, C. B. and Pedersen, N. (2003). Flow in a centrifugal pump impeller at design and off-design conditions—part II: large eddy simulations. *Journal of Fluids Engineering*, 125(1): 73-83.

Brun, K. and Kurz, R. (2005). Analysis of secondary flows in centrifugal impellers. *International Journal of Rotating Machinery*, 2005(1): 45-52.

Birajdar, R., Patil, R. and Khanzode, K. (2009). Vibration and noise in centrifugal pumps-Sources and diagnosis methods. In 3rd International conference on Integrity, Reliability and Failure.

Barrio, R., Blanco, E., Parrondo, J., González, J. and Fernández, J. (2008). The effect of impeller cutback on the fluid-dynamic pulsations and load at the blade-passing frequency in a centrifugal pump. *Journal of Fluids Engineering*, 130(11): 111102.

Barrio, R., Parrondo, J. and Blanco, E. (2010). Numerical analysis of the unsteady flow in the near-tongue region in a volute-type centrifugal pump for different operating points. *Computers & Fluids*, 39(5): 859-870.

Burden, R.L. and Faires, J.D. Numerical Analysis 9th ed., Brooks/Cole, 2011.

Brennen, C.E. Unsteady Flow in Hydraulic Systems, in Hydrodynamics of Pumps, Cambridge University Press, 2011, pp. 172-208.

Brümmer, A., Lehr, C., Linkamp, A. (2019). Entwicklung von grundlagen für instationär betriebene hydraulische pumpensysteme in flexiblen kraftwerken; Teilprojekt TP2, Arbeitspaket AP4: Druckpulsationen in instationär betriebenen hydraulischen Systemen, Technical Report, TU Dortmund.

Chu, S., Dong, R. and Katz, J. (1995). Relationship between unsteady flow, pressure fluctuations, and noise in a centrifugal pump—Part A: Use of PDV data to compute the pressure field. *Journal of Fluids Engineering*, 117(1): 24-29.

Chu, S., Dong, R. and Katz, J. (1995). Relationship between unsteady flow, pressure fluctuations, and noise in a centrifugal pump—part B: effects of blade-tongue interactions. *Journal of Fluids Engineering*, 117(1): 30-35.

Carta, F., Charley, J. and Caignaert, G. (2000). Transfer matrices of single volute centrifugal pumps. *International Journal of Acoustics and Vibration*, 5(4): 159-166.

Carta, F., Bolpaire, S., Charley, J. and Caignaert, G. (2002). Hydroacoustic source characterisation of centrifugal pumps. *International Journal of Acoustics and Vibration*, 7(2): 110-114.

Chudina, M. (2003). Noise as an indicator of cavitation in a centrifugal pump. *Acoustical Physics*, 49(4): 463-474.

Choi, J. S., McLaughlin, D. K. and Thompson, D. E. (2003). Experiments on the unsteady flow field and noise generation in a centrifugal pump impeller. *Journal of Sound and Vibration*, 263(3): 493-514.

Chen, Y. B., Feng, T., Liu, K. and Li, X. H. (2005). Some factors acting on in-pipe noise measurement of fluid-machine. *Technical Acoustics*, 24(z1): 75-76.

Čudina, M. and Prezelj, J. (2009). Detection of cavitation in situ operation of kinetic pumps: effect of cavitation on the characteristic discrete frequency component. *Applied Acoustics*, 70(9): 1175-1182.

Christopher, S. and Kumaraswamy, S. (2013). Identification of critical net positive suction head from noise and vibration in a radial flow pump for different leading edge profiles of the vane. *Journal of Fluids Engineering*, 135(12): 121301.

Cai, J., Pan, J. and Guzzomi, A. (2014). The flow field in a centrifugal pump with a large tongue gap and back blades. *Journal of Mechanical Science and Technology*, 28(11): 4455-4464.

Cheng, X., Wang, P. and Zhang, S. (2020). Correlation research between turbulent pressure pulsation and internal sound field characteristics of centrifugal pump. *Journal of Thermal Science*, 1-11.

Dong, R., Chu, S. and Katz, J. (1997). Effect of modification to tongue and impeller geometry on unsteady flow, pressure fluctuations, and noise in a centrifugal pump. *Journal of Turbomachinery*, 119(3): 506-515.

Durrer, B., Wurm, F. H. and Ag, W. (2006). Noise sources in centrifugal pumps. *Wseas Transactions on Applied and Theoretical Mechanics*, 1(1): 85.

De Roeck, W. and Desmet, W. (2008). Experimental acoustic identification of flow noise sources in expansion chambers. In Proceedings of ISMA, 2008, 455-470.

Elholm, T., Ayder, E. and Van den Braembussche, R. (1990). Experimental study of the swirling flow in the volute of a centrifugal pump. In ASME 1990 International Gas Turbine and Aeroengine Congress and Exposition. American Society of Mechanical Engineers.

Faulkner, L. L. (1976). Handbook of Industrial Noise Control. Industrial Press, New York.

Guelich, J.F. and Bolleter, U. (1992). Pressure pulsations in centrifugal pumps. *Journal of Vibration and Acoustics*, 114(2): 272-279.

Guan X. The theory and design of modern pump, 2nd ed.; Chinese Aerospace Press: Beijing, China, 2011.

Gao, B., Zhang, N., Li, Z., Ni, D. and Yang, M. (2016). Influence of the blade trailing edge profile on the performance and unsteady pressure pulsations in a low specific speed centrifugal pump. *Journal of Fluids Engineering*, 138(5): 051106.

Guo, C., Gao, M., Lu, D. and Wang, K. (2017). An experimental study on the radiation noise characteristics of a centrifugal pump with various working conditions. *Energies*, 10(12): 2139.

Guo, C., Gao, M., Lu, D. and Guan, H. (2018). Experimental study on radiation noise frequency characteristics of a centrifugal pump with various rotational speeds. *Applied Sciences*, 8(5): 796.

Garnell, E., Åbom, M. and Banwell, G. (2019). The use of the two-port method to characterize high-speed small fans. *Applied Acoustics*, 146: 155-163.

Guo, C., Gao, M., Wang, J., Shi, Y. and He, S. (2019). The effect of blade outlet angle on the acoustic field distribution characteristics of a centrifugal pump based on Powell vortex sound theory. *Applied Acoustics*, 155: 297-308.

Guo, C., Gao, M. and He, S. (2020). A review of the flow-induced noise study for centrifugal pumps. *Applied Sciences*, 10(3): 1022.

Hambric, S. A., Hwang, Y. F. and Chyczewski, T. S. (2002). Noise sources and transmission in piping systems. In ASME 2002 International Mechanical Engineering Congress and Exposition (pp. 79-90). *American Society of Mechanical Engineers Digital Collection*.

Han, Y., Smith, B. A. W. and Luloff, B. V. (2003). Use of redundant sensors to determine the acoustic transfer matrix of a pump. In ASME Pressure Vessels and Piping Conference (Vol. 41561, pp. 169-178).

Holmberg, A., Åbom, M. and Bodén, H. (2011). Accurate experimental two-port analysis of flow generated sound. *Journal of Sound and Vibration*, 330(26): 6336-6354.

Hayashi, I. and Kaneko, S. (2014). Pressure pulsations in piping system excited by a centrifugal turbomachinery taking the damping characteristics into consideration.

Journal of Fluids and Structures, 45, 216-234.

Jong, C. D. (1996). Analysis of pulsations and vibrations in fluid-filled pipe systems. Eindhoven: Technische Universiteit Eindhoven. Doctoral Thesis.

Kergourlay, G., Younsi, M., Bakir, F. and Rey, R. (2007). Influence of splitter blades on the flow field of a centrifugal pump: test-analysis comparison. *International Journal of Rotating Machinery*, 2007.

Keller, J., Parrondo, J., Blanco, E., Barrio, R. and Suárez, C. (2013). Influence of pump-circuit coupling on acoustic waves in pipelines and pump velocity fields. In ASME 2013 Pressure Vessels and Piping Conference, American Society of Mechanical Engineers.

Keller, J., Parrondo, J., Barrio, R., Fernández, J. and Blanco, E. (2014). Effects of the pump-circuit acoustic coupling on the blade-passing frequency perturbations. *Applied Acoustics*, 76: 150-156.

Keller, J., Blanco, E., Barrio, R. and Parrondo, J. (2014). PIV measurements of the unsteady flow structures in a volute centrifugal pump at a high flow rate. *Experiments in Fluids*, 55(10): 1820.

Keller, J. (2014). Fluid-dynamic fluctuation and flow structure in centrifugal pumps due to rotor-stator interaction. Departmento de Energía, Universidad of Oviedo, Gijón, Spain. Doctoral Thesis.

Kabral, R. and Åbom, M. (2018). Investigation of turbocharger compressor surge inception by means of an acoustic two-port model. *Journal of Sound and Vibration*, 412: 270-286.

Lighthill, M. J. (1952). On sound generated aerodynamically I. General theory. Proceedings of the Royal Society of London. Series A. *Mathematical and Physical Sciences*, 211(1107): 564-587.

Lavrentjev, J., Åbom, M. and Bodén, H. (1995). A measurement method for determining the source data of acoustic two-port sources. *Journal of Sound and Vibration*, 183(3): 517-531.

Lavrentjev, J. and Åbom, M. (1996). Characterization of fluid machines as acoustic multi-port sources. *Journal of Sound and Vibration*, 197(1): 1-16.

Langthjem, M. A. and Olhoff, N. (2004). A numerical study of flow-induced noise in a two-dimensional centrifugal pump. Part II. Hydroacoustics. *Journal of Fluids and Structures*, 19(3): 369-386.

Larralde, E. and Ocampo, R. (2010). Centrifugal pump selection process. *World Pumps*, 2010(2): 24-28.

Liu, H. L., Wang, Y., Yuan, S. Q. and Tan, M. G. (2012). Effects of impeller outlet width on the vibration and noise from centrifugal pumps induced by flow. *Journal of Huazhong University of Science and Technology* (Natural Science Edition),

40(1):123-127.

Liu, H. L., Ding, J., Tan, M. G., Cui, J. B. and Wang, Y. (2013). Analysis and experimental of centrifugal pump noise based on outlet width of impeller. *Transactions of the Chinese Society of Agricultural Engineering*, 29(16): 66-73.

Li, Y., Yuan, S., Wang, X., Keat Tan, S. and Mao, J. (2016). Comparison of flow fields in a centrifugal pump among different tracer particles by particle image velocimetry. *Journal of Fluids Engineering*, 138(6).

Linkamp, A.; Lehr, C. and Brümmer, A. Simplified one-dimensional model for transient time-domain simulation of centrifugal pumps. In Proceedings of the 24th International Congress on Sound & Vibration, London, UK, 23-27 July 2017; pp. 2377-2385.

Lehr, C., Linkamp, A., Aurich, D. and Brümmer, A. (2019). Simulations and Experimental Investigations on the Acoustic Characterization of Centrifugal Pumps of Different Specific Speed. *International Journal of Turbomachinery, Propulsion and Power*, 4(3): 16.

Munjal, M. L. (1987). Acoustics of ducts and mufflers with application to exhaust and ventilation system design. John Wiley & Sons.

Munjal, M. L. Acoustics of ducts and mufflers 2nd ed., Wiley, 2014.

Morgenroth, M. and Weaver, D. S. (1998). Sound generation by a centrifugal pump at blade passing frequency. *Journal of Turbomachinery*, 120(4): 736-743.

Majidi, K. (2005). Numerical study of unsteady flow in a centrifugal pump. *Journal of Turbomachinery*, 127(2): 363-371.

Mimani, A. and Munjal, M. L. (2010). Transverse plane-wave analysis of short elliptical end-chamber and expansion-chamber mufflers. *International Journal of Acoustics and Vibration*, 15(1): 24-38.

Mousmoulis, G., Karlsen-Davies, N., Aggidis, G., Anagnostopoulos, I. and Papantonis, D. (2019). Experimental analysis of cavitation in a centrifugal pump using acoustic emission, vibration measurements and flow visualization. *European Journal of Mechanics-B/Fluids*, 75: 300-311.

Neill, G. D., Reuben, R. L., Sandford, P. M., Brown, E. R. and Steel, J. A. (1997). Detection of incipient cavitation in pumps using acoustic emission. *Journal of Process Mechanical Engineering*, 211(4): 267-277.

Nashed, M. W., Elnady, T. and Åbom, M. (2018). Modeling of duct acoustics in the high frequency range using two-ports. *Applied Acoustics*, 135: 37-47.

Ni, D., Yang, M., Gao, B., Zhang, N. and Li, Z. (2018). Experimental and numerical investigation on the pressure pulsation and instantaneous flow structure in a nuclear reactor coolant pump. *Nuclear Engineering and Design*, 337: 261-270.

Ni, D., Zhang, N., Gao, B., Li, Z. and Yang, M. (2020). Dynamic measurements on unsteady pressure pulsations and flow distributions in a nuclear reactor coolant pump. *Energy*, 117305.

Parrondo, J., Gonzalez, J. and Fernández, J. (2002). The effect of the operating point on the pressure fluctuations at the blade passage frequency in the volute of a centrifugal pump. *Journal of Fluid Engineering*, 124(3): 784-790.

Pedersen, N., Larsen, P. S. and Jacobsen, C. B. (2003). Flow in a centrifugal pump impeller at design and off-design conditions—part I: particle image velocimetry (PIV) and laser Doppler velocimetry (LDV) measurements. *Journal of Fluids Engineering*, 125(1): 61-72.

Parrondo, J., Pérez, J., Barrio, R. and González, J. (2011). A simple acoustic model to characterize the internal low frequency sound field in centrifugal pumps. *Applied Acoustics*, 72(1): 59-64.

Rzentkowski, G. and Zbroja, S. (2000). Experimental characterization of centrifugal pumps as an acoustic source at the blade-passing frequency. *Journal of Fluids and Structures*, 14(4): 529-558.

Rzentkowski, G. and Zbroja, S. (2000). Acoustic characterization of a CANDU primary heat transport pump at the blade-passing frequency. *Nuclear Engineering and Design*, 196(1): 63-80.

Stirnemann, A., Eberl, J., Bolleter, U. and Pace, S. (1987). Experimental determination of the dynamic transfer matrix for a pump. *Journal of Fluids Engineering*, 109(3): 218-225.

Sinha, M. and Katz, J. (2000). Quantitative visualization of the flow in a centrifugal pump with diffuser vanes—I: on flow structures and turbulence. *Journal of Fluids Engineering*, 122(1): 97-107.

Solis, M., Bakir, F. and Khelladi, S. (2009). Pressure fluctuations reduction in centrifugal pumps: influence of impeller geometry and radial gap. In ASME 2009 fluids engineering division summer meeting. *American Society of Mechanical Engineers*.

Sun, Y. D., Zhong, R., Wang, S. Q., Hao, X. Y. and Wang, J. (2016). Experimental research on hydrodynamic noise of centrifugal pumps based on two-port source characteristic test method. *Journal of Ship Mechanics*, 20(1-2): 198-205.

Si, Q., Ali, A., Yuan, J., Fall, I. and Muhammad Yasin, F. (2019). Flow-induced noises in a centrifugal pump: a review. Science of Advanced Materials, 11(7): 909-924.

Si, Q., Shen, C., He, X., Li, H., Huang, K. and Yuan, J. (2020). Numerical and Experimental Study on the Flow-Induced Noise Characteristics of High-Speed Centrifugal Pumps. *Applied Sciences*, 10(9): 3105.

To, C. W. S. and Doige, A. G. (1979). A transient testing technique for the

determination of matrix parameters of acoustic systems, I: Theory and principles. *Journal of Sound and Vibration*, 62(2): 207-222.

To, C. W. S. and Doige, A. G. (1979). A transient testing technique for the determination of matrix parameters of acoustic systems, II: Experimental procedures and results. *Journal of Sound and Vibration*, 62(2): 223-233.

Tao, F. (2004). The measurement study of flow induced noise in centrifugal pump. *Institute of Acoustics, Chinese Academy of Sciences*, China. Doctoral Thesis.

Wang, H. and Tsukamoto, H. (2003). Experimental and numerical study of unsteady flow in a diffuser pump at off-design conditions. *Journal of Fluids Engineering*, 125(5): 767-778.

Westra, R. W., Broersma, L., van Andel, K. and Kruyt, N. P. (2010). PIV measurements and CFD computations of secondary flow in a centrifugal pump impeller. *Journal of Fluids Engineering*, 132(6): 061104.

Wang, Y., Wang, J., Liu, D. X. and Liu, H. L. (2013). Effects of centrifugal pumps outlet angle on flow induced vibration and noise. *Applied Mechanics and Materials, Trans Tech Publications*, 2013, 249: 460-465.

Wu, D., Ren, Y., Mou, J. and Gu, Y. (2017). Investigation of pressure pulsations and flow instabilities in a centrifugal pump at part-load conditions. *International Journal of Fluid Machinery and Systems*, 10(4): 355-362.

Yang, S., Kong, F. and Chen, B. (2011). Research on pump volute design method using CFD. *International Journal of Rotating Machinery*, 2011.

Yuan, S. Q., Xue, F., Yuan, J. P. and Tang, Y. (2009). Experimental study on impact of pressure fluctuation on flow-noise in centrifugal pump. *Drainage and Irrigation Machinery*, 27(5): 287-290.

Yuan, S., Yang, J., Yuan, J., Luo, Y. and Pei, J. (2012). Experimental investigation on the flow-induced noise under variable conditions for centrifugal pumps. *Chinese Journal of Mechanical Engineering*, 25(3): 456-462.

Yang, J., Yuan, S., Yuan, J., Si, Q. and Pei, J. (2014). Numerical and experimental study on flow-induced noise at blade-passing frequency in centrifugal pumps. *Chinese Journal of Mechanical Engineering*, 27(3): 606-614.

Yamamoto, K., Müller, A., Ashida, T., Yonezawa, K., Avellan, F. and Tsujimoto, Y. (2015). Experimental method for the evaluation of the dynamic transfer matrix using pressure transducers. *Journal of Hydraulic Research*, 53(4): 466-477.

Zhang, N., Yang, M., Gao, B., Li, Z. and Ni, D. (2015). Experimental investigation on unsteady pressure pulsation in a centrifugal pump with special slope volute. *Journal of Fluids Engineering*, 137(6): 061103.

Zhang, N., Yang, M., Gao, B., Li, Z. and Ni, D. (2016). Investigation of rotor-stator interaction and flow unsteadiness in a low specific speed centrifugal pump.

Strojniški vestnik-Journal of Mechanical Engineering, 62(1): 21-31.

Zhang, N., Liu, X., Gao, B. and Xia, B. (2019). DDES analysis of the unsteady wake flow and its evolution of a centrifugal pump. *Renewable Energy*, 141: 570-582.

Zhang, N., Jiang, J., Gao, B. and Liu, X. (2020). DDES analysis of unsteady flow evolution and pressure pulsation at off-design condition of a centrifugal pump. *Renewable Energy*, 153: 193-204.

Articles derived of the thesis:

1) Title: Effect of the discharge piping scheme on the pressure fluctuations induced from a laboratory pump

Authors: Guidong Li, Jorge Parrondo, Yang Wang

Presented at:

2nd International Research Conference on Sustainable Energy, Engineering, Materials and Environment, Mieres, Spain, 25th–27th July 2018

Published as:

Li G, Parrondo J, Wang Y. Effect of the Discharge Piping Scheme on the Pressure Fluctuations Induced from A Laboratory Pump. Proceedings, 2018, 2(23): 1488.

2) Title: Experimental investigation on the acoustic scattering matrix for a centrifugal pump

Authors: Guidong Li, Jorge Parrondo, Yang Wang

Presented at:

2nd International Research Conference on Sustainable Energy, Engineering, Materials and Environment, Mieres, Spain, 25th–27th July 2018

Published as:

Li G, Parrondo J, Wang Y. Experimental Investigation on the Acoustic Scattering Matrix for a Centrifugal Pump. Proceedings. 2018, 2(23): 1489.

3) Title: Geometry dependence of the acoustic transmission and reflection properties of centrifugal pumps based on an internal lumped parameter model

Authors: Guidong Li, Manuel Garc á-D áz, Guillermo Laine, Jorge Parrondo

Journal: Applied Acoustics

Manuscript Submitted